Raman spectroscopic study of inorganic salts present in atmospheric particulate matter, their origin and implications

seit 1558

Dissertation

Zur Erlangung des akademischen Grades
doctor rerum naturalium (Dr. rer. nat.)

vorgelegt dem Rat der Chemisch-Geowissenschaftlichen Fakultät der
Friedrich-Schiller-Universität Jena von

M. Sc. Paul Ernesto Vargas Jentzsch

geb. am 14. März 1979 in Cochabamba

Gutachter:

1. Prof. Dr. Jürgen Popp
   Institut für Physikalische Chemie
   Friedrich-Schiller-Universität Jena

2. Prof. Dr. Falko Langenhorst
   Institut für Geowissenschaften
   Friedrich-Schiller-Universität Jena

Tag der öffentlichen Verteidigung: 12.12.2012

Dedicated to my parents, my sister and my brother.

"Everything should be made as simple as possible, but not simpler." (Albert Einstein)

Contents

Zusammenfassung

Umweltrelevante Themen haben gegenwärtig in Forschung und Wissenschaft grosse Bedeutung erlangt. Besondere Beachtung findet dabei die Luftverschmutzung, da das enorme Anwachsen von Industriegebieten und urbanen Ballungsräumen zu einer erhöhten Abgabe von gasförmigen, flüssigen (mikroskopische Tropfen) und festen (feste Schwebeteilchen) Schadstoffemissionen in die Atmosphäre führt.

Atmosphärische Aerosolpartikel können sowohl die Gesundheit der Bevölkerung als auch das Klima bedrohen. Durch zahlreiche in der Vergangenheit durchgeführte Studien wurde bewiesen, dass den Aerosolen eine grosse Rolle bei der Bewertung des Klimawandels zukommt, da sie die Sonneneinstrahlung absorbieren oder streuen und so die Wolkenbildung und –lebensdauer beeinflussen können.

Die Zusammensetzung der atmosphärischen Aerosolpartikel ist unterschiedlich und hängt von den in den jeweiligen Gebieten vorherrschenden natürlichen und anthropogenen Emissionen ab. So sind beispielsweise in der Atmosphäre über urbanen Räumen vorwiegend anthropogene Bestandteile wie Russ, halbflüchtige organische Verbindungen, bestimmte Metalle, Sulfate, Nitrate usw. zu finden, während Emissionen wie Sodium- und Potassiumsalze, die durch schäumende Wellen der Ozeane bzw. durch Verbrennung von Biomasse entstehen und in die Atmosphäre gelangen, natürlichen Urprung haben.

Besondere Bedeutung ist den anorganischen Salzen in den atmosphärischen Aerosolpartikeln beizumessen, da diese in hohem Masse wasserlöslich und/oder hygroskopisch sind. Aufgrund dieser Eigenschaften können atmosphärische Partikel, die zumindest kleine Mengen anorganischer Salze enthalten, als effiziente Kondensationskerne für die Wasserkondensation (mit oder ohne Eisbildung) fungieren und dadurch das Klima beeinflussen. Unter Berücksichtigung der Interaktionen der atmosphärischen Partikel mit Wasser ermöglicht die Identifizierung der in den Aerosolpartikeln enthaltenen Salze Rückschlüsse auf die in der Atmosphäre stattfindenden Prozesse. Die Analyse atmosphärischer Partikel unter diesen Gesichtspunkten setzt selbstverständlich die Verfügbarkeit geeigneter analytischer Techniken voraus.

Eine Vielzahl bereits veröffentlichter Studien belegen die Eignung der Raman-Spektroskopie zur Identifizierung von bekannten atmosphärischen Salzen, darüber hinaus kann diese Technik jedoch auch zur Aufklärung der Bildungs- und Transformationsprozesse von atmosphärischen Salzen eingesetzt werden.

Im Rahmen dieser Dissertation wurde der Ursprung bestimmter Salze und Salzmischungen unter Mitwirkung von Wasser untersucht. Die an den atmosphärischen Partikeln stattfindenden Kondensations- und Verdampfungszyklen führen zu Veränderungen der ursprünglich ausgestossenen Partikel und zur Kristallisation anderer Salze. In dieser Arbeit wird die atmosphärische Bildung von verschiedenen Salzen vorgeschlagen, insbesondere eines Fe(III)-Salzes, des sogenannten "Ungemachit". Von jedem Salz wurden die Raman-Spektren gemessen und die charakteristischen Banden zugeordnet. Untersucht wurde auch die Reaktivität von festen, alkaline Mineralien und $(NH_4)_2SO_4$ enthaltenden Mischungen im Kontakt mit feuchter Luft, da solche Reaktionen infolge des Koagulationsprozesses an atmosphärischen Partikeln stattfinden können. Sowohl die Zusammensetzung der atmosphärischen Partikel als auch die Reaktivität fester Mischungen stellen nützliche Daten für die Erstellung von Modellen zur Schätzung des Klimawandels dar.

1 Summary

1.1   Motivation

It is known and accepted that human activities have effects on the surrounding environment. These effects depend on the specific geographic location as well as the "magnitude" of the activities in terms of exploitation of natural resources and generation of residues. Air trapped in ice samples dated back to the latter part of the eighteenth century, which coincides with the beginning of the industrial revolution, showed incipient global changes in the atmospheric composition, [1] confirming the important environmental impact caused by the industrial development.

At present, environmental topics related to soil, water and air, as well as the development of new technologies and methods for the environmentally friendly production, are subjects of intense study. Much of the concern is related to the air pollution and how the atmospheric chemistry is affected, since substances emitted into the atmosphere can be transported to remote regions. Illustrative examples are the reports referred to the long-range transport of precursors of acid rain, [2,3] polycyclic aromatic hydrocarbons, [4] and mineral dust. [5-7]

There are different pollutants present in the atmosphere, some of the most important ones are volatile organic compounds (VOCs), sulfur dioxide (SO_2), nitrogen oxides (NO_x), particulate matter, carbon monoxide (CO), carbon dioxide (CO_2)[1], tropospheric ozone (O_3), peroxyacetyl nitrate (PAN), ammonia (NH_3) and chlorofluorocarbons (CFCs). The direct influence and effects of these pollutants depend on their physical and chemical characteristics, e.g., methane (CH_4), which pertains to the category of VOCs, is a gas known to contribute to the global warming, [8] while CFCs participate in the destruction of stratospheric ozone. [9] Furthermore, interactions between pollutants can cause an enhancement or attenuation of atmospheric processes, resulting in dangerous interferences on natural equilibrium.

In the scientific literature a large variety of studies is dedicated to atmospheric particulate matter. Particulate matter contains components of natural and anthropogenic origin, which can even be found in rural areas, where the human influence is minimal. Nevertheless, even in rural areas the anthropogenic impact can be observed; the results of a study carried out in a rural area in Lithuania [10] illustrate this finding. There are no doubts that the human activities have direct and indirect influence on the size

---

[1] In 2007, after a long controversy, the U.S. Supreme Court held that the Clean Air Act gives the Environmental Protection Agency (EPA) the authority to regulate tailpipe emissions of CO_2 and other greenhouse gases. (Massachusetts v. Environmental Protection Agency, No. 05-1120). This decision can be interpreted as a legal acceptance that CO_2 is an air pollutant.

distribution, concentration and composition of atmospheric particles, and these suspended materials in turn are important because of their implications on human health and atmospheric processes. Therefore, the study of atmospheric particulate matter not only requires appropriate analytical methods, but also the interpretation of the observed atmospheric composition, its variations and significance.

Particulate matter has a direct effect on the climate, since particles scatter and absorb the solar radiation. In addition, there are two indirect effects on the climate, both related to water in the hydrological cycle. [11,12]

A remarkable component of the troposphere is water, which can be found in vapor, liquid and solid state. Water in solid state can be found fundamentally in the upper troposphere; the cirrus clouds are probably the most important form due to their radiative effects. [13] Liquid water is present in the troposphere as fog, cloud droplets and wet aerosols; clouds cover ~60% of the Earth's surface and occupy ~7% of the troposphere. [14] In the condensation of both liquid and solid water (ice), atmospheric particulate matter plays a determinant role, since it allows the heterogeneous nucleation of ice [15] and the condensation of water droplets at reasonable supersaturations. [16] The increase in the concentration of particles (more particles per volume unit) results in the formation of more droplets and thus in an increased reflection to space of solar radiation (first indirect radiative forcing). In addition, the condensation of more droplets implies a decrease of the droplet radius and the precipitation efficiency. In other words, the precipitation is inhibited and the clouds contain more water (as droplets), leading to a further increase in the reflection of radiation (second indirect radiative forcing). [11,12]

In this context, when particulate matter interacts with water in the atmosphere, particles can be removed by washout or modified in size and composition (aging processes) until they finally are removed by dry or wet precipitation. What is the composition of these aged particles? It is accepted that the result of aging processes is the formation of internally mixed particles[2], [16] but there are uncertainties associated with the identification of the individual compounds. The ionic composition of atmospheric particulate matter has been a subject of study of several reported works, but there are only a few reports specifying the salt form in which the ions are found.

The identification of the components found in atmospheric particulate matter (in this case inorganic salts) is important for monitoring purposes and also for the study of the atmospheric chemistry. Currently, atmospheric studies are performed not only using aerosol chambers and other related experimental setups, but also using computational models to evaluate different emission scenarios. These models are used to obtain climate projections and to estimate the effects of changes in atmospheric composition. For interpretation purposes, the results obtained by computational calculations require the feed-back and the support of past and current atmospheric measurements.

The aim of this doctoral thesis is to investigate aspects concerning the atmospheric origin of some inorganic salts of known atmospheric occurrence. Moreover, based on laboratory experiments, the atmospheric formation of other inorganic salts is proposed in view of the common presence of certain ions in the atmosphere and their interaction with atmospheric water. Raman spectroscopy is the main analytical tool used in this

---

[2] The terms internal mixture and external mixture are used to indicate whether two or more species are found together in one particle, i.e., as one "internal mixture" or are rather found in separate particles in the same sample, i.e., as an "external mixture". [17]

work, therefore, the bands observed in the Raman spectra of all pure salts considered in this investigation have been properly assigned. The Raman-specific features of some salts were discussed from the point of view of their crystal structure.

In the following section, general aspects of the significance of atmospheric particulate matter to human health, the atmospheric chemistry and climate are outlined. Furthermore, the most common analytical methods used to study atmospheric particulate matter and the advantages of Raman spectroscopy with respect to other methods are summarized. Finally, the results of this doctoral thesis are summarized and conclusions are drawn.

1.2   State of the Art

Many research works have been done on the topic of particulate matter from the point of view of human health effects. [18-20] The researchers agree upon two important parameters to be taken into account: the particle composition and the respirable fraction of aerosol particles which can penetrate into the alveoli of the lungs. The deficit in lung function is associated with a set of pollutants such as fine particulate matter with an aerodynamic diameter[3] below 2.5 µm ($PM_{2.5}$). [21] The relative toxicity of atmospheric substances is important, because obviously it could aggravate the health complications related to inert particles of the same size. An important aspect to be considered in the health impact evaluation is the amount of water-soluble (bioavailable) substances. A Canadian epidemiological study has shown that sulfate, iron, nickel and zinc in ambient $PM_{2.5}$ appear to be more strongly associated with mortality than $PM_{2.5}$ mass. [18] It has also been postulated that iron and other transition metals could act as catalysts in the formation of reactive oxygen species that may be associated with the activation of many biochemical processes. [22]

However, atmospheric particulate matter has environmental implications beyond the human health effects. There are important heterogeneous reactions which can alter the atmospheric composition, e.g., the formation of $HCl(g)$ and $NaNO_3$(s or aq) by the reaction between $HNO_3(g)$ and $NaCl$(s or aq). [23] In addition, photochemical reactions of mineral dust have been the subject of different investigations on the daytime chemistry. [24] Atmospheric particles affect also the weather conditions and climate, since they influence the cloud lifetime and the Earth radiation budget. [25,26] Cloud droplets and ice particles are formed in the atmosphere by condensation of supersaturated water vapor on atmospheric particles; particles which can nucleate liquid cloud droplets and induce the formation of ice crystals are called cloud condensation nuclei (CCN) and ice nuclei (IN), respectively. Undoubtedly, the composition of atmospheric particles is a key factor; particles made from water soluble (organic or inorganic) and insoluble but wettable materials, facilitate the formation of cloud droplets, while the organic hydrophobic compounds act inhibiting the condensation of water, [16] this means that even particles of hydrophobic materials but internally mixed with modest amounts of hydrophilic materials can act as CCN. The effect of the variation in the concentration of CCN on the onset of precipitation was observed in the event of smoke from forest fires, [27] and further implications include the increase of the stratospheric water vapor [28] and even effects on the depletion of stratospheric ozone. [29]

Many researchers have studied the radiative forcing caused by specific components of the atmospheric particulate matter. [25,30-33] It has been found that some materials such as sulfates cause a negative forcing (cooling the atmosphere), while others such as black carbon have a positive forcing effect (warming the atmosphere). [30,33] Moreover, model studies have shown that variations in emissions of a given compound can modify the concentration of several others, [32] resulting in variations of the global radiative forcing.

---

[3] The aerodynamic diameter is defined as the diameter of a spherical particle with a density of 1 g cm^{-3} and a settling velocity equal to that of the particle in question. Particles with the same physical size and shape but different densities have different aerodynamic diameters. [21]

About two decades ago, Preining (1991) [34] estimated that the annual global aerosol[4] production totaled approx. 2 Pg (1 Pg = 10^{15} g), whereof 40% was attributed to direct natural emissions (sea salt, mineral dust and volcanic material), 40% to natural gas emissions converted to aerosols (sulfates, nitrates and hydrocarbons), and 20% to anthropogenic emissions (direct and gas-to-particle conversion). The relative anthropogenic effect on the environment is normally a subject of intense discussion, because it is evident that the dividing line between anthropogenic and naturally-originated pollutants is not always clear. The case of mineral dust transported by wind is illustrative, because the transport of these materials, especially from deserts, has been considered for a long time as a natural process, but now it is known that the progressive expansion of deserts and the soil degradation due to human activities can enhance the mentioned transport process. [35] Tegen and coworkers [36,37] demonstrated by model calculations that not all mineral dust has a natural origin, in fact more than 50% of the total atmospheric dust mass originates from human-disturbed soils. In addition, there are other sources of dust emissions probably underestimated in the past, but important in current scenarios in which human activities already affected the natural equilibrium.

A well-known dramatic example of the destruction of the natural equilibrium by human activities is the desiccation of the Aral Sea due to the excessive exploitation of watercourses for agriculture, industry and human consumption. [38] One of the consequences of the desiccation of lakes is the dust emission from the dry lake beds, since the material therein has a very fine granulometry (clays and evaporite salts). Results from a model study performed by Tegen and coworkers [39] show that dry lake beds (called "preferential source areas" by these authors) make a substantial contribution to global dust emissions. When a saline lake desiccates, the saline fraction of the emitted dust is remarkably high; in the case of the Aral Sea, wind-transportation of huge amounts of salt/dust material (also known as "salt storms") was observed as far as 500 km, affecting not only the health of people, but also the crop productivity by causing a systematic soil salinization in remote areas. [38] Of course, these particles of soluble salts occurring in atmosphere can also affect the weather, since they act as very efficient CCN.

The Aral Sea is the most notorious case due to its magnitude, but not the only one; the Urmia Lake (Iran) is another saline water body in desiccation process, again triggered by an overexploitation of water inflows. [40] Some "soda lakes"[5], e.g., the Owens Lake (USA), were also affected by desiccation processes, releasing large quantities of wind-transported alkaline dust. [41,42] Although the emission of alkaline dust is known, studies on their atmospheric effects are scarce in the scientific literature. Usually, the effect of dust-contained alkaline materials on the atmospheric chemistry is just evaluated in terms of the effect on the pH value of atmospheric water. For atmospheric studies, the neutral pH value is 5.6, since it is considered that cloud- and rainwater are equilibrated with atmospheric CO_2. [43,44] Several studies on the pH of atmospheric water in India above rural and urban areas have been reported in the past. [43-53] The authors agree that the observed pH values higher than 5.6 (in many cases even higher

---

[4] According to the rigorous definition, aerosols are relatively stable suspensions of solid or liquid particles in gas. Thus aerosols differ from particles in that an aerosol includes both the particles and the gas in which they are suspended. However, the term "aerosols" is often used in the atmospheric chemistry literature to denote just the particles. [17]

[5] A soda lake or alkaline lake is a lake with pH values typically between 9 and 12. Generally, they are characterized by high concentrations of CO_3^{2-} and Na^+ ions.

than 7.0) can be attributed fundamentally to the interaction of the atmospheric water with soil dust known to be rich in alkaline materials. There are no doubts about the interaction of mineral dust with water in the atmosphere, and the interaction of dust particles with other atmospheric components and even with other particles of different composition can be expected.

Gas-to-particle conversion processes (secondary particle formation) are other important contributors of atmospheric particulate matter. This kind of processes involves both organic vapors and gases emitted from oceanic and continental areas. Probably the most important gas-to-particle conversion processes are related to the formation in atmosphere of sulfate (SO_4^{2-}) and nitrate (NO_3^-).

There are minor primary sources of sulfate particles (sea salt aerosol and some sulfate minerals in dust), but most of the atmospheric sulfate particles are secondary particles. [16] Sulfur in atmosphere is emitted as SO_x predominantly from volcanoes as a natural source, but also from fossil fuel burning and industry, [54] which then oxidizes to the SO_4^{2-} observed in atmosphere as H_2SO_4 or sulfate salts. [17] However, sulfur is also released into the atmosphere from the ocean in the form of dimethyl sulfide (DMS) and then oxidized to SO_4^{2-} by reaction with the hydroxyl radical ($HO^\bullet$) in presence of solar radiation. [55-57]

The occurrence of nitrate in atmosphere (in snow, in liquid water or as solid salt) is attributed to processes taking place in the atmosphere. In fact, the formation of the most important nitrate deposits in the Antarctic Continent and the deserts of northern Chile was attributed to atmospheric processes. [58] The oxidation of nitrogenous material originated on the ocean surface, [58,59] the formation of nitrate as a product of the auroral activity (and other ionization stratospheric processes) in the upper atmosphere [60,61] and even the production of nitrate by the X- or γ-rays from supernovae [62] are the processes postulated and discussed during several years to explain the natural formation of the nitrate deposits. The emissions of NO_x (which are between 70 and 90% of anthropogenic origin [63]) and the subsequent oxidation processes are remarkable contributions to the atmospheric nitrate.

Besides SO_4^{2-} and NO_3^- ions, other ions are usually found in aerosols: Na^+, K^+, NH_4^+, Mg^{2+}, Ca^{2+} and Cl^-, among others. There are also several reports of metals in the atmospheric environment; iron, manganese, copper and zinc (among others) have been found in atmospheric water samples (cloudwater, wet and bulk precipitation) as well as in atmospheric particulate matter (PM_{10}, $PM_{2.5-10}$ and $PM_{2.5}$). [64-72] The atmospheric occurrence of copper and zinc usually is attributed fundamentally to anthropogenic sources, while iron and manganese (sometimes) have both natural and anthropogenic origin. Zn-rich particles have been found in atmospheric particulate matter sampled in urban areas of China influenced by mining, zinc industries as well as steel production and coal combustion. [71,72] Most of the copper is emitted to the atmosphere by activities including iron and steel manufacturing, nonferrous metal production and fuel combustion, but there are also some contributions from soil, vegetation and sea salt spray. [73] The occurrence of both copper and zinc in cloudwater and atmospheric particles has also been linked to the automobile traffic. [67,74] Iron and manganese in atmosphere can be attributed to resuspended road dust, mechanical wear in road transport and combustion, [66] and also the long-range wind-driven transport of particles (e.g., particles coming from the Saharan desert).

However, there are additional sources of metal emissions; Grassian [75] proposed that nanodust (nanoparticles) generated by the nanomaterial industry may be a source of

metals to the atmospheric environment, since ~50% of the consumer products composed of nanomaterials contain metals. It has been found that the use of organometallic gasoline additives containing Fe and Mn, such as ferrocene, FeC_5H_5 and methylcyclopentadienyl manganese tricarbonyl, $CH_3C_5H_4Mn(CO)_3$, generates the emission of iron and manganese nanoparticles. [76] Adachi and Buseck [77] confirmed that nanoparticles containing transition or post-transition metals are common in polluted air, with consequent effects on the population health.

The presence of metals in atmosphere has also effects on the atmospheric chemistry; some studies revealed that soluble transition metal ions interfere with photochemical reactions in aqueous phase. [78] Matthijsen et al. [79] studied the influence of dissolved Fe and Cu on the in-cloud ozone using cloud model experiments for different photochemical scenarios; they found significant variations in the rate of ozone loss (higher for polluted continental conditions and lower for average continental conditions) and an increased production of $HO^\bullet$, which also boosts the oxidation of organic compounds (e.g., formaldehyde, etc.). Researchers studied with special interest the role of soluble Fe and Cu in S(IV) oxidation processes and a link between iron and sulfur cycles has been suggested. [56,80,81]

It is clear that not only the mass and size distribution of aerosols, but also their composition are important in environmental studies. Depending on the state of the sample (liquid or solid) and the target analytes, different analytic methods and techniques are used to characterize atmospheric aerosols. Gas chromatography-mass spectrometry (GC-MS) [82,83] and high-performance liquid chromatography (HPLC) [84] have been successfully applied to analyze organic species such as the so called humic-like substances (HULIS) and levoglucosan (a typical sugar produced by forest fires). Moreover, the remarkable development of mass spectrometry techniques allows not only the chemical characterization of organic and inorganic aerosols (on-line and off-line), [85-87] but also the study of the aerosol morphology. [88]

Many researchers reported analytical data related to the inorganic composition of atmospheric particulate matter, atmospheric liquid water (rainwater, cloudwater and fog) and snow, collected at different locations. [64-67,73,74,80,83,89-99] The most common methods used in earlier works to analyze atmospheric liquid samples are ion chromatography, atomic absorption spectrometry, colorimetric methods (e.g., Fe(II) by formation of the Fe(II)-ferrozine complex), and electrochemical methods. [64,68,69,73,74,89-91,95,96] For solids, depending on the research goals, the inorganic chemical composition can be elucidated for either all particles *en masse* or individual particles. [100]

Several studies on atmospheric particulate matter can be found in scientific literature, in which the analysis of particles *en masse* (which implies the analysis of a mixture of particles) was reported. According to this type of analysis, the solid material has to be dissolved first in order to identify and quantify the components using a specific analytical technique such as ion chromatography, atomic absorption spectroscopy (AAS) and different types[6] of inductively coupled plasma (ICP). [65-67,83,97,98,101-103] These techniques provide information on the elemental composition of the sample.

---

[6] Inductively Coupled Plasma-Atomic Emission Spectroscopy (ICP-AES), Inductively Coupled Plasma-Mass Spectrometry (ICP-MS) and Inductively Coupled Plasma-Optical Emission Spectrometry (ICP-OES).

Most of the recent works employ the analysis of individual particles, since this information can provide clues on the origin of the particulate matter. The most important analytical techniques used to study individual particles are scanning electron microscopy (SEM), transmission electron microscopy (TEM), energy-dispersive X-ray spectrometry (EDX), X-ray fluorescence (XRF) and selected area electron diffraction (SAED). [92,93,101,104] Both SEM and TEM produce black and white images of the material on the scale of tens of nanometer, which provide valuable morphologic information. On the other hand, EDX and XRF provide information regarding the elemental composition of the sample. Usually the imaging and elemental analysis techniques are combined in order to identify the chemical form of the solid phases, e.g., SEM-EDX. [71,72,99,105] SAED is a technique that can be performed inside a transmission electron and can provide crystallographic information. These techniques can be supported by X-ray powder diffractometry (XRD), since crystalline materials have characteristic peaks in the XRD pattern.

Except XRD, the mentioned techniques fundamentally provide elemental composition data and morphologic information which are only indicative of inorganic salts in atmospheric particles. Moreover, a great disadvantage of SEM and TEM is the necessity to operate in vacuum, as many hydrated inorganic salts can dehydrate under this condition. It was also reported that some inorganic inclusions in organic particles were beam sensitive even at low-intensity electron beams. [92]

An appropriate analytical technique should provide reliable results and its selection requires the knowledge of the analytes. In this case, the goal is to know the chemical form in which the elements can be found in the atmospheric particles in view of their possible modification during the atmospheric transport, therefore the associated atmospheric processes should be known. Since their emission or formation, particles in atmosphere suffer coagulation[7] and/or coalescence[8] processes (growing of the particles), undergo condensation-evaporation cycles (according to estimations, around ten condensation-evaporation cycles [106]) and participate direct or indirectly in chemical reactions, resulting in changes in the composition. The interaction of particles with atmospheric water - process known as "cloud processing" - implies not only the condensation-evaporation of water on the particle, but also the dissolution of the soluble material. Moreover, the aerosol solution generated by the condensation of atmospheric water on the particle can reach extreme low pH values due to the uptake of strong acids (especially H_2SO_4), [107] therefore, the solubility of metals is highly enhanced. For instance, the increase in soluble iron due to cloud processing was evaluated and confirmed in the past by different laboratory experiments. [108-110]

It is not difficult to imagine that the atmospheric processes related to the particle growth, condensation-evaporation cycles and the exposition to solutions with low pH values (above polluted areas), modify both the average size and the composition of the atmospheric particles. Some authors, generally using X-ray powder diffractometry, reported in atmospheric particle samples the occurrence of minerals such as $Na_2Mg(SO_4)_2 \cdot 4H_2O$ (bloedite), $(NH_4)_2Mg(SO_4)_2 \cdot 6H_2O$ (boussingaultite), $(NH_4)_2Ca(SO_4)_2 \cdot H_2O$ (koktaite), $(NH_4)_2Fe(SO_4)_2 \cdot 6H_2O$ (mohrite), $(NH_4)_2SO_4 \cdot 3NH_4NO_3$, $Na_3(NO_3)(SO_4) \cdot H_2O$ (darapskite), among others. [101,111-115] While minerals in atmospheric particles partly originate from blown dust, the

---

[7] Coagulation is the process by which two particles combine to form one.

[8] Coalescence is the process by which two or more droplets merge to form a single droplet.

atmospheric formation should be considered as an important contribution. The possible origin of these (and other similar) minerals should be evaluated in terms of the atmospheric processes.

Raman spectroscopy is acquiring growing importance in mineral analysis; it has already been used to identify the composition of mineral deposits in the study of geologic processes [116] and several investigations reported the suitability of this technique for chemical characterization of atmospheric particles. [117-125] With Raman micro-spectroscopy, which is a non-destructive analytical technique, it is possible to identify different minerals by their characteristic signals. The different hydrated states of inorganic salts, and even the phase in which the salt crystallizes, can be identified by Raman signals, since the Raman spectrum is determined by the crystal structure.

Raman micro-spectroscopy can measure micrometer sized particles in the micrometric range in a relative short time, therefore, this technique is proposed in this work to study inorganic salts in the atmosphere.

1.3   Own research results

The subjects referred to the atmospheric particulate matter are complex, due to their implications on human health, atmospheric chemistry and climate. In order to understand these implications, the atmospheric particulate matter must be studied from the point of view of its concentration, composition and reactivity. A primordial stage in the study of every pollutant is the understanding of the factors and conditions linked to the origin and removal (sink) of the pollutant.

Considering that water is thought to play a fundamental role in atmospheric processes, the atmospheric formation of several salts is postulated. The crystallization in atmosphere of the mineral ungemachite and many other mixed salts including also salts of metals like iron, manganese, copper and zinc, is proposed. It is thought that the condensation-evaporation cycles have a strong influence in the modification of the particles during the transport (aging), resulting in the "rearrangement" of the ions in different salts than those originally emitted. The evaporation of solution droplets containing specific ions resulting in the crystallization of mixed salts (e.g., bloedite, darapskite, koktaite, etc.) and the formation of salt mixtures seem to confirm the preponderant role of water in the modification of the atmospheric particles. Moreover, the reactivity of certain alkaline minerals with an important aerosol component $((NH_4)_2SO_4)$ in contact with humid air shows that water is a key factor to trigger chemical reactions in solid particles. All of these aspects were studied and evaluated using Raman spectroscopy as the main analytical tool. Therefore, the bands in the Raman spectra of the pure substances were assigned and certain features discussed.

In the following subsections, details concerning the experiments and results of the mentioned aspects are presented.

1.3.1   Ungemachite: Vibrational spectra and its possible atmospheric occurrence

Synthetic ungemachite was prepared for the first time by crystallization from an acidic solution containing stoichiometrical proportions of the constituent ions, as described in subsection 2.1 in [PV4].

Ungemachite, $K_3Na_8Fe(SO_4)_6(NO_3)_2 \cdot 6H_2O$ is a rare mineral, which has been found and reported for the first time by Peacock and Bandy. [126,127] As expected for minerals containing nitrate ions (NO_3^-), the first samples of this mineral were taken from an extremely arid region (Chuquicamata, Chile).

Since it is known that ungemachite crystallizes in the trigonal system with the space group $R\bar{3}$ and three molecules in the unit cell, [128] the factor group analysis using the correlation method [129] was possible (Table 1 and Figure 2 in [PV4]). The Raman and infrared spectra were recorded (Figure 3 in [PV4]) and the assignments were proposed for the most important bands; the four strongest bands in the Raman spectrum belong to the NO_3^- symmetric stretching (ν_1) at 1047 cm^{-1}, and the SO_4^{2-} symmetric stretching (ν_1) at 1035, 1011 and 952 cm^{-1}. The infrared spectrum shows strong bands for the H_2O stretching modes at 3422 cm^{-1}, NO_3^- asymmetric stretching (ν_3) at 1402 and 1384 cm^{-1}, SO_4^{2-} asymmetric stretching (ν_3) at 1215, 1195, 1166 and 1131 cm^{-1}, NO_3^- symmetric stretching (ν_1) at 1046 cm^{-1}, and SO_4^{2-} symmetric stretching (ν_1) at 964 cm^{-1}.

Remarkable is the fact that the H_2O bending mode appears at unusually high values, 1711 and 1663 cm^{-1} in the Raman spectrum and at 1769, 1698 and 1635 cm^{-1} in the infrared spectrum.

However, there is a structural characteristic of ungemachite that can be observed in both the Raman and infrared spectra; Fe^{3+} ions are octahedrally coordinated by six oxygen atoms and all six Fe-O bonds are equivalent, [128] therefore the resulting FeO_6 octahedron belongs to the point group symmetry O_h. Six fundamental modes are observed under an O_h symmetry: ν_1 (A_{1g}), ν_2 (E_g), ν_3 (F_{1u}), ν_4 (F_{1u}), ν_5 (F_{2g}), and ν_6 (F_{2u}), where ν_1, ν_2 and ν_5 are Raman active, ν_3 and ν_4 are infrared active, and ν_6 is inactive in both infrared and Raman spectra. [130] In order to assign the bands to these modes (when they are intense enough to be observed), reported spectroscopic data of the compounds known as "alums", $Me^IMe^{III}(SO_4)_2 \cdot 12H_2O$ (where Me^I is a monovalent and Me^{III} is a trivalent metal), [130-135] were used, since they contain a $Me^{III}O_6$ octahedron in their crystal structure. In the Raman spectrum, the band at 534 cm^{-1} was assigned to FeO_6 ν_1, while the bands in the region 400-500 cm^{-1} were assigned to SO_4^{2-} ν_2 + FeO_6 ν_2, as a more distinct differentiation of the modes was impossible. In the infrared spectrum, the band at 511 cm^{-1} was assigned to the FeO_6 ν_3.

As mentioned before, the existence of acidic solutions containing Na^+, K^+, NO_3^-, SO_4^{2-} and Fe^{3+} ions and their subsequent evaporization are the prerequisites for the formation of ungemachite, which can be achieved in atmosphere, since all those chemical species are usually present in the tropospheric environment. Although the origin is variable, the sea salt is considered the most important source of Na^+, while the occurrence of K^+ ions is usually linked to biomass burning. Most of the emitted materials containing Na^+ and K^+ ions are soluble salts such as NaCl and KCl, which can react during the atmospheric transport to form other salts. [93,136] Both NO_3^- and SO_4^{2-} ions are products of atmospheric oxidation processes; their abundance depends on the emission of adequate precursors, which are mostly of anthropogenic origin.

Low pH values are expected in atmospheric water, especially above polluted areas. For atmospheric study purposes, it is considered that the neutral pH value is 5.6, [43,44] but the uptake of H_2SO_4 and HNO_3 causes a drastic reduction in the pH value, so that a pH value of 4.7 would represent normal atmospheric conditions, [137-141] although under certain circumstances the pH of the aerosol solution could even be lower than 1.0. [107]

It seems that the limiting factor of the atmospheric formation of ungemachite could be an insufficient availability of Fe^{3+} ion. The occurrence of iron in atmosphere as well as its transport has been intensively studied in the past, [138,141,142] because iron is an important micronutrient which restricts the growth of phytoplankton [67]. It is recognized that one of the most important pathways for iron to enter in the ocean is the deposition of atmospheric iron transported from continental areas. [107] In addition, aerosol materials originated from biomass burning [143] and fuel combustion, [144] which can be considered fundamentally anthropogenic, are important contributors of atmospheric iron. As explained in [PV4] (subsection 3.2), most researchers agree that the anthropogenic aerosols contribute more soluble iron than the Fe-rich dust emitted from continental areas, but in both cases the solubility of iron increases substantially with the low pH values expected for aerosol solutions.

On the other hand, iron is found in atmosphere as Fe(III) and Fe(II). Some reduction processes from Fe(III) to Fe(II) were suggested in the past [145,146] and even linked to the sulfur cycle. [56] When analyzing dust particle emissions rich in Fe(III) oxides (as usually is the case) transported over long distances, the determination of the

Fe(II)/Fe(III) ratio can provide information on how much time this material was exposed to cloud processing. [56]

Taking into account the mentioned aspects in this subsection, the atmospheric formation of ungemachite is plausible, because the conditions required to crystallize this mineral can be found in the atmospheric environment. Moreover, since ungemachite is a Fe(III) mineral, its presence in atmospheric particles may be an indication of a short-time cloud processing in a polluted atmospheric environment (rich in strong acids) with sea salt and potassium (biomass burning) contributions. The vibrational spectra of ungemachite presented in [PV4] can be used in the future for the analysis of atmospheric materials, mineral deposits and even in planetary exploration.

1.3.2 Salt mixtures and mixed salts in atmospheric particulate matter

Aspects concerning to the origin of salt mixtures and mixed salts in atmospheric particulate matter and their significance are described and discussed in [PV1], [PV2] and [PV5].

As mentioned in Section 1.2, a great variety of compounds can be found in atmospheric particulate matter. Since Na^+, K^+, NH_4^+, Ca^{2+}, Mg^{2+}, SO_4^{2-}, NO_3^- and others are common ions present in atmospheric particles; their interaction with water results in the formation of solutions. When a solution containing many ions evaporates, the salts precipitate (crystallize) according to the relative concentration of the ions; several model studies were published on this topic, in order to predict the precipitation of salts, especially from seawater. [147-152]

Raman spectroscopy is the analytical method proposed to identify the salts expected to form and appear in atmosphere, therefore, the Raman spectra of these salts must be known and the bands assigned. Since the atmosphere contains a great variety of materials, the formation of salt mixtures can be expected, although the formation of mixed salts as the product of recombination of ions should not be ruled out.

The formation of a salt mixture was observed when solutions containing $NaNO_3$ and KNO_3 were evaporated under room conditions (20°C and ~50% relative humidity), as described in [PV2]. A droplet containing a saturated solution of $NaNO_3$ and KNO_3 in an equimolar ratio and placed on a microscope slide was vaporized in contact with ambient air. The Raman spectrum of the first crystal occurring in the solution was recorded and the following spectra were obtained successively during the water vaporization process until the droplet was dry (Figure 1 in [PV2]). As expected according to the solubility of the salts, KNO_3 crystallized before $NaNO_3$, but the Raman spectrum at t = 0 s (this means when the first crystal appeared) showed features of KNO_3 in phase III (high temperature phase) with the strongest band at 1050 cm^{-1}, rather than the stable phase at room temperature, phase II. Only when enough water was evaporated and the crystal was exposed to air, bands of phase II with the strongest band at 1047 cm^{-1}, were observed. Xu and Schweiger [153] reported a similar phase transition for Na_2SO_4, which crystallizes from a saturated solution in phase III (high temperature phase) and transforms to phase V which is stable at room temperature. The solid resulting after the total evaporation of water was a mixture of the stable phases of $NaNO_3$ and KNO_3, both in phase II. In this case, a salt mixture of $NaNO_3$ and KNO_3 was observed; both salts crystallized independently of each other, maintaining their own crystal properties as space group, unit cell dimensions, etc., and therefore the resulting Raman spectrum of

the mixture looks like the sum of the individual Raman spectra of the constituent salts. If a similar evaporating process takes place in aerosol droplets, the resulting particles would form an internal mixture. The crystallization from a solution of KNO_3 at room temperature in phase III instead of phase V, reported for the first time in [PV2], is not a minor point, since the crystal structure of a solid can affect the rate of reactions in which this solid participates. For instance, Takahashi and coworkers [154][9] reported differences in the rate of singlet oxygen ($^1O_2$) formation from the irradiation of anatase and rutile, both polymorphs of TiO_2. Many reports of heterogeneous reactions taking place on aerosols were published in the past; the formation of SO_4^{2-} by heterogeneous reaction of SO_2 on mineral particles, [155] and the loss of ozone on carbon soot aerosol [156] are examples of this kind of reactions. Although KNO_3 in phase III can only be stable in contact with the saturated solution, atmospheric heterogeneous reactions involving this species cannot be ruled out.

The formation of mixed salts by evaporation processes should also be considered. When a solution containing $NaNO_3$ and Na_2SO_4 evaporates at room temperature, the Raman spectrum of the resulting solid shows not only bands belonging to $NaNO_3$ and Na_2SO_4, but also of a third salt. The Raman spectra of individual particles of the milled residue obtained from solutions containing $NaNO_3$ and Na_2SO_4 at the end of the total vaporization process usually showed two strong bands at 1060 and 993 cm^{-1}. These values are different from the characteristic values observed for Na_2SO_4 (SO_4^{2-} ν_1 at 989 cm^{-1}) and $NaNO_3$ (NO_3^- ν_1 at 1065 cm^{-1}), but they are equal to the values observed in the unpolarized spectra of synthetic $Na_3(NO_3)(SO_4) \cdot H_2O$[10], also known by its mineral name darapskite. Since it is known that darapskite crystallizes in the monoclinic system with the space group *P2₁/m* and that it has two molecules in the unit cell, [158] it was possible to apply the factor group analysis using the correlation method [129] (Table 1 in [PV2]). Considering these results and the observed bands in the polarized Raman spectra as well as in the infrared spectrum, the assignments for the most important bands (related to NO_3^- and SO_4^{2-} ions) were proposed (Table 2 in [PV2]). These data are valuable for Raman-based analytical methods when applied to the analysis of atmospheric particulate matter.

An earlier observation of darapskite in atmospheric particles was attributed to acid (H_2SO_4 and HNO_3) attack upon marine NaCl. [114] It is accepted that NaCl reacts with H_2SO_4 and HNO_3 to form Na_2SO_4 and $NaNO_3$, respectively, [23,93,112,159] but it is not clear if there is a direct process in which the action on NaCl of H_2SO_4 and HNO_3 together, as suggested by Harrison and Sturges, generates darapskite. It seems that simple dissolution-crystallization processes - due to condensation and evaporation of water - on earlier-formed Na_2SO_4 and $NaNO_3$ can explain the formation of darapskite in the atmosphere. Regardless of whether Na_2SO_4 and $NaNO_3$ are formed together in the same particle or whether they are formed by separate processes and bind together by coagulation processes, the condensation of water on this particle triggers the dissolution of the salts and the subsequent evaporation results in the crystallization of variable amounts of darapskite, depending on the ion concentration and the temperature.

Sulfate mixed salts containing sodium and magnesium are another important case of study. Both sodium and magnesium represent the most abundant cations in sea water

---

[9] Study on the $^1O_2$ formation for oral bacterial disinfection.

[10] $Na_3(NO_3)(SO_4) \cdot H_2O$ (darapskite) was crystallized from a solution containing $NaNO_3$ and Na_2SO_4 in the same proportion as previously reported. [157]

and their atmospheric occurrence is fundamentally attributed to oceanic contributions. [160] When a solution containing $MgSO_4$ and Na_2SO_4 evaporates, four mixed salts can be formed: $Na_2Mg(SO_4)_2 \cdot 4H_2O$ (bloedite), $Na_2Mg(SO_4)_2 \cdot 5H_2O$ (konyaite), $Na_6Mg(SO_4)_4$ (vanthoffite), and $Na_{12}Mg_7(SO_4)_{13} \cdot 15H_2O$ (loeweite). Among these mixed salts, only bloedite was found in atmospheric particulate matter, [101,115,125] therefore some questions arise: Can other mixed salts of magnesium and sodium be found in atmospheric particulate matter? If so, what conditions are necessary? Furthermore, knowing that bloedite was observed in atmospheric particles, how does it form? To answer these questions, a series of crystallization experiments was performed within droplets, as described in [PV1] (Section II).

According to earlier studies, the crystallization of $Na_2Mg(SO_4)_2 \cdot 4H_2O$ (bloedite) on saturation of equal molar solutions of $MgSO_4$ and Na_2SO_4 is expected. [161,162] The partial evaporation of a droplet containing $MgSO_4$ and Na_2SO_4 in an equimolar ratio resulted in the formation of small crystals with sizes ~10 μm, which were identified as bloedite. Crystals with the same characteristics were also observed, when solutions containing $MgSO_4$ and Na_2SO_4 in molar ratios of 1:2, 1:3, 2:1 and 3:1 were partially evaporated. Accordingly, crystallization of anhydrous Na_2SO_4 (thenardite) was observed when evaporating partially solutions with an excess of Na_2SO_4 respect to $MgSO_4$ (molar ratios of 1:2 and 1:3). Figure 3 in [PV1] shows the bloedite crystals and a circular crystal formation identified as thenardite within a solution droplet with a molar ratio of 1:2, as well as the Raman spectra of these crystals. No other salts were observed until complete water elimination and it was at this point when the abrupt precipitation of different salts was observed in all solution droplets, leading to the formation of salt mixtures. The Raman spectra of these salt mixtures showed additional strong bands at 1039 and 1003 cm^{-1}, which could not be explained considering only Na_2SO_4, bloedite and different hydration salts of $MgSO_4$. In order to identify the components present in these mixtures, konyaite, vanthoffite and loeweite were synthesized and the Raman spectra recorded. Figure 2 in [PV1] shows the Raman spectra of the four mixed salts of the $MgSO_4$-Na_2SO_4 system. The band observed at 1039 cm^{-1} belongs to loeweite, while the band at 1003 cm^{-1} belongs to konyaite. Considering the spectroscopic data of the pure salts, it is possible to summarize that the resulting salt mixtures contained variable proportions of thenardite, $MgSO_4 \cdot 6H_2O$ (hexahydrite), bloedite, konyaite and loeweite. In no case vanthoffite was detected because, probably, its crystallization requires higher temperatures.

Konyaite, bloedite and loeweite can be produced by evaporation of solutions at tropospheric temperatures, but the specific characteristics of the condensation-evaporation cycles taking place in atmosphere seem to favor the formation of konyaite. Konyaite has been found in cave environments, [163] marine deposits, [164] and saline soils. [165-167] Keller and coworkers [168] reported the persistence of konyaite for long periods of time in dry efflorescences and that it was metastable in contact with saturated solutions containing Na^+, Mg^{2+} and SO_4^{2-} ions. They also postulated that konyaite precipitates before the nucleation of bloedite. This seems to be highly unlikely, since the results of the evaporation experiments in droplets clearly showed that only bloedite and thenardite (in some cases) were present in partially evaporated droplets. Friedel [169] observed that the transformation from $Na_2Mg(SO_4)_2 \cdot 5H_2O$ to $Na_2Mg(SO_4)_2 \cdot 4H_2O$ in a saturated solution occurs in a matter of days. As a consequence, if konyaite was formed in an earlier stage, it had to be detected together with bloedite within the solution; however, konyaite was observed only after all water was evaporated from the droplet. Therefore, the formation of konyaite may be

attributed to a fast evaporation process (the final evaporative stage in the mentioned droplet experiments), as suggested also by Shayan and Lancucki. [164] With all these aspects in mind, it is possible to conclude that konyaite is the main mixed salt produced in atmosphere when the aerosol solutions containing Na^+, Mg^{2+} and SO_4^{2-} ions evaporate. Nevertheless, special conditions including slow evaporation processes of aerosol solutions, further condensation-evaporation cycles taking place on early-formed konyaite particles or the exposition of konyaite particles to dry conditions (low relative humidities), could result in the formation of variable amounts of bloedite with (internally mixed) or without konyaite. Additionally, the formation of loeweite by an eventual further reaction between bloedite and konyaite, as it was considered for soil systems by Keller [168], should not be completely ruled out.

The combined effect of the great mineralogical variety on the terrestrial crust susceptible to erosion and wind-transport, the release into the atmosphere of oceanic materials and the anthropogenic emissions result in primary particles of different composition but with the potential to combine during aging processes. As mentioned before, aging processes are strongly influenced by water and can modify the composition of the atmospheric particles. Moreover, the low pH values of aerosol solutions can favor the dissolution of metals occurring in mineral dust, particles from mechanical wear, fly ash and other specific industrial emissions, resulting later in the precipitation of simple and mixed salts. Many salts can be produced by the combined effect of coagulation, coalescence, chemical reactions and condensation-evaporation cycles, and the detection of these processes can provide valuable information on pollution sources and atmospheric mechanisms. Taking into account the atmospheric processes mentioned before as well as the wind-transport of crust material, the Raman spectra of forty-five atmospheric salts including sulfates, nitrates, carbonates, bicarbonates, sulfate-carbonate and sulfate-nitrates were recorded and the bands assigned ([PV5]). The characteristic bands observed in the Raman spectra of these salts not only allow the appropriate identification of the salts, but also the assessment of similarities/differences in the crystal structure of the salts.

The atmospheric formation of sulfates containing iron, manganese, copper and zinc was postulated ([PV5]). The considered salts were: $FeSO_4 \cdot H_2O$, $FeSO_4 \cdot 4H_2O$, $FeSO_4 \cdot 7H_2O$, $MnSO_4 \cdot H_2O$, $ZnSO_4 \cdot 7H_2O$, $CuSO_4 \cdot 5H_2O$, $(NH_4)_2Fe(SO_4)_2 \cdot 6H_2O$, $(NH_4)Fe(SO_4)_2 \cdot 12H_2O$, $(NH_4)_2Mn(SO_4)_2 \cdot 6H_2O$, $(NH_4)_2Zn(SO_4)_2 \cdot 6H_2O$, $(NH_4)_2Cu(SO_4)_2 \cdot 6H_2O$, $K_2Zn(SO_4)_2 \cdot 6H_2O$, $K_2Cu(SO_4)_2 \cdot 6H_2O$, $Na_2Mn(SO_4)_2 \cdot 2H_2O$, $Na_2Zn(SO_4)_2 \cdot 4H_2O$ and $Na_2Cu(SO_4)_2 \cdot 2H_2O$. All these salts crystallize at 20°C from the evaporation of aqueous solutions containing the appropriate ions. Iron salts require also acidic pH values, which can be found in aerosol solutions. The occurrence of these salts in atmospheric particles can be used as an indicator not only of the emission of these metals, but also provide information on the relative solubility of the emitted metal-rich material and the "history" of the particulate matter.

The solubility of metals is frequently correlated with their bioavailability; [170] for instance, the soluble fraction of iron in mineral dust and other suspended particulate materials has been a subject of intense study, because iron is considered a critical micronutrient for the primary productivity over the ocean. [171,172] Mn(II), Zn(II), Cu(I), Cu(II), Fe(II) and Fe(III) are the soluble metal forms that can be expected, each one with specific characteristics. The occurrence of Mn in rainwater was studied by Deutsch et al. [90] and Willey et al. [95] and they observed that only Mn(II) can be found in a dissolved state, while the insoluble phase is related to Mn(IV) as oxide. These authors agree in the conclusion that Mn(III) is unstable under atmospheric

conditions and that only a very short-lived occurrence during the oxidation of S(IV) can be expected. Both Cu(I) and Cu(II) were detected in fog and rain water, [89,73] but Cu(II) seems to be the predominant form. Fe is considered ubiquitous in atmosphere, [146] as it was found in atmospheric aqueous samples (fog, cloud and rain water) as both Fe(II) and Fe(III), in variable ratios. [64,91,96,171]

The history of the particulate matter, i.e. the processes suffered by the material and the atmospheric conditions during transport, can also be deduced from the chemical form in which the metal is found in the particles. Considering the redox reactions of iron taking place in atmosphere and their relation to the sulfur cycle, [56] three iron (II) sulfate salts[11] can be expected in atmospheric particles: $FeSO_4 \cdot 7H_2O$ (melanterite), $FeSO_4 \cdot 4H_2O$ (rozenite), and $FeSO_4 \cdot H_2O$ (szomolnokite). $FeSO_4 \cdot 7H_2O$ crystallizes from slightly acidic solutions containing Fe^{2+} and SO_4^{2-} ions, while $FeSO_4 \cdot 4H_2O$ and $FeSO_4 \cdot H_2O$ can result from dehydration-hydration processes at reasonable tropospheric conditions. The exposition of $FeSO_4 \cdot 7H_2O$ at room temperature to dry air or to strong acidic solutions results in the elimination of six H_2O molecules. $FeSO_4 \cdot 4H_2O$ can be obtained by either dehydration of $FeSO_4 \cdot 7H_2O$ or hydration of $FeSO_4 \cdot H_2O$, since rozenite is the stable form of iron (II) sulfate at normal temperatures and humidities. [173] These three iron (II) sulfate salts can provide information on particle-affecting processes, because if $FeSO_4 \cdot 7H_2O$ is found, the particle (produced by crystallization from a solution) is "young" and/or maintained in this chemical form by a high relative humidity. If $FeSO_4 \cdot H_2O$ and $FeSO_4 \cdot 4H_2O$ are observed, their occurrence could be explained in terms of an atmospheric aging, i.e. due to variations in atmospheric conditions promoting the mentioned dehydration-hydration processes.

As described in this subsection, the crystallization process of certain salts due to the evaporation of solution droplets was observed using Raman micro-spectroscopy. This kind of experiments showed that mixed salts and salt mixtures in atmospheric particulate matter can be the products of the evaporation of aerosol solutions. Depending on regional conditions as well as the influence of specific emissions, many simple and mixed salts can be formed in the atmosphere, some of which are considered in [PV5]. The Raman spectroscopic information of the salts depicted in [PV5] can be used in the study of atmospheric particulate matter not only for the chemical characterization of materials, but also to study atmospheric processes and the influence of human activities on the air quality.

1.3.3 Calcium mixed salts in atmosphere

Aspects concerning to the origin of four calcium mixed salts in atmospheric particulate matter are described and discussed in [PV3].

Different sources contribute calcium to the atmosphere. Wind-blown dust [5] and marine biogenic material (coccoliths) [101] introduce $CaCO_3$ (calcite) into the atmosphere. There are also reports of calcium emissions from continental areas in the form of calcium sulfate. [159] The evaporation of sea-spray, cloud and rain droplets can result in the crystallization of $CaSO_4 \cdot 2H_2O$ (gypsum). [174] The anthropogenic sources

---

[11] Jambor and Traill [173] reported that the pentahydrate salt of iron (II) sulfate (siderotil) is produced by dehydration instead of $FeSO_4 \cdot 4H_2O$ when impurities of Cu^{2+} ions substitute some Fe^{2+} ions in the $FeSO_4 \cdot 7H_2O$ structure, but our attempts to produce siderotil by dehydration (short-time exposition of $FeSO_4 \cdot 7H_2O$ to temperatures of 30-40°C) were unsuccessful.

are also important; gypsum emission is generally associated to combustion processes, while calcite is present in dust from metallurgical, chemical and cement industries. [175]

It is clear that the originally emitted calcium species are modified during the atmospheric transport, and then calcium is found in other chemical forms (simple and mixed salts). Some works suggest that calcite can react in atmosphere with $(NH_4)_2SO_4$, H_2SO_4 and gaseous HNO_3 to produce $(NH_4)_2Ca(SO_4) \cdot H_2O$ [5], $CaSO_4$ ($CaSO_4 \cdot 2H_2O$), [105] and $Ca(NO_3)_2$, [176] respectively.

The calcium mixed salts $Na_2Ca(SO_4)_2$ (glauberite), $K_2Ca(SO_4)_2 \cdot H_2O$ (syngenite), $(NH_4)_2Ca(SO_4)_2 \cdot H_2O$ (koktaite), and $K_2Ca_2Mg(SO_4)_4 \cdot 2H_2O$ (polyhalite) have been reported in atmospheric particles by many studies, [71,72,104,111,177] but only a few attempts were made to explain their origin.

Syngenite, koktaite, glauberite and polyhalite were synthesized and the Raman spectra recorded. The Raman spectra of these four calcium mixed salts are shown in Figure 1 in [PV3], while the proposed band assignments are summarized in table 1 in [PV3]. Since the crystal structure as well as the number of molecules in the unit cell of syngenite, koktaite, glauberite and polyhalite are known, [178-182] the factor group analysis using the correlation method [129] could be applied for the four mixed salts. The infrared spectra were recorded only for syngenite and koktaite, because for glauberite and polyhalite small amounts of gypsum were detected in the bulk substance (using X-ray diffractometry)[12], which probably formed during the separation of these compounds from the mother liquor.

The strongest band in the Raman spectra of the four calcium mixed salts belongs to the SO_4^{2-} symmetric stretching (ν_1). The Raman spectra depend on the structural characteristics of the mixed salts, therefore two bands belonging to the SO_4^{2-} ν_1 were observed for syngenite (at 1003 and 979 cm^{-1}), koktaite (at 996 and 980 cm^{-1}) and polyhalite (at 1014 and 987 cm^{-1}), while only one band was observed for glauberite (at 998 cm^{-1}). On comparison of the spectra (Figure 1 in [PV3]) the similarities between the spectra of syngenite and koktaite are evident; the number of bands observed for each SO_4^{2-} mode is equal and only small differences in the wavenumbers of the SO_4^{2-} bands can be observed. The Raman spectra of these mixed salts also suggest the structural relationships among them. Despite these similarities, the unambiguous differentiation between these mixed salts is possible when using the broad bands of NH_4^+ (ν_2 and ν_4), as these are absent in the spectra of syngenite. As expected from the crystal structure of glauberite and polyhalite, the Raman spectra of these mixed salts are clearly different compared to the spectra of syngenite and koktaite. These data are valuable for Raman-based analytical methods when applied to the analysis of atmospheric particulate matter.

Considering that water plays a fundamental role in atmospheric processes, experiments of crystallization within droplets, as described in [PV3] (Subsection 2.2), were performed.

---

[12] The pellet necessary to record the infrared spectrum is prepared with the bulk substance, so if this material contains even small amounts of an impurity, the resulting spectrum will not be of the pure substance. This is the reason why the infrared spectra of glauberite and polyhalite were not included. On the other hand, the Raman spectra of synthetic salts were recorded using micro Raman spectroscopy, which allows to record the Raman spectrum of individual micrometric particles (or microcrystals), therefore the interference of eventual impurities is avoided.

A droplet of a saturated solution containing $CaSO_4$ and K_2SO_4 in molar ratio 1:50 was evaporated under room conditions (20°C and ~50% relative humidity). The Raman spectrum of the first crystal occurring in the solution was recorded and the following spectra were obtained during the evaporation process until the droplet was dry. Figure 2 in [PV3] shows microphotographs of the crystal formation and the Raman spectra at different times. The first crystal occurring within the droplet was identified as syngenite and the total evaporation of water results in the crystallization of the remaining K_2SO_4. The Raman spectrum at t = 234 s (dry droplet) indicates that the resulting solid was a mixture of syngenite and K_2SO_4.

Like for the $CaSO_4$-K_2SO_4 system, a droplet of a saturated solution containing $CaSO_4$ and $(NH_4)_2SO_4$ in molar ratio 1:50 was evaporated under room conditions to evaluate the crystallization process. Figure 3 in [PV3] shows microphotographs of the crystal formation and the Raman spectra at different times. The first crystal occurring within the droplet was identified as koktaite and the total evaporation of water results in the crystallization of the remaining $(NH_4)_2SO_4$. The Raman spectrum at t = 210 s (dry droplet) indicates that the resulting solid was a mixture of koktaite and $(NH_4)_2SO_4$.

According to experiments of a recent study [PV6], a reaction in a solid mixture of gypsum and $(NH_4)_2SO_4$ exposed to humid air (70% RH) can take place to produce koktaite. The following reaction is proposed:

$$CaSO_4 \cdot 2H_2O + (NH_4)_2SO_4 \rightarrow (NH_4)_2Ca(SO_4)_2 \cdot H_2O + H_2O \qquad (1)$$

It seems that koktaite can be produced not only by precipitation from aerosol solutions, but also by a reaction of solid material in the presence of humid air. This reaction is reported for the first time in [PV6].

The attempts to crystallize glauberite and polyhalite under room conditions were unsuccessful. Using different concentrations of solutions containing $CaSO_4$ and Na_2SO_4 for experiments of crystallization within droplets, only gypsum or Na_2SO_4 in phase III, but no glauberite were observed. The crystallization of Na_2SO_4 in phase III from solutions containing Na^+ and SO_4^{2-} ions and its relatively high stability at room temperature was earlier reported by Xu and Schweiger. [153] The evaporation of different solutions containing $CaSO_4$, K_2SO_4 and $MgSO_4$ resulted, in the majority of cases, in the crystallization of syngenite, whereas the crystallization of polyhalite was not observed. It was suggested that the crystallization of glauberite requires the presence of NaCl in the solution and/or higher temperatures. [183] A phase diagram for the $MgSO_4$-K_2SO_4-$CaSO_4$ system at 83ºC [184] suggests that a high temperature is also necessary to crystallize polyhalite.

A possible explanation for the occurrence of glauberite and polyhalite in atmospheric particles may be the back-reaction of early-formed minerals. Harvie and co-workers, [185] based on computer calculations, suggested back-reactions of early-formed $CaSO_4$ (anhydrite) or gypsum and glauberite, in order to explain the formation of glauberite and polyhalite. This theory is accepted in geology to explain the origin of certain evaporite deposits, and may also apply to the atmospheric environment.

The crystallization process of calcium mixed salts due to the evaporation of solution droplets was observed using Raman micro-spectroscopy. This kind of experiments showed not only the formation of the mixed salts syngenite and koktaite, but also the formation of salt mixtures. This is the first time experimental evidence is presented of

the formation of koktaite by the interaction of water vapor with a solid mixture containing $CaSO_4 \cdot 2H_2O$ and $(NH_4)_2SO_4$. Since glauberite and polyhalite do not crystallize from solutions at ordinary temperatures, it is reasonable to explain the atmospheric formation of these salts by back-reactions of calcium sulfate. The Raman spectroscopic data of these four calcium mixed salts depicted in [PV3] can be used in the future for the analysis of atmospheric materials, mineral deposits and in planetary exploration.

1.3.4 Reactions of alkaline minerals in solid mixtures exposed to humid air

The reactions between some common alkaline minerals and $(NH_4)_2SO_4$ are presented and discussed in [PV6].

The emission of alkaline minerals into the atmosphere is a fact; some reported cases are the dust emissions from playas[13] in the Mojave Desert (USA) [186] and from the Owens (dry) Lake. [187] Studies concerning alkaline minerals in atmosphere should be performed with respect to their reactivity with other atmospheric components. In order to understand the effects of airborne alkaline particles on human health as well as their weather and climate implications, the atmospheric chemical reactions (intermediate and final products) of these materials should be investigated.

In general, wind-transported particles, depending on their size, can sediment or remain suspended for many days. The suspended material (fine particles) undergoes different atmospheric processes, one of them is the coagulation, which can produce internally mixed particles (each particle is a mixture). The presence of water condensed on particles from air due to hygroscopicity of the solid material, can trigger chemical reactions between the components of the mixture, resulting in modifications of the particles composition and thus their properties.

In order to evaluate the reactivity in certain solid mixtures expected to occur in atmospheric particles, a macroscopic approach was proposed in [PV6]. The reactants, as fine powders, were intimately mixed, exposed to humid air and then the course of the reaction was monitored using Raman spectroscopy. Using this methodology, the reactions of synthetic $Na_2CO_3 \cdot H_2O$ (thermonatrite), $Na_3(HCO_3)(CO_3) \cdot 2H_2O$ (trona) and $Na_6(CO_3)(SO_4)_2$ (burkeite) with $(NH_4)_2SO_4$ were studied.

The experiments showed that when the solid mixtures containing the alkaline salt (thermonatrite, trona or burkeite) and $(NH_4)_2SO_4$ were exposed to ordinary conditions - i.e. temperatures ranging between 21 and 23°C and a relative humidity (RH) of air below 50% - the chemical reaction rate was very slow; the Raman spectra of mixtures exposed to room conditions during 24 h show no or only weak bands of the reaction products. However, when the mixtures were exposed to humid air (~70% RH), there was a remarkable increase in reactivity. The unequivocal sign that reactions were taking place in the mixtures was the release of NH_3, which is a product of acid-base reactions involving CO_3^{2-} and/or HCO_3^-, and NH_4^+ ions. Although the CO_2 release from the

---

[13] The Spanish word "playa" means "beach". The term "playa" is commonly used by scientists to denote the dry lakes. From the point of view of dust emissions, playas are classified as wet and dry (see reference [186]).

reacting mixture was not directly measured, the mentioned acid-base reactions imply its formation.

The Raman spectra acquired at different times from equimolar mixtures of thermonatrite-$(NH_4)_2SO_4$, trona-$(NH_4)_2SO_4$ and burkeite-$(NH_4)_2SO_4$ exposed to humid air at ordinary temperatures (21-23°C) (Figure 1 and 3 in [PV6]) showed the formation of the mixed salt $NH_4NaSO_4 \cdot 2H_2O$ (lecontite). It seems that lecontite and also $NaHCO_3$ are intermediate products in the solid reactions of these three systems, while Na_2SO_4 and NH_4HCO_3 are the final products.

Two phases of anhydrous Na_2SO_4 can remain stable at environmental temperatures: V and III. Phase V is the stable phase at room temperature. Evaporation experiments performed in droplets by Xu and Schweiger [153] at 23°C showed that Na_2SO_4 crystallizes in phase III, and this result was confirmed during the attempts to crystallize glauberite within droplets ([PV3]). It seems that Na_2SO_4 crystallizes in phase III when a fast crystallization process is taking place, e.g., during the room temperature evaporation of droplets. Since Na_2SO_4 in phase III can remain unmodified for long periods, [188] the occurrence of this phase should be considered in studies of atmospheric processes. Using Raman spectroscopy phase III and phase V can be distinguished from each other, since the strongest band in their Raman spectra (SO_4^{2-} symmetric stretching) appear at 996 and 993 cm^{-1}, respectively.

The Raman spectra acquired at different times for the three studied mixtures show the formation of Na_2SO_4 in phase III within the first hours of reaction and the subsequent formation of Na_2SO_4 in phase V (Figure 1 and 3 in [PV6]). This indicates that the phase transition $Na_2SO_4(III) \rightarrow Na_2SO_4(V)$ takes place in the reacting mixtures, probably due to the contact with humid air.

Considering the behavior (emergence and disappearance) of the characteristic bands of carbonate, bicarbonate and sulfate salts, the equations for the chemical reactions taking place in the three studied systems were proposed (Eq. (1)-(8) in [PV6]).

The reactivity in the solid mixtures was attributed to the formation of a "liquid H_2O film" on the solids due to the prolonged exposition to humid air and the hygroscopicity of at least one of the components (see Figure 2 in [PV6]). In this "film", a partial dissolution of the solids and the reactions of CO_3^{2-} and/or HCO_3^- with NH_4^+ take place, resulting in the crystallization of new salts. This can explain the formation of $NaHCO_3$, NH_4HCO_3, lecontite and Na_2SO_4 in the solid mixtures at different times.

The proposed macroscopic approach used to study the chemical reactions taking place between the three alkaline salts (thermonatrite, trona and burkeite) and $(NH_4)_2SO_4$ is appropriate to identify the intermediate and final products, and therefore the equations of the chemical reactions can be proposed. If there is a chemical reaction between two solid compounds present in a single micrometer particle, this reaction takes also place in a macro scale, i.e., a bulk powder mixture. It is clear that kinetic differences between experiments in micro and macro scale can be expected, fundamentally due to differences in surface area and gas diffusion. Since the reaction rate in a bulk solid mixture may be lower than in a single particle, it is more likely to detect intermediate products under this condition. Essentially, this is the reason why the use of bulk powder mixtures was chosen.

Considering that $(NH_4)_2SO_4$ is a well-known anthropogenic salt occurring in atmospheric particulate matter and the coagulation processes favor the formation of solid mixtures in atmospheric particles, the reactions presented in this work (and their

implications on the atmospheric chemistry) should be considered in regions influenced by alkaline dust emissions.

Although the coagulation of particles is a well-known atmospheric process, reactions involving solid mixtures have not been considered in atmospheric models. Since most of the current scientific efforts are focused on the study of changes in the atmospheric composition and their consequences, it is now imperative that future investigations address the reactivity of other solid mixtures of atmospheric importance.

1.4 Conclusions and Outlook

The possible atmospheric formation of the rare mineral ungemachite, $K_3Na_8Fe(SO_4)_6(NO_3)_2 \cdot 6H_2O$, is proposed on the basis of its synthetic preparation, the atmospheric occurrence of the necessary ions, and the low pH values expected in aerosol solutions. The synthetic conditions necessary to crystallize ungemachite are similar to those to be found in the troposphere, therefore the atmospheric formation of ungemachite is plausible. The Raman and infrared spectra of ungemachite were recorded and the bands assigned considering crystal structure details. This information provides valuable data for analytical purposes.

A series of crystallization experiments was performed within solution droplets and the formation of both salt mixtures and mixed salts was observed using micro-Raman spectroscopy. These experiments provide evidence concerning the origin of certain salts observed in the atmospheric particulate matter. The atmospheric occurrence of $Na_2Mg(SO_4)_2 \cdot 4H_2O$ (bloedite), which is a known salt in atmospheric particles, can be attributed to crystallization processes from aerosol solutions. Moreover, the occurrence in the atmosphere of other mixed salts of the $MgSO_4$-Na_2SO_4 system can be expected. In addition, considering the condensation-evaporation cycles in which water plays a fundamental role, the formation of other salts can be postulated.

The crystallization within solution droplets of KNO_3 in phase III (high temperature phase) rather than phase II (stable phase at room temperature) was observed and documented for the first time. It seems that KNO_3 in phase III crystallizes as a consequence of fast evaporation processes and is stable at room temperature only in contact with the saturated solution. The existence of a crystalline phase achieved by fast crystallization of a salt (as occurs in droplets) has importance not only from an analytical point of view, but is also a fact to be considered when investigating further heterogeneous reactions taking place in atmosphere. The possible effect of the crystal structure of crystalline materials in the atmosphere should be evaluated in future works. It cannot be ruled out that the crystal structure has effects on certain catalytic reactions in the atmosphere.

The atmospheric formation of four calcium mixed salts was evaluated using micro-Raman spectroscopy. The results of the crystallization experiments within solution droplets suggest that $K_2Ca(SO_4)_2 \cdot H_2O$ (syngenite) and $(NH_4)_2Ca(SO_4)_2 \cdot H_2O$ (koktaite) can crystallize at ordinary temperatures from solutions containing the necessary ions, while the atmospheric origin of $Na_2Ca(SO_4)_2$ (glauberite) and $K_2Ca_2Mg(SO_4)_4 \cdot 2H_2O$ (polyhalite) probably is linked to more complex processes. Considering the atmospheric conditions in which water interacts with suspended particles, the origin of glauberite and polyhalite in atmospheric particles may be attributed to back-reactions of early-

formed minerals. The Raman spectroscopic data of these salts can be used for Raman-based analytical methods.

The reactions of some solid mixtures containing the alkaline minerals $Na_2CO_3 \cdot H_2O$ (thermonatrite), $Na_3(HCO_3)(CO_3) \cdot 2H_2O$ (trona) and $Na_6(CO_3)(SO_4)_2$ (burkeite) and the typical atmospheric salt $(NH_4)_2SO_4$ were studied using Raman spectroscopy. The equations of the chemical reactions taking place between each of the mentioned alkaline mineral and $(NH_4)_2SO_4$ in the presence of humid air (~70% relative humidity) were proposed. The final products of these reactions are Na_2SO_4 (in phase V) and NH_4HCO_3, while $NaHCO_3$, $(NH_4)NaSO_4 \cdot 2H_2O$ (lecontite) and Na_2SO_4 (in phase III) are intermediate products. Furthermore, the formation of koktaite by the reaction between $CaSO_4 \cdot 2H_2O$ (gypsum) and $(NH_4)_2SO_4$ within a solid mixture exposed to humid air, demonstrates that these reactions in solid state and in contact with humidity are not limited to carbonate minerals. Future works should consider reactions in solid state, because they can be important during the coagulation and transport of atmospheric particles.

In order to get more accurate climate projections, future model studies should consider the condensation-evaporation cycles as well as solid state reactions as important factors in the investigation of changes in the composition and/or properties of atmospheric particulate matter.

Bibliography

[1]   Crutzen P. J. (2002) Geology of mankind. *Nature* **415**, 23.

[2]   Jickells T., Knap A., Church T., Galloway J. and Miller J. (1982) Acid rain on Bermuda. *Nature* **297**, 55-57.

[3]   Nordø J. (1976) Long range transport of air pollutants in Europe and acid precipitation in Norway. *Water Air Soil Poll.* **6**, 199-217.

[4]   Björseth A., Lunde G. and Lindskog A. (1979) Long-range transport of polycyclic aromatic hydrocarbons. *Atmos. Environ.* **13**, 45-53.

[5]   Mori I., Nishikawa M. and Iwasaka Y. (1998) Chemical reaction during the coagulation of ammonium sulphate and mineral particles in the atmosphere. *Sci. Total Environ.* **224**, 87-91.

[6]   Querol X., Alastuey A., Rodríguez S., Viana M. M., Artíñano B., Salvador P., Mantilla E., García do Santos S., Fernandez Patier R., de La Rosa J., Sanchez de la Campa A., Menéndez M. and Gil J. J. (2004) Levels of particulate matter in rural, urban and industrial sites in Spain. *Sci. Total Environ.* **334-335**, 359-376.

[7]   Prospero, J. M. (1999) Long-range transport of mineral dust in the global atmosphere: Impact of African dust on the environment of the southeastern United States. *Proc. Natl. Acad. Sci. USA* **96**, 3396-3403.

[8]   Lashof D. A. and Ahuja D. R. (1990) Relative contributions of greenhouse gas emissions to global warming. *Nature* **344**, 529-531.

[9]   Molina M. J. and Rowland F. S. (1974) Stratospheric sink for chlorofluoromethanes: Chlorine atom-catalysed destruction of ozone. *Nature* **249**, 810-812.

[10]   Sopauskiene D. and Budvytyte D. (1994) Chemical characteristics of atmospheric aerosol in rural site of lithuania. *Atmos. Environ.* **28**, 1291-1296.

[11]   Ramanathan V., Crutzen P. J., Kiehl J. T. and Rosenfeld D. (2001) Aerosols, climate, and the hydrological cycle. *Science* **294**, 2119-2124.

[12]   Takemura T., Nozawa T., Emori S., Nakajima T. Y. and Nakajima T. (2005) Simulation of climate response to aerosol direct and indirect effects with aerosol transport-radiation model. *J. Geophys. Res.* **110**, D02202.

[13]   Ramaswamy V. and Ramanathan V. (1989) Solar absorption by cirrus clouds and the maintenance of the tropical troposphere thermal structure. *J. Atmos. Sci.* **46**, 2293-2310.

[14]   Myriokefalitakis S., Tsigaridis K., Mihalopoulos N., Sciare J., Nenes A., Kawamura K., Segers A. and Kanakidou M. (2011) In-cloud oxalate formation in the global troposphere: a 3-D modeling study. *Atmos. Chem. Phys.* **11**, 5761-5782.

[15] Cantrell W. and Heymsfield A. (2005) Production of ice in tropospheric clouds: A review. *Bull. Amer. Meteor. Soc.* **86**, 795-807.

[16] Andreae M. O. and Rosenfeld D. (2008) Aerosol–cloud–precipitationinteractions. Part 1. The nature and sources of cloud-active aerosols. *Earth-Sci. Rev.* **89**, 13-41.

[17] Finlayson-Pitts B. J. and Pitts J. N. Jr. (2000) *Chemistry of the upper and lower atmosphere: Theory, experiments, and applications.* Academic Press, U.S.A.

[18] Burnett R. T., Brook J., Dann T., Delocla C., Philips O., Cakmak S., Vincent R., Goldberg M. S. and Krewski D. (2000) Association between particulate- and gas-phase components of urban air pollution and daily mortality in eight Canadian cities. *Inhal Toxicol.* **12**, 15-39.

[19] Godoi R. H. M., Braga D. M., Makarovska Y., Alfoldy B., Carvalho Filho M. A. S., Van Grieken R. and Godoi A. F. L. (2008) Inhale particulate matter from lime industries: Chemical composition and deposition in human respiratory tract. *Atmos. Environ.* **42**, 7027-7033.

[20] Polichetti G., Cocco S., Spinali A., Trimarco V. and Nunziata A. (2009) Effects of particulate matter (PM_{10}, $PM_{2.5}$ and PM_1) on the cardiovascular system. *Toxicology* **261**, 1-8.

[21] Wilson W. E., Chow J. C., Claiborn C., Fusheng W., Engelbrecht J. and Watson J. G. (2002) Monitoring of particulate matter outdoors. *Chemosphere* **49**, 1009-1043.

[22] Huggins F. E., Huffman G. P., Linak W. P. and Miller C. A. (2004) Quantifying hazardous species in particulate matter derived from fossil-fuel combustion. *Environ. Sci. Technol.* **38**, 1836-1842.

[23] Gard E. E., Kleeman M. J., Gross D. S., Hughes L. S., Allen J. O., Morrical B. D., Fergenson D. P., Dienes T., Gälli M. E., Johnson R. J., Cass G. R. and Prather K. A. (1998) Direct observation of heterogeneous chemistry in the atmosphere. *Science* **279**, 1184-1187.

[24] Rubasinghege G., Elzey S., Baltrusaitis J., Jayaweera, P. M. and Grassian V. H. (2010) Reactions on atmospheric dust particles: surface photochemistry and size-dependent nanoscale redox chemistry. *J. Phys. Chem. Lett.* **1**, 1729-1737.

[25] Charlson R. J., Schwartz S. E., Hales J. M., Cess R. D., Coakley J. A. Jr., Hansen J. E. and Hofmann D. J. (1992) Climate forcing by anthropogenic aerosols. *Science* **255**, 423-430.

[26] Andreae M. O., Jones C. D. and Cox P. M. (2005) Strong present-day aerosol cooling implies a hot future. *Nature* **435**, 1187-1190.

[27] Andreae M. O., Rosenfeld D., Artaxo P., Costa A. A., Frank G. P., Longo K. M. and Silva-Dias M. A. F. (2004) Smoking rain clouds over the Amazon. *Science* **303**, 1337-1342.

[28] Sherwood S. (2002) A microphysical connection among biomass burning, cumulus clouds, and stratospheric moisture. *Science* **295**, 1272-1275.

[29] Kirk-Davidoff D. B., Hintsa E. J., Anderson J. G. and Keith D. W. (1999) The effect of climate change on ozone depletion through changes in stratospheric water vapour. *Nature* **402**, 399-401.

[30] Haywood J. and Boucher O. (2000) Estimates of the direct and indirect radiative forcing due to tropospheric aerosols: A review. *Rev. Geophys.* **38**, 513-543.

[31]   Shindell D. and Faluvegi G. (2009) Climate response to regional radiative forcing during the twentieth century. *Nature Geosci.* **2**, 294-300.

[32]   Shindell D. T., Faluvegi G., Koch D. M., Schmidt G. A., Unger N. and Bauer S. E. (2009) Improved attribution of climate forcing to emissions. *Science* **326**, 716-718.

[33]   Arneth A., Unger N., Kulmala M. and Andreae M.O. (2009) Clean the air, heat the Planet?" *Science* **326**, 672-673.

[34]   Preining O. (1991) Aerosol and climate - an overview. *Atmos. Environ. A* **25**, 2443-2444.

[35]   Schlesinger W. H., Reynolds J. F., Cunningham G. L., Huenneke L. F., Jarrell W. M., Virginia R. A. and Whitford W. G. (1990) Biological feedbacks in global desertification. *Science* **247**, 1043-1048.

[36]   Tegen I. and Fung I. (1995) Contribution to the atmospheric mineral aerosol load from land surface modification. *J. Geophys. Res.* **100**, 18707-18726.

[37]   Tegen I., Lacis A. A. and Fung I. (1996) The influence on climate forcing of mineral aerosols from disturbed soils. *Nature* **380**, 419-422.

[38]   Micklin P. (2007) The Aral Sea disaster. *Annu. Rev. Earth Planet. Sci.* **35**, 47-72.

[39]   Tegen I., Harrison S. P., Kohfeld K., Prentice I. C., Coe M. and Heimann M. (2002) Impact of vegetation and preferential source areas on global dust aerosol: Results from a model study. *J. Geophys, Res.* **107**, 4576.

[40]   Eimanifar A. and Mohebbi F. (2007) Urmia Lake (Northwest Iran): a brief review. *Saline Systems* **3**, 5.

[41]   Cahill T. A., Gill T. E., Gillette D. A., Gearhart E. A., Reid J. S. and Yau M. -L., (1994) *Generation, characterization and transport of Owens (dry) lake dust*, Contract No. A132-105, California Air Resources Board Research Division, Final Report, U.S.A.

[42]   Cahill T. A., Gill T. E., Reid J. S., Gearhart E. A. and Gillete D. A. (1996) Saltating particles, playa crust and dust aerosols at Owens (dry) lake, California. *Earth Surf. Process. Landforms* **21**, 621-639.

[43]   Khemani L. T., Momin G. A., Naik M. S., Prakasa Rao P. S., Safai P. D. and Murty A. S. R. (1987) Influence of alkaline particulates on pH of cloud and rain water in India. *Atmos. Environ.* **21**, 1137-1145.

[44]   Tiwari S., Chate D. M., Bisht D. S., Srivastava M. K. and Padmanabhamurty B. (2012) Rainwater chemistry in the North Western Himalayan Region, India. *Atmos. Res.* **104-105**, 128-138.

[45]   Khemani L. T., Momin G. A., Naik M. S., Prakasa Rao P. S., Kumar R. and Ramana Murty BH. V. (1985) Impact of alkaline particulates on pH of rain water in India. *Water Air Soil Poll.* **25**, 365-376.

[46]   Varma G. S. (1989) Background trends of pH of precipitation over India. *Atmos. Environ.* **23**, 747-751.

[47]   Khemani L. T., Momin G. A., Prakasa Rao P. S., Safai P. D., Singh G., Chatterjee R. N. and Prakash P. (1989) Long-term effects of pollutants on pH of rain water in North India. *Atmos. Environ.* **23**, 753-756.

[48] Jain M., Kulshrestha U. C., Sarkar A. K. and Parashar D. C. (2000) Influence of crustal aerosols on wet deposition at urban and rural sites in India. *Atmos. Environ.* **34**, 5129-5137.

[49] Kulshrestha U. C., Kulshrestha M. J., Sekar R., Sastry G. S. R. and Vairamani M. (2003). Chemical characteristics of rainwater at an urban site of south-central India. *Atmos. Environ.* **37**, 3019-3026.

[50] Rastogi N. and Sarin M. M. (2005) Chemical characteristics of individual rain events from a semi-arid region in India: Three-year study. *Atmos. Environ.* **39**, 3313-3323.

[51] Lakhani A., Parmar R. S., Satsangi G. S. and Prakash S. (2007) Chemistry of fogs at Agra, India: Influence of soil particulates and atmospheric gases. *Environ. Monit. Assess.* **133**, 435-445.

[52] Lekouch I., Mileta M., Muselli M., Milimouk-Melnytchouk I., Šojat V., Kabbachi B. and Beysens D. (2010) Comparative chemical analysis of dew and rain water. *Atmos. Res.* **95**, 224-234.

[53] Salve P. R., Gobre T., Lohkare H., Krupadam R. J., Bansiwal A., Ramteke D. S. and Wate S. R. (2011) Source identification and variation in the chemical composition of rainwater at coastal and industrial areas of India. *J. Atmos. Chem.* **68**, 183-198.

[54] Dignon J. (1992) NO_x and SO_x emissions from fossil fuels: A global distribution. *Atmos. Environ. A* **26**, 1157-1163.

[55] Hastie D. R., Schiff H. I., Whelpdale D. M., Peterson R. E., Zoller W. H. and Anderson D. L. (1988) Nitrogen and sulphur over the Western Atlantic Ocean. *Atmos. Environ.* **22**, 2381-2391.

[56] Zhuang G., Yi Z., Duce R. A. and Brown P. R. (1992) Link between iron and sulphur cycles suggested by detection of Fe(II) in remote marine aerosols. *Nature* **355**, 537-539.

[57] Andreae M. O. and Crutzen P. J. (1997) Atmospheric aerosols: Biogeochemical sources and role in atmospheric chemistry. *Science* **276**, 1052-1058.

[58] Claridge G. G. C. and Campbell I. B. (1968) Origin of nitrate deposits. *Nature* **217**, 428-430.

[59] Mueller G. (1968) Genetic histories of nitrate deposits from Antarctica and Chile. *Nature* **219**, 1131-1134.

[60] Wilson A. T. and House D. A. (1965) Fixation of nitrogen by aurora and its contribution to the nitrogen balance of the Earth. *Nature* **205**, 793-794.

[61] Parker B. C., Heiskell L. E., Thompson W. J. and Zeller E. J. (1978) Non-biogenic fixed nitrogen in Antarctica and some ecological implications. *Nature* **271**, 651-652.

[62] Rood R. T., Sarazin C. L., Zeller E. J. and Parker B. C. (1979) X- or γ-rays from supernovae in glacial ice. *Nature* **282**, 701-703.

[63] Singh H. B. (1987) Reactive nitrogen in the troposphere. *Environ. Sci. Technol.* **21**, 320-327.

[64] Hofmann H., Hoffmann P. and Lieser K. H. (1991) Transition metals in atmospheric aqueous samples, analytical determination and speciation. *Fresenius J. Anal. Chem.* **340**, 591-597.

[65] Querol X., Zhuang X., Alastuey A., Viana M., Lv W., Wang Y., López A., Zhu Z., Wei H. and Xu S. (2006) Speciation and sources of atmospheric aerosols in a highly industrialized emerging mega-city in Central China. *J. Environ. Monit.* **8**, 1049-1059.

[66] Fujiwara F., Dos Santos M., Marrero J., Polla G., Gómez D., Dawidowski L. and Smichowski P. (2006) Fractionation of eleven elements by chemical bonding from airborne particulate matter collected in an industrial city in Argentina. *J. Environ. Monit.* **8**, 913-922.

[67] Cheng M. -T., Chou W. -C., Chio C. -P., Hsu S. -C., Su Y. -R., Kuo P. -H., Tsuang B. -J., Lin S. -H. and Chou C. C. -K. (2008) Compositions and source apportionments of atmospheric aerosol during Asian dust storm and local pollution in central Taiwan. *J. Atmos. Chem.* **61**, 155-173.

[68] Migliavacca D., Teixeira E.C., Pires M. and Fachel J. (2004) Study of chemical elements in atmospheric precipitation in South Brazil. *Atmos. Environ.* **38**, 1641-1656.

[69] Migliavacca D., Teixeira E. C., Wiegand F., Machado A. C. M. and Sanchez J. (2005) Atmospheric precipitation and chemical composition of an urban site, Guaíba hydrographic basin, Brazil. *Atmos. Environ.* **39**, 1829-1844.

[70] Lee S. -H., Murphy D. M., Thomson D. S. and Middlebrook A. M. (2002) Chemical components of single particles measured with Particle Analysis by Laser Mass Spectrometry (PALMS) during the Atlanta SuperSite Project: Focus on organic/sulfate, lead, soot, and mineral particles. *J. Geophys. Res.* **107**, 4003.

[71] Xie R. K., Seip H. M., Leinum J. R., Winje T. and Xiao J. S. (2005) Chemical characterization of individual particles (PM_{10}) from ambient air in Guiyang City, China. *Sci. Total Environ.* **343**, 261-272.

[72] Xie R. K., Seip H. M., Liu L. and Zhang D. S. (2009) Characterization of individual airborne particles in Taiyuan City, China. *Air Qual. Atmos. Health* **2**, 123-131.

[73] Kieber R. J., Skrabal S. A., Smith C. and Willey J. D. (2004) Redox speciation of copper in rainwater: Temporal variability and atmospheric deposition. *Environ. Sci. Technol.* **38**, 3587-3594.

[74] Sedlak D. L., Hoigné J., David M. M., Colvile R. N., Seyffer E., Acker K., Wiepercht, W., Lind J. A. and Fuzzi S. (1997) The cloudwater chemistry of iron and copper at Great Dun Fell, U.K. *Atmos. Environ.* **31**, 2515-2526.

[75] Grassian V. H. (2009) New Directions: Nanodust - A source of metals in the atmospheric environment? *Atmos. Environ.* **43**, 4666-4667.

[76] Gidney J. T., Twigg M. V. and Kittelson D. B. (2010) Effect of organometallic fuel additives on nanoparticle emissions from a gasoline passenger car. *Environ. Sci. Technol.* **44**, 2562-2569.

[77] Adachi K. and Buseck P. R. (2010) Hosted and free-floating metal-bearing atmospheric nanoparticles in Mexico city. *Environ. Sci. Technol.* **44**, 2299-2304.

[78] Graedel T. E., Weschler C. J. and Mandich M. L. (1985) Influence of transition metal complexes on atmospheric droplet acidity. *Nature* **317**, 240-242.

[79] Matthijsen J., Builtjes P. J. H. and Sedlak D. L. (1995) Cloud model experiments of the effect of iron and copper on tropospheric ozone under marine and continental conditions. *Meteorol. Atmos. Phys.* **57**, 43-60.

[80] Sedlak D. L. and Hoigné J. (1993) The role of copper and oxalate in the redox cycling of iron in atmospheric waters. *Atmos. Environ. A* **27**, 2173-2185.

[81] Sedlak D. L. and Hoigné J. (1994) Oxidation of S(IV) in atmospheric water by photooxidants and iron in the presence of copper. *Environ. Sci. Technol.* **28**, 1898-1906.

[82] Stone E. A., Hedman C. J., Sheesley R. J., Shafer M. M. and Schauer J. J. (2009) Investigating the chemical nature of humic-like substances (HULIS) in North American atmospheric aerosols by liquid chromatography tandem mass spectrometry. *Atmos. Environ.* **43**, 4205-4213.

[83] Stone E., Schauer J., Quraishi T. A. and Mahmood A. (2010) Chemical characterization and source apportionment of fine and coarse particulate matter in Lahore, Pakistan. *Atmos. Environ.* **44**, 1062-1070.

[84] Pio C.A., Legrand M., Alves C.A., Oliveira T., Afonso J., Caseiro A., Puxbaum H., Sanchez-Ochoa A. and Gelencsér A. (2008) Chemical composition of atmospheric aerosols during the 2003 summer intense forest fire period. *Atmos. Environ.* **42**, 7530-7543.

[85] Mensah A. A., Buchholz A., Mentel Th. F., Tillmann R. and Kiendler-Scharr A. (2011) Aerosol mass spectrometric measurements of stable crystal hydrates of oxalates and inferred relative ionization efficiency of water. *J. Aerosol Sci.* **42**, 11-19.

[86] Pratt K. A. and Prather K. A. (2012) Mass spectrometry of atmospheric aerosols - Recent developments and applications. Part I: Off-line mass spectrometry techniques *Mass Spectrom. Rev.* **31**, 1-16.

[87] Pratt K. A. and Prather K. A. (2012) Mass spectrometry of atmospheric aerosols - Recent developments and applications. Part II: On-line mass spectrometry techniques. *Mass Spectrom. Rev.* **31**, 17-48.

[88] Loh N. D., Hampton C. Y., Martin A. V., Starodub D., Sierra R. G., Barty A., Aquila A., Schulz J., Lomb L., Steinbrener J., Shoeman R. L., Kassemeyer S., Bostedt C., Bozek J., Epp S. W., Erk B., Hartmann R., Rolles D., Rudenko A., Rudek B., Foucar L., Kimmel N., Weidenspointner G., Hauser G., Holl P., Pedersoli E., Liang M., Hunter M. S., Gumprecht L., Coppola N., Wunderer C., Graafsma H., Maia F. R. N. C., Ekeberg T., Hantke M., Fleckenstein H., Hirsemann H., Nass K., White T. A., Tobias H. J., Farquar G. R., Benner W. H., Hau-Riege S. P., Reich C., Hartmann A., Soltau H., Marchesini S., Bajt S., Barthelmess M., Bucksbaum P., Hodgson K. O., Strüder L., Ullrich J., Frank M., Schlichting I., Chapman H. N. and Bogan M. J. (2012) Fractal morphology, imaging and mass spectrometry of single aerosol particles in flight. *Nature* **486**, 513-517.

[89] Xue H., Gonçalves M. S., Reutlinger M., Sigg L. and Stumm W. (1991) Copper (I) in fogwater: Determination and interactions with sulfite. *Environ. Sci. Technol.* **25**, 1716-1722.

[90] Deutsch F., Hoffmann P. and Ortner H. M. (1997) Analytical characterization of manganese in rainwater and snow samples. *Fresenius J. Anal. Chem.* **357**, 105-111.

[91]   Deutsch F., Hoffmann P. and Ortner H. M. (2001) Field experimental investigations on the Fe(II)- and Fe(III)-content in cloudwater samples. *J. Atmos. Chem.* **40**, 87-105.

[92]   Pósfai M., Simonics R., Li, J., Hobbs P. V. and Buseck P. R. (2003) Individual aerosol particles from biomass burning in southern Africa: 1. Compositions and size distributions of carbonaceous particles. *J. Geophys. Res.* **108**, 8483.

[93]   Li J., Pósfai M., Hobbs P. V. and Buseck P. R. (2003) Individual aerosol particles from biomass burning in southern Africa: 2, Compositions and aging of inorganic particles. *J. Geophys. Res.* **108**, 8484.

[94]   Lee Y. C. and Hills P. R. (2003) Cool season pollution episodes in Hong Kong, 1996-2002. *Atmos. Environ.* **37**, 2927-2939.

[95]   Willey J. D., Inscore M. T., Kieber R. J. and Skrabal S. A. (2009) Manganese in coastal rainwater: Speciation, photochemistry and deposition to seawater. *J. Atmos. Chem.* **62**, 31-43.

[96]   Willey J. D., Kieber R. J. and Yavari J. R. (2009) Fe(II) in coastal rainwater: Changing stability and concentrations. *Aquat. Sci.* **71**, 144-150.

[97]   Shah M. H. and Shaheen N. (2010) Seasonal behaviours in elemental composition of atmospheric aerosols collected in Islamabad, Pakistan. *Atmos. Res.* **95**, 210-223.

[98]   Safai P. D., Budhavant K. B., Rao P. S. P., Ali K. and Sinha A. (2010) Source characterization for aerosol constituents and changing roles of calcium and ammonium aerosols in the neutralization of aerosol acidity at a semi-urban site in SW India. *Atmos. Res.* **98**, 78-88.

[99]   Ault A. P., Peters T. M., Sawvel E. J., Casuccio G. S., Willis R. D., Norris G. A. and Grassian V. H. (2012) Single-particle SEM-EDX analysis of iron-containing coarse particulate matter in an urban environment: sources and distribution of iron within Cleveland, Ohio. *Environ. Sci. Technol.* **46**, 4331-4339.

[100]   Vallero D. A. (2008) *Fundamentals of air pollution.* Academic Press, U.S.A.

[101]   Andreae M. O., Charlson R. J., Bruynseels F., Storms H., Van Grieken R. and Maenhaut W. (1986) Internal mixture of sea salt, silicates and excess sulfate in marine aerosols. *Science* **232**, 1620-1623.

[102]   Flament P., Deboudt K., Cachier H., Châtenet B. and Mériaux X. (2011) Mineral dust and carbonaceous aerosols in West Africa: Source assessment and characterization. *Atmos. Environ.* **45**, 3742-3749.

[103]   Chuang P. Y., Duvall R. M., Shafer M. M. and Schauer J. J. (2005) The origin of water soluble particulate iron in the Asian atmospheric outflow. *Geophys. Res. Lett.* **32**, L07813.

[104]   Chabas A. and Lefèvre R. A. (2000) Chemistry and microscopy of atmospheric particulates at Delos (Cyclades-Greece). *Atmos. Environ.* **34**, 225-238.

[105]   Zhou G. and Tazaki K. (1996). Seasonal variation of gypsum in aerosol and its effect on the acidity of wet precipitation on the Japan Sea side of Japan. *Atmos. Environ.* **30**, 3301-3308.

[106]   Pruppacher H. R. and Jaenicke R. (1995) The processing of water vapor and aerosols by atmospheric clouds, a global estimate. *Atmos. Res.* **38**, 283-295.

[107] Zhu X., Prospero J. M., Millero F. J., Savoie D. L. and Brass G. W. (1992) The solubility of ferric ion in marine mineral aerosol solutions at ambient relative humidities. *Mar. Chem.* **38**, 91-107.

[108] Spokes L. J., Jickells D. and Lim B. (1994) Solubilisation of aerosol trace metals by cloud processing: A laboratory study. *Geochim. Cosmochim. Acta* **58**, 3281-3287.

[109] Desboeufs K. V., Sofikitis A., Losno R., Colin J. L. and Ausset P. (2005) Dissolution and solubility of trace metals from natural and anthropogenic aerosol particulate matter. *Chemosphere* **58**, 195-203.

[110] Shi Z., Bonneville S., Krom M. D., Carslaw K. S., Jickells T. D., Baker A. R. and Benning L. G. (2011) Iron dissolution kinetics of mineral dust at low pH during simulated atmospheric processing. *Atmos. Chem. Phys.* **11**, 995-1007.

[111] Voigt R. and Lieser K. H. (1984) Identification of chemical species in air dust by powder diffractometry. *Naturwissenschaften* **71**, 377-378.

[112] Sturges W. T., Harrison R. M. and Barrie, L. A. (1989) Semi-quantitative x-ray diffraction analysis of size fractionated atmospheric particles. *Atmos. Environ.* **23**, 1083-1098.

[113] Querol X., Alastuey A., Puicercus J. A., Mantilla E., Ruiz C. R., Lopez-Soler A., Plana F. and Juan R. (1998) Seasonal evolution of suspended particles around a large coal-fired power station: Chemical characterization. *Atmos. Environ.* **32**, 719-731.

[114] Harrison R. M. and Sturges W. T. (1984) Physico-chemical speciation and transformation reactions of particulate atmospheric nitrogen and sulphur compounds. *Atmos. Environ.* **18**, 1829-1833.

[115] Rodríguez I., Gali S. and Marcos C. (2009) Atmospheric inorganic aerosol of a non-industrial city in the centre of an industrial region of the North of Spain, and its possible influence on the climate on a regional scale. *Environ. Geol.* **56**, 1551-1561.

[116] Ciobotă V., Salama W., Tarcea N., Rösch P., Aref M. E., Gaupp R. and Popp J. (2012) Identification of minerals and organic materials in Middle Eocene ironstones from the Bahariya depression in the Western desert of Egypt by means of micro-Raman spectroscopy. *J. Raman Spectrosc.* **43**, 405-410.

[117] Schweiger G. (1989) Single microparticle analysis by Raman spectroscopy. *J. Aerosol Sci.* **20**, 1621-1624.

[118] Fung K. H., Imre D. G. and Tang I. N. (1994) Detection limits for sulfates and nitrates in aerosol particles by Raman spectroscopy. *J. Aerosol Sci.* **25**, 479-485.

[119] Trunk M., Popp J., Hartmann I., Lankers M., Urlaub E. and Kiefer W. (1996) Chemical composition and reaction analysis of single aerosol particles. *Fresenius J. Anal. Chem.* **355**, 354-356.

[120] Trunk M., Popp J. and Kiefer W. (1998) Investigations of the composition changes of an evaporating, single binary-mixture microdroplet by inelastic and elastic light scattering. *Chem. Phys. Lett.* **284**, 377-381.

[121] Musick J., Popp J., Trunk M. and Kiefer W. (1998) Investigations of radical polymerization and copolymerization reactions in optically levitated microdroplets by simultaneous Raman spectroscopy, Mie scattering, and radiation pressure measurements. *Appl. Spectrosc.* **52**, 692-701.

[122] Musick J., Popp J. and Kiefer W. (2000) Observation of a phase transition in an electrodynamically levitated NH_4NO_3 microparticle by Mie and Raman scattering. *J. Raman Spectrosc.* **31**, 217-219.

[123] Batonneau Y., Sobanska S., Laureyns J. and Bremard C. (2006) Confocal microprobe Raman imaging of urban tropospheric aerosol particles. *Environ. Sci. Technol.* **40**, 1300-1306.

[124] Schumacher W., Kühnert M., Rösch P. and Popp J. (2011) Identification and classification of organic and inorganic components of particulate matter via Raman spectroscopy and chemometric approaches. *J. Raman Spectrosc.* **42**, 383–392.

[125] Sobanska S., Hwang H., Choël M., Jung H. -J., Eom H. -J., Kim H., Barbillat J. and Ro C. -U. (2012) Investigation of the chemical mixing state of individual Asian dust particles by the combined use of Electron Probe X-ray microanalysis and Raman microspectrometry. *Anal. Chem.* **84**, 3145-3154.

[126] Peacock M. A. and Bandy M. C. (1937) Ungemachite and clinoungemachite, new minerals from Chile. *Am. Mineral.* **22**, 207.

[127] Peacock M. A. and Bandy M. C. (1938) Ungemachite and clino-ungemachite: New minerals from Chile. *Am. Mineral.* **23**, 314-328.

[128] Groat L. A. and Hawthorne F. C. (1986) Structure of ungemachite, $K_3Na_8Fe(SO_4)_6(NO_3)_2 \cdot 6H_2O$, a mixed sulfate-nitrate mineral. *Am. Mineral.* **71**, 826-829.

[129] Fateley W. G., Dollish F. R., McDevitt N. T., Bentley F. F. (1972) *Infrared and Raman selection rules for molecular and lattice vibrations: The Correlation Method*, Wiley-Interscience, U.S.A.

[130] Heyns A. M. (1977) The i.r. and Raman spectra of sodium hexafluorophosphate monohydrate, $NaPF_6 \cdot H_2O$. *Spectrochim. Acta A* **33**, 315-322.

[131] Best S. P., Armstrong R. S. and Beattie J. K. (1980) Infrared metal-ligand vibrations of hexaaquametal (III) ions in alums. *Inorg. Chem.* **19**, 1958-1961.

[132] Best S. P., Armstrong R. S. and Beattie J. K. (1982) Vibrational spectroscopic studies of trivalent hexa-aqua-cations: single-crystal Raman spectra of caesium aluminium alums between 300 and 1200 cm^{-1}. *J. Chem. Soc. Dalton Trans.* 1655-1664.

[133] Best S. P., Beattie J. K. and Armstrong R. S. (1984) Vibrational spectroscopic studies of trivalent hexa-aqua-cations: single-crystal Raman spectra between 275 and 1200 cm^{-1} of the caesium alums of titanium, vanadium, chromium, iron, gallium, and indium. *J. Chem. Soc. Dalton Trans.* 2611-2624.

[134] Jarzęcki A. A., Anbar A. D. and Spiro T. G. (2004) DFT analysis of $Fe(H_2O)_6^{3+}$ and $Fe(H_2O)_6^{2+}$ structure and vibrations; implications for isotope fractionation. *J. Phys. Chem. A* **108**, 2726-2732.

[135] Boujelbene M. and Mhiri T. (2011) Polarized Raman Spectra of $NH_4Al(SO_4)_2 \cdot 12H_2O$. *Inter. J. Spectrosc.* ID 128401.

[136] Andreae M. O. (1983) Soot carbon and excess fine potassium: Long-range transport of combustion-derived aerosols. *Science* **220**, 1148-1151.

[137] Desboeufs K. V., Losno R. and Colin J. L. (2001) Factors influencing aerosol solubility during cloud processes. *Atmos. Environ.* **35**, 3529-3537.

[138]   Sarthou G., Baker A. R., Blain S., Achterberg E. P., Boye M., Bowie A. R., Croot P., Laan P., De Baar H. J. W., Jickells T. D. and Worsfold P. J. (2003) Atmospheric iron deposition and sea-surface dissolved iron concentrations in the eastern Atlantic Ocean. *Deep-Sea Res. I* **50**, 1339-1352.

[139]   Baker A. R., Jickells T. D., Witt M. and Linge K. L. (2006) Trends in the solubility of iron, aluminium, manganese and phosphorus in aerosol collected over the Atlantic Ocean. *Mar. Chem.* **98**, 43-58.

[140]   Paris R., Desboeufs K. V. and Journet E. (2011) Variability of dust iron solubility in atmospheric waters: Investigation of the role of oxalate organic complexation. *Atmos. Environ.* **45**, 6510-6517.

[141]   Sholkovitz E. R., Sedwick P. N. and Church T. M. (2009) Influence of anthropogenic combustion emissions on the deposition of soluble aerosol iron to the ocean: Empirical estimates for island sites in the North Atlantic. *Geochim. Cosmochim. Acta* **73**, 3981-4003.

[142]   Paris R., Desboeufs K. V., Formenti P., Nava S. and Chou C. (2010) Chemical characterization of iron in dust and biomass burning aerosols during AMMA-SOP0/DABEX: implication for iron solubility. *Atmos. Chem. Phys.* **10**, 4273-4282.

[143]   Guieu C., Bonnet S., Wagener T. and Loÿe-Pilot M. -D. (2005) Biomass burning as a source of dissolved iron to the open ocean? *Geophys. Res. Lett.* **32**, L19608.

[144]   Smith R. D. (1980) The trace element chemistry of coal during combustion and the emissions from coal-fired plants. *Prog. Energy Combust. Sci.* **6**, 53-119.

[145]   Behra P. and Sigg L. (1990) Evidence for redox cycling of iron in atmospheric water droplets. *Nature* **344**, 419-421.

[146]   Faust B. C. and Hoigné J. (1990) Photolysis of Fe (III)-hydroxy complexes as sources of OH radicals in clouds, fog and rain. *Atmos. Environ. A* **24**, 79-89.

[147]   Harvie C. E. and Weare J. H. (1980) The prediction of mineral solubilities in natural waters: the $Na-K-Mg-Ca-Cl-SO_4-H_2O$ system from zero to high concentration at 25° C. *Geochim. Cosmochim. Acta* **44**, 981-997.

[148]   Harvie C. E., Møller N. and Weare J. H. (1984) The prediction of mineral solubilities in natural waters: The $Na-K-Mg-Ca-H-Cl-SO_4-OH-HCO_3-CO_3-CO_2-H_2O$ system to high ionic strengths at 25°C. *Geochim. Cosmochim. Acta* **48**, 723-751.

[149]   Møller N. (1988) The prediction of mineral solubilities in natural waters: A chemical equilibrium model for the $Na-Ca-Cl-SO_4-H_2O$ system, to high temperature and concentration. *Geochim. Cosmochim. Acta* **52**, 821-837.

[150]   Spencer R. J., Møller N. and Weare J. H. (1990) The prediction of mineral solubilities in natural waters: A chemical equilibrium model for the $Na-K-Ca-Mg-Cl-SO_4-H_2O$ system at temperatures below 25°C. *Geochim. Cosmochim. Acta* **54**, 575-590.

[151]   Clegg S. L. and Whitfield M. (1995) A chemical model of seawater including dissolved ammonia and the stoichiometric dissociation constant of ammonia in estuarine water and seawater from -2 to 40°C. *Geochim. Cosmochim. Acta* **59**, 2403-2421.

[152]   Marion G. M. and Farren R. E. (1999) Mineral solubilities in the Na-K-Mg-Ca-Cl-SO$_4$-H$_2$O system: a re-evaluation of the sulfate chemistry in the Spencer-Møller-Weare model. *Geochim. Cosmochim. Acta* **63**, 1305-1318.

[153]   Xu B. and Schweiger G. (1999) In-situ Raman observation of phase transformation of Na$_2$SO$_4$ during the hydration/dehydration cycles on single levitated microparticle. *J. Aerosol Sci.* **30**, S379-S380.

[154]   Takahashi C., Tsujimoto Y. and Yamamoto Y. (2012) The effect of irradiation wavelengths and the crystal structures of titanium dioxide on the formation of singlet oxygen for bacterial killing. *J. Clin. Biochem. Nutr.* **51**, 128-131.

[155]   Zhang X., Zhuang G., Chen J., Wang Y., Wang X., An Z. and Zhang P. (2006) Heterogeneous reactions of sulfur dioxide on typical mineral particles. *J. Phys. Chem. B* **110**, 12588-12596.

[156]   Kamm S., Möhler O., Naumann K. -H., Saathoff H. and Schurath U. (1999) The heterogeneous reaction of ozone with soot aerosol. *Atmos. Environ.* **33**, 4651-4661.

[157]   Ericksen G. E. and Mrose M. E. (1970) Mineralogical studies of the nitrate deposits of Chile. II. Darapskite Na$_3$(NO$_3$)(SO$_4$)·H$_2$O. *Am. Mineral.* **55**, 1500-1517.

[158]   Redden M. J. (1968) *The crystal structure of darapskite.* Master Thesis, Massachusetts Institute of Technology, U.S.A.

[159]   Bruynseels F., Storms H. and Van Grieken R. (1988) Characterization of North Sea aerosols by individual particle analyses. *Atmos. Environ.* **22**, 2593-2602.

[160]   Zhao L. -J., Zhang Y. -H., Wei Z. -F., Cheng H. and Li X. -H. (2006) Magnesium sulfate aerosols studied by FTIR spectroscopy: Hygroscopic properties, supersaturated structures, and implications for seawater aerosols. *J. Phys. Chem. A* **110**, 951-958.

[161]   Zhang Y. -H. and Chan C. K. (2002) Understanding the hygroscopic properties of supersaturated droplets of metal and ammonium sulfate solutions using Raman spectroscopy *J. Phys. Chem. A* **106**, 285-292.

[162]   Platford R. F. (1974) Thermodynamics of the system H$_2$O-NaCl-Na$_2$SO$_4$-MgSO$_4$ to the saturation limit of NaCl at 25ºC. *J. Solution Chem.* **3**, 771-780.

[163]   Onac B. P., White W. B. and Viehmann I. (2001) Leonite [K$_2$Mg(SO$_4$)$_2$·4H$_2$O], konyaite [Na$_2$Mg(SO$_4$)$_2$·5H$_2$O] and syngenite [K$_2$Ca(SO$_4$)$_2$·H$_2$O] from Tausoare Cave, Rodnei Mts, Romania. *Mineral. Mag.* **65**, 103-109.

[164]   Shayan A. and Lancucki C. J. (1984) Konyaite in salt efflorescence from a tertiary marine deposit near Geelong, Victoria, Australia. *Soil Sci, Soc. Am. J.* **48**, 939-942.

[165]   Van Doesburg J. D. J., Vergouwen L. and Van der Plas L. (1982) Konyaite, Na$_2$Mg(SO$_4$)$_2$.5H$_2$O, a new mineral from the Great Konya Basin, Turkey. *Am. Mineral.* **67**, 1035-1038.

[166]   Kohut C. K. and Dudas M. J. (1993) Evaporite mineralogy and trace-element content of salt-affected soils in Alberta. *Can. J. Soil Sci.* **73**, 399-409.

[167]   Ducloux J., Guero Y., Fallavier P. and Valet S. (1994) Mineralogy of salt efflorescences in paddy field soils of Kollo, southern Niger. *Geoderma* **64**, 57-71.

[168] Keller L. P., McCarthy G. J. and Richardson J. L. (1986) Laboratory modeling of Northern Great Plains salt efflorescence mineralogy. *Soil Sci, Soc. Am. J.* **50**, 1363-1367.

[169] Friedel B. (1976) $Na_2Mg(SO_4)_2 \cdot 5H_2O$, ein metastabilies Salz bei der Krustenbildung auf Boden. *Neues Jahrb. Miner.* **126**,187-198.

[170] Karthikeyan S., Joshi U. M. and Balasubramanian R. (2006) Microwave assisted sample preparation for determining water-soluble fraction of trace elements in urban airborne particulate matter: Evaluation of bioavailability. *Anal. Chim. Acta* **576**, 23-30.

[171] Theodosi C., Markaki N. and Mihalopoulos N. (2010) Iron speciation, solubility and temporal variability in wet and dry deposition in the Eastern Mediterranean. *Mar. Chem.* **120**, 100-107.

[172] Fu H., Lin J., Shang G., Dong W., Grassian V. H., Carmichael G. R., Li Y. and Chen J. (2012) Solubility of iron from combustion source particles in acidic media linked to iron speciation. *Environ. Sci. Technol.* **46**, 11119-11127.

[173] Jambor J. L. and Traill R. J. (1963) On rozenite and siderotil. *Can. Mineral.* **7**, 751-763.

[174] Parungo F. P., Nagamoto C. T. and Harris J. M. (1986) Temporal and spatial variations of marine aerosols over the Atlantic Ocean. *Atmos. Res.* **20**, 23-37.

[175] Hoornaert S., Van Malderen H. and Van Grieken R. (1996) Gypsum and other calcium-rich aerosol particles above the North Sea. *Environ. Sci. Technol.* **30**, 1515-1520.

[176] Grassian V. H. (2002) Chemical reactions of nitrogen oxides on the surface of oxide, carbonate, soot, and mineral dust particles: Implications for the chemical balance of the troposphere. *J. Phys. Chem. A* **106**, 860-877.

[177] Derbez M. and Lefèvre R. (2003) Chemical and mineralogical composition and sources of urban atmospheric particles, specially sulphates - a study at Tours (France). *Pollut. Atmos.* **177**,103-125.

[178] Corazza E. and Sabelli C. (1967) The crystal structure of syngenite, $K_2Ca(SO_4)_2 \cdot H_2O$. *Z. Kristallogr.* **124**, 398-408.

[179] Bokii G. B., Pal'chik N. A. and Antipin M. Y. (1981) Genesis and structure of koktaite. *Trudy Instituta Geologii i Geofiziki* **487**, 4-8.

[180] Cocco G., Corazza E. and Sabelli C. (1965) The crystal structure of glauberite, $CaNa_2(SO_4)_2$. *Z. Kristallogr.* **122**, 175-184.

[181] Araki T. and Zoltai T. (1967) Refinement of the crystal structure of a glauberite. *Am. Mineral.* **52**, 1272-1277.

[182] Bindi L. (2005) Reinvestigation of polyhalite, $K_2Ca_2Mg(SO_4)_4 \cdot 2H_2O$. *Acta Crystallogr. E* **61**, i135-i136.

[183] Block J. and Waters Jr. O. B. (1968) The $CaSO_4$-Na_2SO_4-$NaCl$-H_2O system at 25° to 100°C. *J. Chem. Eng. Data* **13**, 336-344.

[184] Jänecke E. (1906) Über eine neue Darstellungsform der wässerigen Lösungen zweier und dreier gleichioniger Salze, reziproker Salzpaare und der van't Hoffschen Untersuchungen über ozeanische Salzablagerungen. *Z. Anorg. Chem.* **51**, 132-157.

[185] Harvie C. E., Weare J. H., Hardie L. A. and Eugster H. P. (1980) Evaporation of seawater: Calculated mineral sequences. *Science* **208**, 498-500.

[186] Reynolds R. L., Yount J.C., Reheis M., Goldstein H., Chavez P. Jr., Fulton R., Whitney J., Fuller C. and Forester R. M. (2007) Dust emission from wet and dry playas in the Mojave Desert, USA. *Earth Surf. Process. Landforms* **32**, 1811-1827.

[187] Reheis M. C. (1997) Dust deposition downwind of Owens (dry) Lake, 1991–1994: Preliminary findings. *J. Geophys. Res.* **102**, 25999-26008.

[188] Choi B. -K., Labbé H. J. and Lockwood D. J. (1990) Raman spectrum of Na_2SO_4 (phase III). *Solid State Commun.* **74**, 109-113.

2 Publications

2.1 Raman spectroscopic study of crystallization from solutions containing MgSO$_4$ and Na$_2$SO$_4$: Raman spectra of double salts [PV1]

Authorship of Publication

Paul Vargas Jentzsch: concept development

mixed salts preparation

experiments of crystallization within droplets

factor group analysis and bands assigment

writing of manuscript

Bernd Kampe: Raman spectra processing

aplication of the evolutionary strategy (for salt misxtures)

Petra Rösch: discussion of experimental concept and results

proofreading of manuscript

Jürgen Popp: project management

discussion of concepts and results

discussion and proofreading of manuscript

Raman Spectroscopic Study of Crystallization from Solutions Containing MgSO₄ and Na₂SO₄: Raman Spectra of Double Salts

Paul Vargas Jentzsch,[†] Bernd Kampe,[†] Petra Rösch,[†] and Jürgen Popp*,[†,‡]

[†]Institut für Physikalische Chemie, Friedrich-Schiller-Universität Jena, D-07743 Jena, Germany
[‡]Institut für Photonische Technologien e.V. (IPHT), D-07745 Jena, Germany

Ⓢ Supporting Information

ABSTRACT: Mg^{2+}, Na^+, and SO_4^{2-} are common ions in natural systems, and they are usually found in water bodies. Precipitation processes have great importance in environmental studies because they may be part of complex natural cycles; natural formation of atmospheric particulate matter is just one case. In this work, $Na_2Mg(SO_4)_2 \cdot 5H_2O$ (konyaite), $Na_6Mg(SO_4)_4$ (vanthoffite), and $Na_{12}Mg_7(SO_4)_{13} \cdot 15H_2O$ (loeweite) were synthesized and their Raman spectra reported. By slow vaporization (at 20 °C and relative humidity of 60−70%), crystallization experiments were performed within small droplets (diameter ≤ 1−2 mm) of solutions containing $MgSO_4$ and Na_2SO_4, and crystal formations were studied by Raman spectroscopy. Crystallization of $Na_2Mg(SO_4)_2 \cdot 4H_2O$ (bloedite) was observed, and the formation of salt mixtures was confirmed by Raman spectra. Bloedite, konyaite, and loeweite, as well as Na_2SO_4 and $MgSO_4 \cdot 6H_2O$, were the components found to occur in different proportions. No crystallization of $Na_6Mg(SO_4)_4$ (vanthoffite) was observed under the crystallization condition used in this study.
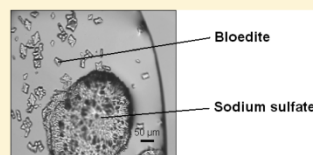
I. INTRODUCTION

At present, environmental topics are acquiring growing importance worldwide; different subjects related to water, soil, and atmospheric pollution are intensively studied not only to understand natural phenomena and processes but also to monitor/protect and control the environmental quality.

A large variety of studies are dedicated to the atmospheric particulate matter. Particulate matter contains components of natural and anthropogenic origin; atmospheric particulate matter can even be found in rural areas where the human influence is minimal. As is the case of other pollutants, pollution is aggravated by human activities like, e.g., industry, construction activities, mining, and others. In order to control the pollution levels countries and specialized agencies have set up laws and standards. Although there is a discussion on the parameters and factors to be considered by laws and standards, researchers generally agree on two important parameters related to particulate matter: the particle composition and the respirable fraction of aerosol particles which can penetrate into the pulmonary alveoli.

In order to analyze environmental samples, new methods including spectroscopic techniques were developed and reported during recent years. Considering that legislation is changing continuously and standards are more and more strict, analytical techniques for specific analytes must be made available quickly and, of course, those techniques should be cheap and fast. In the case of atmospheric particulate matter, Raman spectroscopy offers important advantages; therefore, several investigations of this kind were reported.[1−10]

The presence of sodium and magnesium as well as sulfates in soil and water reservoirs is well known. In particular, seawater is rich in ions of many types; the most abundant are Na^+, Cl^-, Mg^{2+}, and SO_4^{2-}.[11] A large proportion of salt is injected into the atmosphere as aerosol by breaking waves and bursting bubbles on the ocean surface,[12] and considering the abundance of ions in seawater, NaCl or $MgSO_4$ may be expected in atmospheric particles. The natural process of erosion incorporates salts into rainwater. When this water washes the soil and rocks as part of the natural water cycle, it affects the resulting water quality, e.g., the total hardness of water, which is defined as the sum of the calcium and magnesium concentrations.[13]

Recently, exploration of other planets and satellites in our solar system has motivated the study of magnesium salts, especially the spectroscopic properties, due to the fact that analytical methods of this kind are the basis of exploration missions. Specifically, it is well known that many efforts have been made to locate water on other planets, because water is an essential ingredient of life, and the existence of hydrated salts could indicate some water activity (past or current). With this in mind, Chaban et al.[14] reported theoretical work about the infrared and Raman spectra of magnesium sulfate salts with different hydration degrees and a few years later Wang et al.[15] reported a complete work which included Raman spectra from 10 hydrated and anhydrous magnesium sulfates.

Sodium sulfate undergoes several phase transformations; depending on the temperature four phases can be observed and distinguished by their Raman spectra: V, III, II, and I. Phase

ACS Publications   © 2011 American Chemical Society

5540

dx.doi.org/10.1021/jp200142n | J. Phys. Chem. A 2011, 115, 5540–5546

V is the room-temperature phase. The Raman spectra of Na_2SO_4 phases were intensively studied in early works, and band assignments were made.[16–19] Also, the phase transformation was an important subject in the studies reported by Xu and co-workers[20,21] investigating the Raman spectra evolution of a single levitated microparticle.

In natural systems it is not common to find pure substances; actually, complex mixtures may be expected. The process of solubilization of salts present in soil and rocks as a consequence of natural phenomena like rain involves several kinds of inorganic and organic compounds, and a subsequent crystallization (by water vaporization) produces a complex solid mixture. According to an earlier report, evaporite salts like Na_2SO_4 (thenardite), $Na_2SO_4 \cdot 10H_2O$ (mirabilite), $MgSO_4 \cdot 6H_2O$ (hexahydrite), $MgSO_4 \cdot 7H_2O$ (epsomite), $Na_2Mg(SO_4)_2 \cdot 4H_2O$ (bloedite), and $Na_2Mg(SO_4)_2 \cdot 5H_2O$ (konyaite) can be found in saline soil.[22] Due to different environmental factors, mixtures and minerals can be transported to the atmosphere; hence, these mixtures and minerals are expected to form particles during this process. It is clear that the Raman spectra of these mixtures and minerals must be known when used for analytical purposes.

In the present study, we attempt to answer two main questions: (1) which salts precipitate when solutions containing $MgSO_4$ and Na_2SO_4 in different proportions vaporize at 20 °C, and (2) what are Raman spectra of particles generated by this process expected to look like?

Also, in this contribution we provide the Raman spectra of synthetic $Na_6Mg(SO_4)_4$ (vanthoffite), $Na_2Mg(SO_4)_2 \cdot 5H_2O$ (konyaite), and $Na_{12}Mg_7(SO_4)_{13} \cdot 15H_2O$ (loeweite).

II. EXPERIMENTAL SECTION

Vanthoffite, Konyaite, and Loeweite Synthesis. Sodium chloride, NaCl (min. 99.5%), and sodium sulfate anhydrous, Na_2SO_4 (≥99%) purchased from Sigma-Aldrich, were used without further purification. Magnesium sulfate anhydrous (min. 99.5%) purchased from VWR was dried in an oven at 250 °C for 2 h before use due to its high hygroscopicity.

The vanthoffite used in this study was synthesized following the method (and reactants amounts) described by Dancy[23] using $MgSO_4$ anhydrous and NaCl. Konyaite was synthesized by evaporation of a solution containing Na_2SO_4 and $MgSO_4$ in a molar ratio of 1:1 in a Petri dish at a temperature of 35 °C, according to the method reported earlier.[24]

Loeweite was synthesized by crystallization from an aqueous solution at 80 °C, as described before.[25] Two solutions containing $MgSO_4$ and Na_2SO_4 were tested in order to obtain the crystals. One of them was prepared in a molar ratio of 4:3 used before by Schneider to synthesize double salts with loeweite crystal structure using manganese,[26] and the other one had a molar ratio of 7:6 equal to the proportion of magnesium and sodium in loeweite. Both methods produced loeweite, and the Raman spectra showed the same features.

Sample Preparation: Crystallization within a Droplet. Saturated solutions containing $MgSO_4$ and $NaSO_4$ in molar ratios of 1:1, 1:2, 1:3, 2:1, and 3:1 were prepared, and droplets (diameter ≤ 1–2 mm) of these solutions were disposed on separate microscope slides. In order to produce crystallization, the microscope slides containing the droplets were vaporized several hours under room conditions (20 °C and 60–70% relative humidity). Several Raman spectra were recorded at different points of each droplet immediately after the start of

the slow vaporization, after ~36 h and after more than 48 h (when the droplet was dry). It should be noted that the solutions containing high concentrations of $MgSO_4$ show a delay in water vaporization; this effect was also observed in early works.[27–29] With the Raman spectra recorded at these three stages it is possible to observe the crystallization sequence of the different kinds of salts typically contained in the $MgSO_4$–Na_2SO_4 system.

As standard samples, recrystallized Na_2SO_4 and $MgSO_4$ samples were also prepared by slow vaporization (several hours) of saturated solutions of each compound on individual microscope slides. Vaporization was performed under room conditions.

Spectroscopic Instrumentation. The Raman spectra of samples (powder and/or crystals) were recorded in the range from 250 to 3400 cm^{-1} with a micro-Raman setup (HR LabRam inverse system, Jobin Yvon Horiba). Raman scattering was excited by a frequency-doubled Nd/YAG laser at a wavelength of 532 nm with a laser power of about 2 mW incident on the sample. The laser beam was focused on individual particles (crystals) by means of an Olympus 50× microscope objective. The dispersive spectrometer has an entrance slit of 100 μm and a focal length of 800 mm and is equipped with a grating of 300 and 1200 lines mm^{-1} (depending on the case). The Raman-scattered light was detected by a CCD camera operating at 220 K. The acquisition time per spectrum was 5 s. For the calibration procedure, titanium dioxide (anatase) and 4-acetamidophenol (4AAP) were measured daily as a reference control and for subsequent data processing.

Data Processing. All data were processed using the "R" software.[30] Raman spectra of pure salts (and double salts) related with this study were collected and average spectra obtained. In order to achieve a reliable identification of the salts in the samples using Raman spectroscopic features, a sequence of algorithms was applied to the spectroscopic data. For all spectra, a background reduction was performed using the R package baselineWavelet, and the calibration procedure was completed performing a shift correction with 4AAP using an R script.[31,32] Interpolation and normalization methods as well removal of the baseline (to avoid fitting against noise) complete the preprocessing process. In order to evaluate Raman spectra of mixtures, two steps were applied using an evolutionary strategy (ES),[33] the first to identify all potential substances in the mixture and the second to quantify them. We used blind identification in the first step, removing all substances afterward that were estimated to account for less than 1% of the mixture. Then, the ES iteratively reduced the difference between the spectrum of the mixture and the quantified sum of all remaining spectra of substances.

III. RESULTS AND DISCUSSION

The most intense bands expected in the Raman spectra of sulfate salts are related to vibrations of the sulfate ion (SO_4^{2-}). Considering the free ion symmetry of SO_4^{2-} (T_d), there are four normal modes of vibration: ν_1 (A_1) symmetric stretching, ν_2 (E) symmetric bending, ν_3 (F_2) asymmetric stretching, and ν_4 (F_2) asymmetric bending; all of them are Raman active. The stretching modes usually occur in the 950–1200 cm^{-1} region, and the bending modes occur in the 400–650 cm^{-1} region.[34] The feature produced by the $\nu_1(A_1)$ mode is expected to be the most intense.

Raman spectra of recrystallized Na_2SO_4 show the most intense band at 989 cm^{-1} (SO_4^{2-} symmetric stretching mode), and all the other features are in good agreement with wavenumbers reported earlier for the anhydrous salt in phase V (stable at room temperature), as shown in Table S1 (Supporting Information).
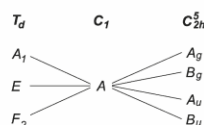
Figure 1. Correlation scheme of free-ion site and factor species for the SO_4^{2-} ion.

Taking into account the obtained wavenumbers, we discard the formation of crystals of Na_2SO_4 in the metastable phase III because the SO_4^{2-} symmetric stretching mode (ν_1) for this phase appears at 996 cm^{-1}.[18] Although Na_2SO_4 (III) according to earlier reports[18,35] appears fairly stable at room temperature, it was not detected under the crystallization conditions of this study.

When the crystallization of $MgSO_4$ is performed using a saturated solution at room temperature, the crystallization of $MgSO_4 \cdot 7H_2O$ may be expected.[36] Nevertheless, the Raman spectra of crystals obtained by slow vaporization at room temperature in this work show features of $MgSO_4 \cdot 6H_2O$,[15] probably due to the long time of exposure to environmental air. The wavenumber difference of the SO_4^{2-} symmetric stretching mode (ν_1) between the hexahydrate and the heptahydrate salt is less than 1 cm^{-1}; consequently, this band (the most intense) is not enough to perform a proper identification, but with the other fundamental modes it is possible to identify the hydration of the salt. As an example, in the Raman spectra of the obtained crystals we observed bands at 1145 and 1084 cm^{-1} attributed to the SO_4^{2-} asymmetric stretching mode (ν_3); these values fit very well with values reported by Wang and co-workers for $MgSO_4 \cdot 6H_2O$ (1146 and 1085 cm^{-1}). Also, for SO_4^{2-} symmetric bending (ν_2) and asymmetric bending (ν_4) the characteristics bands observed in the Raman spectrum fit very well with those reported previously for $MgSO_4 \cdot 6H_2O$. Table S2, Supporting Information, shows the observed wavenumbers of obtained crystals as well as the previously reported wavenumbers for $MgSO_4 \cdot 6H_2O$ and $MgSO_4 \cdot 7H_2O$.

As for the properties of $MgSO_4 \cdot 7H_2O$, it is known that exposure of the crystal to dry air at ordinary temperatures produces the loss of one water molecule: In this specific case the crystals were exposed to air at 20 °C with a relative humidity of 60−70%, i.e., conditions similar to the natural environment, so this loss process can occur in natural soils and minerals. Some studies related to saline soils reported the presence of both $MgSO_4 \cdot 7H_2O$ and $MgSO_4 \cdot 6H_2O$, also known by their mineral names epsomite and hexahydrite, respectively.[22] Both are classified as evaporite minerals; this means that they result naturally by vaporization of water from aqueous solutions containing magnesium and sulfate. It may be assumed that $MgSO_4 \cdot 7H_2O$ is the stable salt generated in first instance, which after contact of the crystals with air gradually produces $MgSO_4 \cdot 6H_2O$; hence, both salts can be observed in conventional soil analyzes.

$Na_2Mg(SO_4)_2 \cdot 4H_2O$ is present in nature as a mineral called bloedite and crystallizes in a monoclinic system with the space group $P2_1/a$ (C^5_{2h}) and has two molecules in the unit cell.[37] Considering the results obtained applying the correlation method,[38] 150 fundamental modes (including the acoustic modes) are expected and split into

$$\Gamma_{150} = 36A_g + 36B_g + 39A_u + 39B_u$$

The species with subscript g are Raman active. In the bloedite crystal, the SO_4^{2-} ion occupies sites of lower symmetry than its
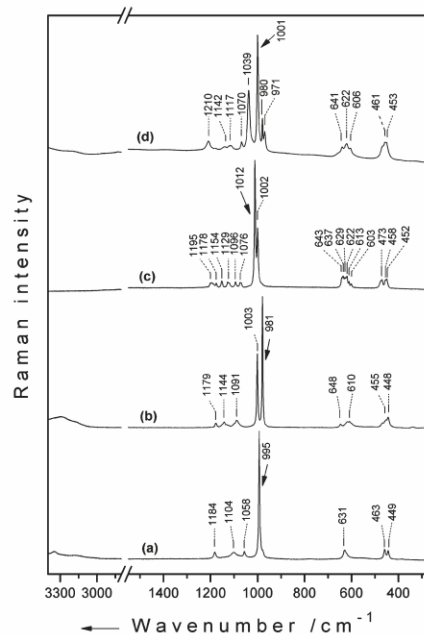

Figure 2. Raman spectra of double salts: (a) $Na_2Mg(SO_4)_2 \cdot 4H_2O$ (bloedite), (b) $Na_2Mg(SO_4)_2 \cdot 5H_2O$ (konyaite), (c) $Na_6Mg(SO_4)_4$ (vanthoffite), and (d) $Na_{12}Mg_7(SO_4)_{13} \cdot 15H_2O$ (loeweite).

free-ion symmetry. The correlation for the fundamental modes of the SO_4^{2-} ion between the free-ion symmetry T_d, the site of symmetry C_1 (general position), and the unit-cell symmetry C_{2h} is shown in Figure 1.

As a consequence of the elimination of degeneration, a splitting of the SO_4^{2-} modes is expected in the Raman spectrum. For synthetic bloedite, we observed one strong band at 995 cm^{-1} assigned to the SO_4^{2-} symmetric stretching mode (ν_1) and another weak one at 631 cm^{-1} assigned to the SO_4^{2-} asymmetric bending mode (ν_4). The SO_4^{2-} symmetric bending mode (ν_2) splits in two bands at 463 and 449 cm^{-1} and the SO_4^{2-} asymmetric stretching mode (ν_3) in three bands at 1184, 1104, and 1058 cm^{-1}. Also, a broad band above 3000 cm^{-1} was observed and assigned to stretching modes of water. The Raman spectrum of bloedite is shown in Figure 2a.

$Na_2Mg(SO_4)_2 \cdot 5H_2O$ is present in nature as a mineral called konyaite. This salt crystallizes in a monoclinic system with the space group $P2_1/c$ (C_{2h}) and has four molecules in the unit cell.[39] Considering the results obtained applying the correlation method, 336 fundamental modes (including the acoustic modes) are expected and split into

$$\Gamma_{336} = 78A_g + 78B_g + 90A_u + 90B_u$$

The species with subscript g are Raman active. The difference between the molecular formula of bloedite and konyaite is only one molecule of water, but important differences can be observed in the crystal structure. Although both bloedite and konyaite have sheet structures, konyaite has a much more densely packed sheet
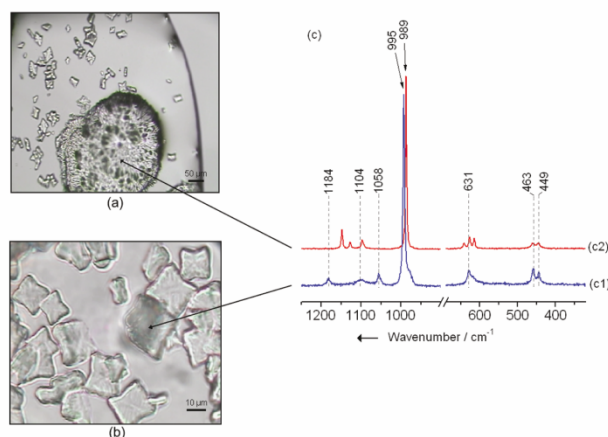
Figure 3. (a) Na_2SO_4 crystal formation precipitated within a droplet of $MgSO_4-Na_2SO_4$ solution with a molar ratio of 1:2 surrounded by crystals of $Na_2Mg(SO_4)_2\cdot4H_2O$. (b) $Na_2Mg(SO_4)_2\cdot4H_2O$ crystal precipitated by slow vaporization of a droplet of $MgSO_4-Na_2SO_4$ solution at a molar ratio of 1:2. (c) Raman spectra of precipitates within the droplet: (c1) $Na_2Mg(SO_4)_2\cdot4H_2O$; (c2) Na_2SO_4.

arrangement compared to the open-sheet configuration of bloedite.[39] This structural characteristic of konyaite allows this double salt to accommodate more molecules per unit cell than bloedite, and several differences can be expected in the Raman spectrum. There are eight SO_4^{2-} ions per unit cell, but only four can be accommodated in general positions; the other four ions must be placed in special positions. This assumption is supported by the crystal structure of konyaite, which suggests the existence of two symmetrically distinct sulfate tetrahedra.[39] Considering this structural characteristic, at least two strong bands are expected for the SO_4^{2-} symmetric stretching (ν_1), and we observed them at 1003 and 981 cm^{-1}. The SO_4^{2-} asymmetric stretching (ν_3) splits in three bands at 1179, 1144, and 1091 cm^{-1}. For the SO_4^{2-} asymmetric bending (ν_4) we observed bands at 648, 619, 610, and 602 cm^{-1}, and for the SO_4^{2-} symmetric bending (ν_2) bands are at 471, 455, and 448 cm^{-1}. As in the spectrum of bloedite, we also observed a broad band assigned to H_2O stretching above 3000 cm^{-1}. The Raman spectrum of konyaite is shown in Figure 2b.

$Na_6Mg(SO_4)_4$, also known as vanthoffite, is a mineral occurring in oceanic salt deposits. The structure belongs to the monoclinic system with the space group $P2_1/c$ (C_{2h}^5) and has two molecules in the unit cell.[40,41] Considering the results obtained applying the correlation method, 162 fundamental modes (including the acoustic modes) are expected and split into

$$\Gamma_{162} = 33A_g + 33B_g + 48A_u + 48B_u$$

The species with subscript g are Raman active. As in the case of konyaite, there are eight SO_4^{2-} ions per unit cell but only four can be accommodated in general positions; the other four ions must be placed in special positions. Again, at least two strong bands are expected for the SO_4^{2-} symmetric stretching mode (ν_1), which were observed at 1012 and 1002 cm^{-1}. The SO_4^{2-} asymmetric stretching mode (ν_3) splits in 10 bands at 1202,1195, 1190, 1178, 1154, 1129, 1122, 1096, 1076, and 1071 cm^{-1}. Bands for the SO_4^{2-} asymmetric bending mode (ν_4) were observed at

643, 637, 629, 622, 613, and 603 cm^{-1}. Four bands at 478, 473, 458, and 452 were assigned to the SO_4^{2-} symmetric bending mode (ν_2). The Raman spectrum of vanthoffite is shown in Figure 2c.

The crystal structure of loeweite reported by Fang and Robinson,[42] who considered that there was one unit of $6Na_2SO_4\cdot7MgSO_4\cdot15H_2O$ (or $Na_{12}Mg_7(SO_4)_{13}\cdot15H_2O$) in the cell, shows the existence of two kinds of octahedral Mg and three tetrahedral S. The octahedron $Mg(2)$ is located in the center of the cell, and alternate linkages of octahedra $Mg(1)$ and the tetrahedra S (1 and 2) emanate radially from its six corners. The tetrahedron $S(3)$ is isolated from this linkage and located at the corner of the cell. Specifically, this tetrahedron $S(3)$ sulfate gives special complexity to the structure because, according to Fang and Robinson,[42] it is shifting its location and can never be found simultaneously at both possible sites.

The Raman spectrum recorded for synthetic loeweite shows four bands in the region of the SO_4^{2-} symmetric stretching; two of them are strong bands at 1039 and 1001 cm^{-1}. Probably, these bands are originated by tetrahedral $S(1)$ and $S(2)$. There are several differences between the tetrahedral coordination around $S (1, 2, \text{and } 3)$ related to the interatomic distances and tetrahedral angles around the S atom. For the tetrahedron $S(3)$, the four S—O distances are 1.601 Å and the tetrahedral angles are between 108.9° and 110.0°,[42] while for SO_4^{2-} ion in the free state all distances and angles are ~1.48 Å and 109.47°, respectively.[43] Despite the fact that interatomic distances in the tetrahedron $S(3)$ are larger than those obtained for SO_4^{2-} in the free state, this tetrahedron is less distorted than tetrahedral $S(1)$ and $S(2)$; therefore, similar features can be expected for the tetrahedron $S(3)$ as for SO_4^{2-} in the free state. In the free state SO_4^{2-}, the symmetric stretching mode (ν_1) appears at 981 cm^{-1} [34] and we observed two bands located at 980 and 971 cm^{-1}, probably related to the tetrahedron $S(3)$ and its characteristic shift location in loeweite's structure.

The SO_4^{2-} asymmetric stretching mode (ν_3) splits in four bands at 1210, 1142, 1117, and 1070 cm^{-1}. For the SO_4^{2-} asymmetric bending mode (ν_4) we observed bands at 641, 622,

ARTICLE

Table 1. Estimated Composition of Mixtures Using Their Raman Spectra

MgSO$_4$:Na$_2$SO$_4$ molar ratio	sample number	composition of the mixture (%)				
		Na$_2$Mg(SO$_4$)$_2$·4H$_2$O (bloedite)	Na$_2$Mg(SO$_4$)$_2$·5H$_2$O (konyaite)	Na$_{12}$Mg$_7$(SO$_4$)$_{13}$·15H$_2$O (loeweite)	MgSO$_4$·6H$_2$O (hexahydrite)	Na$_2$SO$_4$ (thenardite)
1:1	6	9.7	15.4		55.7	19.2
1:1	7	5.2			83.1	11.7
1:1	8		1.7		16.7	81.6
1:1	10	8.0	14.8		57.3	19.9
1:1	12	91.5			8.5	
2:1	13	26.7	26.8		46.6	
2:1	14		36.9	7.3	55.8	
2:1	15	86.2	6.8	3.7	3.3	
2:1	16	68.7			31.3	
2:1	18		28.3	15.3	56.5	
2:1	21	3.8	17.1	66.6	12.4	
2:1	22	3.0	19.8	65.5	11.8	
2:1	23	2.7	20.3	65.0	12.0	
3:1	3	72.3	3.3		24.4	
3:1	6		42.2	12.1	45.7	
3:1	8		33.7		66.3	
3:1	14	96.4			3.6	
3:1	18	2.2	16.5	67.3	14.1	
3:1	22		16.2		83.8	
1:3	7		31.6		68.4	
1:3	11		18.7		81.3	
1:3	12		30.5		12.1	57.4
1:3	14		17.1			82.9
1:3	15		-		89.4	10.6
1:3	20		36.0		56.1	7.9

and 606 cm^{-1}. Three bands at 471 (shoulder), 461, and 453 cm^{-1} were assigned to the SO$_4$$^{2-}$ symmetric bending mode (ν_2). The Raman spectrum of loeweite is shown in Figure 2d.

With respect to the experiments of crystallization within a solution droplet, starting with a MgSO$_4$—Na$_2$SO$_4$ solution (all proportions under study), it is assumed that the gradual crystallization of the salts occurs in accordance with their water solubilities; Raman spectra were recorded as soon as the first crystals appeared. As mentioned before, the concentrated MgSO$_4$ solutions show a considerable delay in vaporization of the solvent (water) compared to solutions of other salts. After ~36 h of vaporization, we observed the first crystals within the droplets of all solutions under study. According to earlier studies, the crystallization of Na$_2$Mg(SO$_4$)$_2$·4H$_2$O (bloedite) on saturation of equal molar solutions of MgSO$_4$ and Na$_2$SO$_4$ is expected,[28,44] so small crystals with sizes ~10 μm observed in the droplet of the solution of a molar ratio of 1:1 were identified as bloedite. In addition, an earlier reported Raman spectrum obtained from natural bloedite shows similar features.[45] The same crystals were observed in droplets of MgSO$_4$ and Na$_2$SO$_4$ solutions of molar ratios of 1:2, 2:1, 1:3, and 3:1, and the same features were observed in their Raman spectra.

For solutions with Na$_2$SO$_4$ in excess, i.e., MgSO$_4$—Na$_2$SO$_4$ solutions of molar ratios of 1:2 and 1:3, we observed also circular precipitate formations identified as Na$_2$SO$_4$. In other words, in these cases Na$_2$SO$_4$ and bloedite crystallized and it was possible to distinguish both precipitated salts easily by their Raman

spectra. Figure 3 shows microphotographs of a droplet of MgSO$_4$—Na$_2$SO$_4$ solution of molar ratio of 1:2, where it is possible to distinguish the crystal formation identified as Na$_2$SO$_4$ surrounded by small crystals of bloedite (Figure 3a) and crystals of bloedite (Figure 3b) with the Raman spectra recorded for each case (Figure 3c).

On complete vaporization of the solvent (water) in all solution droplets the Raman spectra were recorded in different regions of the crystalline formation, showing not only characteristic bands of Na$_2$SO$_4$, MgSO$_4$·6H$_2$O, and bloedite but also other intense bands at 1003 and 1039 cm^{-1}. Zhang and Chan,[28] in a Raman spectroscopic study about the hygroscopic properties of Na$_2$SO$_4$/MgSO$_4$ droplets using an electrodynamic balance system, reported the emergence of bands at 1007 and 1043 cm^{-1} and assigned those two bands to bloedite. Nevertheless, those bands were not observed in the Raman spectrum of bloedite, so according to our recorded spectra those two bands belong to konyaite and loeweite, respectively.

As a consequence of this last vaporization step for complete water elimination, an abrupt and almost simultaneous precipitation of different salts may be expected, leading to salt mixtures. In this work, we present 25 of the most representative spectra of the observed mixtures and their estimated composition (see Table 1); one of them is shown in Figure 4. The other 24 spectra are shown in Figures S1—S24 (Supporting Information).

As it can be seen in the specific case of the Raman spectrum shown in Figure 4 representing sample 6, a dry droplet of
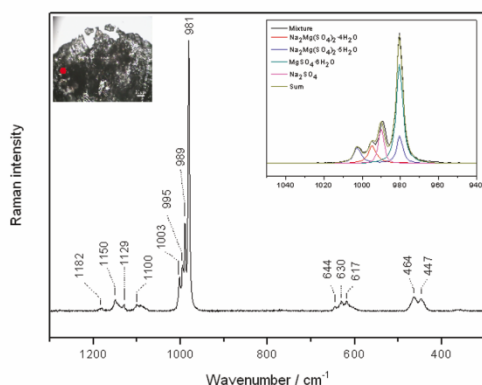
5544

dx.doi.org/10.1021/jp200142n |*J. Phys. Chem. A* 2011, 115, 5540–5546

Figure 4. Raman spectrum of sample 6, measured in the dry droplet of $MgSO_4-Na_2SO_4$ solution with a molar ratio of 1:1.

solution with a molar ratio of 1:1, it is possible to identify clearly bloedite, konyaite, $MgSO_4 \cdot 6H_2O$, and Na_2SO_4 as components of the mixture, in this case with estimated percentages of 10.3%, 15.2%, 54.8%, and 19.8%, respectively.

The phase diagram of the ternary system $MgSO_4-Na_2SO_4-H_2O$, studied theoretically and experimentally by Harvie and Weare,[46] shows the occurrence of three different phases in accordance with the relative concentrations of $MgSO_4$ and Na_2SO_4:$Na_2SO_4 \cdot 10H_2O$, $MgSO_4 \cdot 7H_2O$, and bloedite; this means that these salts are in equilibrium with the solution depending on the relative concentration of the ions. In contact with dry air (or air with moderate humidity), $Na_2SO_4 \cdot 10H_2O$ eliminates the water to produce the anhydrous salt, while $MgSO_4 \cdot 7H_2O$ can eliminate one water molecule to generate $MgSO_4 \cdot 6H_2O$, as mentioned before. In our experiments, we observed that the first salt which precipitates from solutions containing $MgSO_4$ and Na_2SO_4 is bloedite, and in solutions with excess Na_2SO_4 crystal formation of this salt was also observed, as predicted by the phase diagram. However, in the final salt mixture resulting from total water vaporization, we observed also characteristic bands of konyaite and loeweite, probably formed during the last stage of the water vaporization process. Thus, the phase diagram cannot predict the occurrence of konyaite and loeweite.

Finally, it is important to note that in no case vanthoffite was detected, probably because its formation requires a higher temperature.

IV. CONCLUSION

We confirmed that it is possible to obtain $MgSO_4 \cdot 6H_2O$ by slow vaporization of solutions containing $MgSO_4$. As reported in early works, the slow vaporization at room temperature of $MgSO_4$ solution initially produces crystallization of $MgSO_4 \cdot 7H_2O$, but further exposition to air at 20 °C and 60–70% relative humidity causes the gradual loss of one water molecule resulting in crystals of $MgSO_4 \cdot 6H_2O$. The simultaneous occurrence of $MgSO_4 \cdot 7H_2O$ and $MgSO_4 \cdot 6H_2O$ in soil samples reported previously by other authors confirm this assumed sequence.

The total number of fundamental modes was calculated for bloedite, konyaite, and vanthoffite. In this paper we report

the Raman spectra of four double salts characteristic of the $MgSO_4-Na_2SO_4$ system, proposing the assignments of the most intense bands observed in the spectra. For konyaite, vanthoffite, and loeweite, two, two, and four bands, respectively, were assigned to the SO_4^{2-} symmetric stretching (ν_1) due to the specific crystal characteristics of those double salts. The presence of symmetrically different sulfate ions in the crystal structures of those double salts can explain these assignments.

The experiments with droplets show that the first double salt that crystallizes during the slow vaporization process at 20 °C is bloedite, as predicted by the phase diagram. However, the phase diagram of the ternary system $MgSO_4-Na_2SO_4-H_2O$ does not consider the double salts konyaite and loeweite, which are formed during the last stage of the water vaporization process (when all water is eliminated). Both double salts in addition to $MgSO_4 \cdot 6H_2O$, Na_2SO_4, and bloedite were observed by Raman spectroscopy in different proportions in salt mixtures originated from total vaporization of solutions containing $MgSO_4$ and Na_2SO_4. In no case vanthoffite was detected because, probably, its crystallization requires higher temperatures.

The crystallization of salts and double salts from the $MgSO_4-Na_2SO_4$ system under the specified conditions produces different salt mixtures and we attach to this work some Raman spectra representing mixtures of different compositions (Supporting Information). The composition of each mixture can be estimated by Raman spectroscopy using Evolutionary Strategies (ES) according to the above-mentioned data processing.

■ ASSOCIATED CONTENT

ⓢ Supporting Information. Wavenumbers and assignments of the Raman signals obtained for Na_2SO_4 and $MgSO_4 \cdot 6H_2O$, and Raman spectra of samples measured in dry droplets of $MgSO_4-Na_2SO_4$ solutions. This material is available free of charge via the Internet at http://pubs.acs.org.

■ AUTHOR INFORMATION

Corresponding Author
*E-mail: juergen.popp@uni-jena.de.

■ ACKNOWLEDGMENT

■ REFERENCES

(1) Schweiger, G. *J. Aerosol Sci.* **1989**, *20* (8), 1621–1624.
(2) Tang, I. N.; Fung, K. H. *J. Aerosol Sci.* **1989**, *20* (5), 609–617.
(3) Schweiger, G. *J. Aerosol Sci.* **1990**, *21* (4), 483–509.
(4) Fung, K. H.; Imre, D. G.; Tang, I. N. *J. Aerosol Sci.* **1994**, *25* (3), 479–485.
(5) Trunk, M.; Popp, J.; Hartmann, I.; Lankers, M.; Urlaub, E.; Kiefer, W. *Fresenius J. Anal. Chem.* **1996**, *355* (3–4), 354–356.
(6) Trunk, M.; Popp, J.; Lankers, M.; Kiefer, W. *Chem. Phys. Lett.* **1997**, *264* (1–2), 233–237.
(7) Trunk, M.; Popp, J.; Kiefer, W. *Chem. Phys. Lett.* **1998**, *284* (5–6), 377–381.
(8) Musick, J.; Kiefer, W.; Popp, J. *Appl. Spectrosc.* **2000**, *54* (8), 1136–1141.

5545

dx.doi.org/10.1021/jp200142n |*J. Phys. Chem. A* 2011, 115, 5540–5546

(9) Musick, J.; Popp, J.; Kiefer, W. *J. Raman Spectrosc.* **2000**, *31* (3), 217–219.

(10) Schumacher, W.; Kühnert, M.; Rösch, P.; Popp, J. *J. Raman Spectrosc.* **2011**, *42* (3), 383–392.

(11) Zhao, L.-J.; Zhang, Y.-H.; Wei, Z.-F.; Cheng, H.; Li, X.-H. *J. Phys. Chem. A* **2006**, *110*, 951–958.

(12) Tolocka, M. P.; Saul, T. D.; Johnston, M. V. *J. Phys. Chem. A* **2004**, *108* (14), 2659–2665.

(13) In *Standard Methods for the examination of Water and Wastewater*, 20th ed.; Clesceri, L. S., Greenberg, A. E., Eaton, A. D., Eds.; United Book Press, Inc.: Baltimore, MD, 1998.

(14) Chaban, G. M.; Huo, W. M.; Lee, T. J. *J. Chem. Phys.* **2002**, *117* (6), 2532–2537.

(15) Wang, A.; Freeman, J. J.; Jolliff, B. L.; Chou, I.-M. *Geochim. Cosmochim. Acta* **2006**, *70* (24), 6118–6135.

(16) Montero, S. *Spectrochim. Acta A* **1976**, *32*, 843–849.

(17) Choi, B.-K.; Lockwood, D. J. *Solid State Commun.* **1989**, *72* (1), 133–137.

(18) Choi, B.-K.; Labbé, H. J.; Lockwood, D. J. *Solid State Commun.* **1990**, *74* (2), 109–113.

(19) Choi, B.-K.; Lockwood, D. J. *Solid State Commun.* **1990**, *76* (6), 863–866.

(20) Xu, B.; Vehring, R.; Schweiger, G. *J. Aerosol Sci.* **1998**, *29* (2), S865–S866.

(21) Xu, B.; Schweiger, G. *J. Aerosol Sci.* **1999**, *30* (1), S379–S380.

(22) Zielinski, R. A.; Otton, J. K.; Johnson, C. A. *J. Environ. Qual.* **2001**, *30* (4), 1237–1248.

(23) Dancy, W. B. Method of producing Vanthoffite. U.S. Patent 2,952,515, 1958.

(24) Van Doesburg, J. D. J.; Vergouwen, L.; Van der Plas, L. *Am. Mineral.* **1982**, *67* (9−10), 1035–1038.

(25) Von Hodenberg, R.; Kühn, R.; Rosskoff, F. *Kali Steinsalz* **1969**, *5* (5), 178–189.

(26) Schneider, W. *Z. Anorg. Allg. Chem.* **1960**, *303*, 113–116.

(27) Chan, C. K.; Ha, Z.; Choi, M. Y. *Atmos. Environm.* **2000**, *34* (28), 4795–4803.

(28) Zhang, Y.-H.; Chan, C. K. *J. Phys. Chem. A* **2002**, *106*, 285–292.

(29) Tepavitcharova, S.; Balarew, Chr.; Rull, F.; Rabadjieva, D.; Iliev, A. *J. Raman Spectrosc.* **2005**, *36* (9), 891–897.

(30) R Development Core Team. R: A language and environment for statistical computing. R Foundation for Statistical Computing: Vienna, Austria, 2009. ISBN 3-900051-07-0, URL http://www.R-project.org.

(31) Zhang, Z.-M.; Chen, S.; Liang, Y.-Z.; Liu, Z.-X.; Zhang, Q.-M.; Ding, L.-X.; Ye, F.; Zhou, H. *J. Raman Spectrosc.* **2010**, *41* (6), 659–669.

(32) Dörfer, T.; Bocklitz, T.; Tarcea, N.; Schmitt, M.; Popp, J. *Z. Phys. Chem.* **2011**, DOI 10.1524/zpch.2011.0077.

(33) Beyer, H.-G.; Schwefel, H.-P. *Nat. Comput.* **2002**, *1* (1), 3–52.

(34) Ramakrishnan, V.; Nayar, V. U.; Aruldhas, G. *Infrared Phys.* **1985**, *25* (4), 607–610.

(35) Dong, J.-L.; Xiao, H.-S.; Zhao, L.-J.; Zhang, Y.-H. *J. Raman Spectrosc.* **2009**, *40* (3), 338–343.

(36) Emons, H.-H.; Ziegenbalg, G.; Naumann, R.; Paulik, F. *J. Therm. Anal. Cal.* **1990**, *36* (4), 1265–1279.

(37) Vizcayno, C.; Garcia-Gonzalez, M. T. *Acta Crystallogr. C* **1999**, *55* (1), 8–11.

(38) Fateley, W. G.; Dollish, F. R.; McDevitt, N. T.; Bentley, F. F. *Infrared and Raman selection rules for molecular and lattice vibrations: The Correlation Method*; Wiley-Interscience, New York, 1972.

(39) Leduc, E. M. S.; Peterson, R. C.; Wang, R. *Am. Mineral.* **2009**, *94* (7), 1005–1011.

(40) Fischer, W.; Hellner, E. *Acta Crystallogr.* **1964**, *17* (12), 1613.

(41) Keester, K. L.; Eysel, W. *Acta Crystallogr. B* **1977**, *33* (1), 306–307.

(42) Fang, J. H.; Robinson, P. D. *Am. Mineral.* **1970**, *55*, 378–386.

(43) Barashkov, M. V.; Komyak, A. I.; Shashkov, S. N. *J. Appl. Spectrosc.* **1999**, *66* (1), 100–104.

(44) Platford, R. F. *J. Solution Chem.* **1974**, *3* (10), 771–780.

(45) Downs R. T. The RRUFF Project: an integrated study of the chemistry, crystallography, Raman and infrared spectroscopy of minerals. Program and Abstracts of the 19th General Meeting of the International Mineralogical Association in Kobe, Japan. 2006, O03-13. URL http://rruff.info/.

(46) Harvie, C. E.; Weare, J. H. *Geochim. Cosmochim. Acta* **1980**, *44* (7), 981–997.

5546

dx.doi.org/10.1021/jp200142n |*J. Phys. Chem. A* 2011, 115, 5540–5546

2.2 Origin of salt mixtures and mixed salts in atmospheric particulate matter [PV2]

Authorship of Publication

Paul Vargas Jentzsch: concept development

experiments of crystallization within droplets

unpolarized Raman measurements

darapskite preparation

factor group analysis and bands assigment

writing of manuscript

Valerian Ciobotă: polarized Raman measurements

factor group analysis and bands assigment

Bernd Kampe: Raman spectra processing

Petra Rösch: discussion of experimental concept and results

proofreading of manuscript

Jürgen Popp: project management

discussion of concepts and results

discussion and proofreading of manuscript

Research Article

Origin of salt mixtures and mixed salts in atmospheric particulate matter

Paul Vargas Jentzsch,[a][†] Valerian Ciobotă,[a][†] Bernd Kampe,[a] Petra Rösch[a] and Jürgen Popp[b]*

The atmospheric particulate matter contains components of natural and anthropogenic origin, some of them are sulphates and nitrates. Considering the usual occurrence of many ions in the atmosphere and the presence of water, the generation of salt mixtures and mixed salts is possible as a consequence of dissolution–precipitation processes within water droplets, e.g., in fog or haze. This contribution presents the Raman spectroscopic study of the sodium–potassium nitrate system, which generates a salt mixture of both compounds. A phase transition of a KNO_3 crystal within a single solution droplet was observed. Additionally, we postulate the atmospheric generation of the mixed salt $Na_3(NO_3)(SO_4)\cdot H_2O$ (darapskite) by dissolution–precipitation processes, because Na^+, SO_4^{2-}, and NO_3^- can be usually found in the atmosphere. The polarized Raman spectra of synthetic darapskite are reported. Copyright © 2011 John Wiley & Sons, Ltd.

Supporting information may be found in the online version of this article.

Keywords: atmospheric particles; Raman spectroscopy; salt mixtures; phase transition; synthetic darapskite

Introduction

Natural processes produce a great proportion of compounds currently classified as pollutants; volcanic eruptions release a large amount of sulfur dioxide, SO_2[1] and carbon dioxide, and seasonal dust events carry important amounts of mineral dust across thousands of kilometers.[2–5]

Nevertheless, in addition to natural sources of pollutants, there are also anthropogenic ones. Investigations in different areas agree in the conclusion that human activities have a great impact on the delicate global environmental equilibrium. There is no doubt that pollution levels have increased as a consequence of demographic growth, not only because of the increase of industrial activities, but also because more and more food is required to feed a growing population in the whole world. SO_2 is one of the most important pollutants emitted in industrial areas and cities, while the emission of ammonia, NH_3, is originated fundamentally by intensive agriculture (which uses fertilizers) and livestock. Although nitrogen compounds including NH_3 are also emitted by natural sources, e.g., sea water,[6] the anthropogenic contribution to the emission of ammonia increases significantly.[7,8]

Many authors, generally using X-ray diffractometry, have reported the atmospheric occurrence of simple salts like $(NH_4)_2SO_4$, $NaNO_3$, $CaSO_4\cdot 2H_2O$, and mixtures of these salts, and mixed salts like $Na_2Mg(SO_4)_2\cdot 4H_2O$ (bloedite), $(NH_4)_2Mg(SO_4)_2\cdot 6H_2O$ (boussingaultite), $(NH_4)_2Ca(SO_4)_2\cdot H_2O$ (koktaite), $(NH_4)_2Fe(SO_4)_2\cdot 6H_2O$ (mohrite), and others.[9–11] Obviously, in the atmospheric system, where many different inorganic compounds coexist, the formation of mixtures of two or more salts is expected. The presence of sulfates and nitrates in atmosphere are due to oxidative processes; both SO_2 and NH_3 tend to be oxidized to sulfates and nitrates, respectively, and afterwards to be removed from the atmosphere by deposition processes.[1,12,13] At this stage the formation of sulphate and nitrate anions occurs, and the crystallization as salt mixtures and mixed salts is possible in the presence of water.

For analytical purposes, the chemical composition can be elucidated for either individual particles or all particles *en masse*.[14] Analysis of particles *en masse* in different studies showed usually the presence of sulfate, nitrates, and cations like sodium and potassium.[15–17] The composition of individual particles is likewise important, because, according to recent studies, atmospheric particles have climate impacts depending on their composition.[18–20] Furthermore, the surface area of specific airborne minerals provides conditions for water condensation (depending on the hygroscopic properties) and some heterogeneous chemical reactions.[9] The reaction between gaseous nitric acid, $HNO_3(g)$, and solid sodium chloride, $NaCl(s)$, as reported by Gard *et al.*,[21] is an example of an heterogeneous reaction that takes place in the atmosphere involving specific characteristics of airborne particles.

Individual particles may be analyzed by Raman spectroscopy; several investigations of this kind have been reported showing the suitability of this technique for chemical characterization of atmospheric particles.[22–29]

In this contribution, we postulate the possible generation of atmospheric particles as mixtures of salts and/or mixed salts based on the fundamental role of water. When Raman spectroscopy is used as an analytical technique, the assignment and interpretation of the Raman signals is crucial. Therefore, we present the

* Correspondence to: Jürgen Popp, Institut für Physikalische Chemie, and Abbe Center of Photonics, Friedrich-Schiller-Universität Jena, D-07743 Jena, Germany. E-mail: juergen.popp@uni-jena.de

a Institut für Physikalische Chemie, and Abbe Center of Photonics, Friedrich-Schiller-Universität Jena, D-07743 Jena, Germany

b Institut für Photonische Technologien e.V. (IPHT), D-07745 Jena, Germany

† These authors contributed equally to this work.

Origin of salt mixtures and mixed salts in atmospheric particulate matter

Raman spectroscopic study of two systems: (1) sodium nitrate, $NaNO_3$, and potassium nitrate, KNO_3, which involves the formation of a mixture of those two salts; and (2) sodium sulfate, Na_2SO_4 and $NaNO_3$, which includes the formation of the mixed salt $Na_3(NO_3)(SO_4)\cdot H_2O$, known by its mineral name darapskite. A specific study of the vaporization process of a single droplet for the $NaNO_3$–KNO_3 system is reported as the first evidence of a phase transition of crystalline KNO_3 taking place in a solution at room temperature. On the other hand, considering the occurrence of darapskite as a product originating in solutions of the Na_2SO_4–$NaNO_3$ system, we focused our attention on the Raman spectroscopic study of this compound. This is the first time that polarized Raman spectra of darapskite are reported.

Materials and Methods

Chemicals and darapskite synthesis

Potassium nitrate, KNO_3 (≥99%), and sodium sulfate anhydrous, Na_2SO_4 (≥99%), were purchased from Sigma–Aldrich, while sodium nitrate, $NaNO_3$ (min. 99%), was purchased from VWR. All these reactants were used without further purification.

The darapskite used in this study was crystallized at room temperature from a solution containing $NaNO_3$ and Na_2SO_4 in the same proportion as reported previously by Ericksen and Mrose.[30] The darapskite crystallized forming characteristic aggregates of square tabular crystals; this agrees with the morphology observed by Ericksen and Mrose for their synthetic darapskite.

$NaNO_3$–KNO_3 system: crystallization within a droplet

A saturated solution containing $NaNO_3$ and KNO_3 in molar ratio of 1:1 was prepared, and a droplet (diameter ≤ 1–2 mm) of this solution was placed on a microscope slide. The droplet was vaporized within a few minutes under room conditions (20 °C and ~50% relative humidity) to induce crystallization. The Raman spectrum of the first crystal occurring in the solution was recorded and the following spectra were obtained during the water vaporization process until the droplet was dry.

Additionally, a saturated solution containing $NaNO_3$ and KNO_3 in equimolar ratio was vaporized until total water elimination, and the salt residue was milled to simulate a mechanical particle generation. Raman spectra of individual particles were recorded and characterized.

Spectroscopic instrumentation and data processing

The Raman spectra of crystals within a droplet and individual particles (particles mechanically generated) were recorded in the range from 250 to 3600 cm^{-1} with a micro-Raman setup (HR LabRam inverse system, Jobin Yvon Horiba). Raman scattering was excited by a frequency-doubled Nd/YAG laser at a wavelength of 532 nm with a laser power incident on the sample of about 2 mW. The laser beam was focused on individual crystals or particles using an Olympus 50× microscope objective. The dispersive spectrometer has an entrance slit of 100 μm and a focal length of 800 mm and is equipped with a grating of 600, 1200 or 1800 lines mm^{-1} (spectral resolution ~3, ~1.5 or ~1 cm^{-1}, respectively), depending on the case. For the study of the $NaNO_3$–KNO_3 system the gratings 600 and 1200 lines mm^{-1} were used, the first one to record the Raman spectra during the

crystallization process within the drop and the second one to evaluate the bands (wavenumbers) of individual particles. The measurements of the $NaNO_3$–KNO_3 system were performed using unpolarized radiation. The measurements of individual particles of the $NaNO_3$–Na_2SO_4 system were performed using unpolarized radiation and the grating 1200 lines mm^{-1} to evaluate the bands (wavenumbers) in their spectra. The whole polarized Raman spectroscopic study of darapskite was performed using the grating 1800 lines mm^{-1}. The Raman scattered light was detected by a charge-coupled device camera operating at 220 K. The acquisition time per spectrum was 10 s. More details of the Raman polarized study of darapskite are presented in the Section on Polarized Raman spectra of synthetic Darapskite. For the calibration procedure, titanium dioxide (anatase) and 4-acetamidophenol (4AAP) were measured daily as a reference control for subsequent data preprocessing.

All spectroscopic data were processed using the 'R' software.[31] Raman spectra of darapskite were collected and average spectra obtained. For all spectra, a background reduction was performed using the R package baselineWavelet, and the calibration procedure was completed performing a shift correction with 4AAP using an R script.[32,33]

Polarized Raman spectra of synthetic darapskite

For the polarization-dependent micro-Raman measurements, the same Raman device described in the previous paragraph was used. The input polarization was selected with a half-waveplate. The 532 nm laser was focused on the samples using an Olympus 10× objective. A polarizer was used as an analyzer in front of the entrance slit of the spectrometer. The depolarization ratios were checked with a reference sample of CCl_4. The total acquisition time for one Raman spectrum was 60 s. The Raman spectra were recorded in backscattered geometry.

Fourier transform infrared measurements

The infrared spectroscopic measurements were carried out using a Bruker IFS66 Fourier transform infrared spectrometer. The spectra were registered with a spectral resolution of 4 cm^{-1} within 400–6000 cm^{-1} range. The transmission measurements at normal incidence were performed on a pellet of milled darapskite dispersed in a KBr host matrix.

Results and Discussion

From the environmental point of view, systems including Na^+, K^+, NO_3^-, and SO_4^{2-} can be particularly interesting, because they are common ions not only in soil and water bodies, but also in atmospheric particulate matter as has been reported earlier by many researchers.[15–17] The origin of these ions in the atmosphere is variable, but the oceans are an important natural source.[6,34,35] Wilson[34] reported that the potassium/sodium ratio in snow (and thus in atmosphere) is one order of magnitude larger than that of sea water. The argument to justify this phenomenon was that a thin layer of plankton, microorganisms, and other organic materials rich in potassium accumulates on the sea water surface and that these materials are incorporated into the atmosphere by wave breaks. Claridge and Campbell[6] used similar arguments to explain the origin of nitrate deposits in Antarctica. They postulated that the nitrogenous material in the atmosphere originates in this thin sea water layer and that the nitrogen is

P. V. Jentzsch *et al.*

incorporated into the atmosphere as ammonia and protein compounds (albuminoid nitrogen). This is an important natural source of nitrogen compounds in the atmosphere, but much of the environmental concern is due to the anthropogenic sources.

Some of the most important anthropogenic sources of nitrogen compounds in atmosphere are agriculture activities and livestock, in both cases the emissions are in the form of ammonia.[7] There are also important emissions of nitrogen oxides ($NO_x = NO + NO_2$), which are between 70 and 90% of anthropogenic origin.[36]

On the other hand, there are important emissions of sulfur oxides, SO_x, that originate predominantly from volcanoes as natural source, but also from fossil fuel burning and industry.[37]

In presence of oxidation agents, ammonia and NO_x can oxidize to NO_3^-, and SO_x to SO_4^{2-}. The hydroxyl radical, HO·, and ozone, O_3, are the most common atmospheric oxidation agents, actually, the first one is often called the 'detergent of the atmosphere'[38] because of its role in atmosphere self-cleaning. According to several earlier reactivity studies,[12] the tropospheric concentration of both oxidants can be considerably increased by human activities. A specific case is the ozone generation by chemical reactions between volatile organic compounds and nitrogen oxide in the presence of solar light (UV radiation).[39]

Because of the increase of O_3 and HO·, especially in urban areas, an increase of nitrate and sulfate salts is predictable and expected in the atmosphere, and Raman spectroscopy is a reliable and fast technique to perform the chemical characterization of this kind of salts present in atmospheric particulate matter.

The most intense bands expected in Raman spectra of nitrate salts are related with vibrations of the nitrate ion (NO_3^-). Considering the free ion symmetry of NO_3^- (D_{3h}), there are four normal modes of vibration: ν_1 (A_1') symmetric stretching, ν_2 (A_2'') symmetric bending, ν_3 (E') asymmetric stretching, and ν_4 (E') asymmetric bending, only ν_2 is not Raman active. In the free NO_3^- ion, ν_1 occurs at 1049 cm^{-1}, ν_2 at 830 cm^{-1} while ν_3 and ν_4 occur at 1355 and 690 cm^{-1}, respectively.[40]

It is well known that sodium nitrate, $NaNO_3$, exists at room temperature in phase II and undergoes a phase transition at high

temperature to give phase I. Additionally, at high pressures phase II' and III have been reported earlier.[41] The Raman spectrum of room temperature $NaNO_3$ shows the most intense band at 1065 cm^{-1} (NO_3^- symmetric stretching mode) and all the other features are in good agreement with wavenumbers reported earlier for the salt in phase II,[42,43] as shown in Table S1.

Under atmospheric pressure, potassium nitrate, KNO_3, exists in three phases depending on the temperature: I, II, and III (ferroelectric), while it exists in phase IV at high pressure.[44,45] The room temperature phase of KNO_3, phase II, has the aragonite structure (space group D_{2h}^{16}), and at 402 K a phase transition starts to phase I (space group D_{3d}^5); when the crystal in phase I is cooled, the inverse transition to phase II undergoes first a transition to phase III (space group C_{3v}^5) at a temperature ranging from 389 to 385 K, and when the temperature drops lower than 313 K the crystal transforms again into phase II.[46] The Raman spectrum of KNO_3 recorded at room temperature shows the most intense band at 1047 cm^{-1} (NO_3^- symmetric stretching mode) and all the other features are similar to wavenumbers reported earlier for the salt in phase II, as shown in Table S2.

When a saturated solution containing $NaNO_3$ and KNO_3 vaporizes, a process that can be expected in small water droplets of fog or haze, the successive crystallization of both salts is expected according to their individual solubilities, because there is no known possibility of a mixed salt formation. Figure 1 shows a sequence of the crystal growth process from an equimolar solution of $NaNO_3$ and KNO_3. Time zero ($t = 0$) was arbitrarily selected on appearance of the first crystal and afterwards the crystal growth was controlled. Two regions of the Raman spectra for each stage of the vaporization process are also shown in Figs 1(a) and (b).

The first salt expected to crystallize is KNO_3. The Raman spectrum of the crystal at $t = 0$ shows a strong band at 1050 cm^{-1}, shifted by 3 cm^{-1} with respect to the expected ν_1 band for KNO_3 in phase II (stable at room temperature). There are also shifts for ν_3; the spectrum at $t = 0$ shows a broad band with a maximum at 1390 cm^{-1} and another sharp one at 1351 cm^{-1}, both clearly shift with respect to the expected values for phase
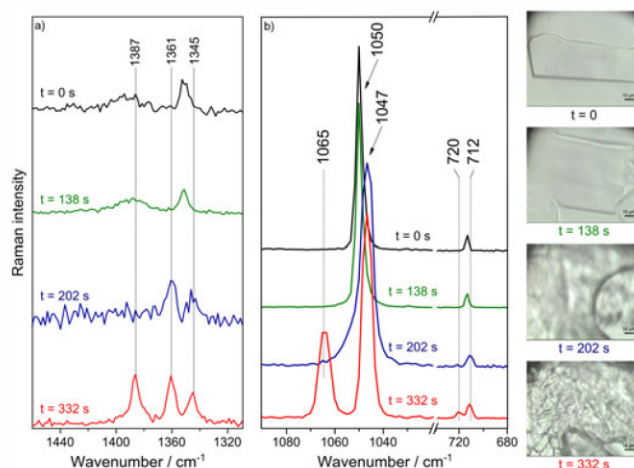

Figure 1. Microphotographs and Raman spectra of vaporization process stages of an equimolar saturated solution containing $NaNO_3$ and KNO_3.

Origin of salt mixtures and mixed salts in atmospheric particulate matter

II, and the same features were also observed in the spectrum at $t = 138$ s. Only after almost complete elimination of water and exposition of the crystal to air, at $t = 202$ s, all shifts disappear. The bands of ν_3 observed for $t = 0$ and 138 s have similar shapes as those observed by Murugan et al.[46] for KNO_3 in phase III, and the shifts observed between bands of KNO_3 in phase II and III are consistent with earlier reported values, as shown in Table S2. A similar experiment using only KNO_3 was performed with the same results; therefore it is possible to postulate that KNO_3 crystallizes from a solution containing K^+ and NO_3^- first in phase III and on contact of the crystal with air, there is a phase transition to phase II. Xu and Schweiger[47] reported a similar phase transition for Na_2SO_4, which crystallizes from a saturated solution in phase III and transforms to phase V (stable at room temperature). Finally, at $t = 332$ s, the Raman spectrum shows bands of KNO_3 and $NaNO_3$ in phase II. At this point, all water was eliminated; because of the high solubility of $NaNO_3$ in water and the small size of the solution droplet used in this experiment, the time between the crystallization of $NaNO_3$ and the complete elimination of water was very short (≤ 2 s). When solutions of $NaNO_3$ and KNO_3 are vaporized at room temperature and the salt residue is milled, the resulting particles are salt mixtures and their Raman spectra show bands of the two individual compounds in variable proportions (see sample spectra in Figs S1–S3), but this does not apply for all systems.

When recording the Raman spectra of individual particles of the milled residue obtained during the total vaporization process of solutions containing $NaNO_3$ and Na_2SO_4, we observed two strong bands at 1060 and 993 cm^{-1} (in most of the cases). These values are different from the characteristic values observed for Na_2SO_4 (SO_4^{2-} ν_1 at 989 cm^{-1}) and $NaNO_3$ (NO_3^- ν_1 at 1065 cm^{-1}), but they are equal to the values observed in the unpolarized spectra of synthetic $Na_3(NO_3)$ $(SO_4) \cdot H_2O$. The Raman spectra of two individual particles obtained by room temperature vaporization of an equimolar solution of $NaNO_3$ and Na_2SO_4 and subsequent milling, are shown in Figs S4 and S5. Note that both particles are composed mostly of darapskite containing $NaNO_3$ as an impurity.

The mixed salt $Na_3(NO_3)(SO_4) \cdot H_2O$ crystallizes at room temperature from solutions containing those three ions. $Na_3(NO_3)(SO_4) \cdot H_2O$ is present in nature as a mineral called darapskite, which was also found by Holtkamp and Heijnen[48] in the efflorescent salts on the walls of two churches in The Netherlands; in this case, its presence was attributed to moisture transport. Darapskite has also been found in atmospheric particles, and Harrison and Sturges attributed its occurrence to acid attack upon marine NaCl.[11] On the basis of our experiments, we believe that the formation mechanism may not be as complex as Harrison and

Sturges presumed and that simple dissolution–crystallization processes can explain the formation of darapskite (and other mixed salts) in the atmosphere.

Darapskite crystallizes in a monoclinic system with the space group $P2_1/m$ and has two molecules in the unit cell. In the crystal, the SO_4^{2-} and NO_3^- ions, and the H_2O molecules, occupy sites of lower symmetry than their free-ion and molecular symmetry, respectively.

According to the results of the X-ray diffraction analysis reported by Redden,[49] all the SO_4^{2-} and NO_3^- ions and the H_2O molecules in the unit cell occupy special positions. In the case of the six Na^+ ions present in the unit cell, four of them are in general positions and two are in special positions. The correlation for the fundamental modes of the SO_4^{2-} and NO_3^- ions (T_d and D_{3h}, respectively) and the H_2O molecule (C_{2v}) with the site of symmetry C_s and the unit-cell symmetry C_{2h}, are shown in Fig. S6.

Considering the results obtained by applying the correlation method,[50] 90 fundamental modes (including the acoustic modes) are expected and split into

$$\Gamma_{90} = 27A_g + 18B_g + 18A_u + 27B_u$$

The species with subscript g are Raman active, while the species with subscript u are infrared active. A summary of the vibrational analysis of the darapskite crystal is shown in Table 1.

The polarized Raman spectroscopic study of a darapskite single crystal allows the identification of different signals observed in the Raman spectrum and their assignment to symmetry species characteristic from the crystal factor group (C_{2h}). The band assignments of the polarized Raman spectra and the infrared spectrum are presented in Table 2.

It is important to note that the factor group C_{2h}, according to the character table,[50] has a center of inversion, i therefore it is not possible that Raman and infrared bands show the same frequency (rule of mutual exclusion). This characteristic is useful for the assignment of bands of species with subscript u, because they are only infrared active. However, as to the symmetric bending, the asymmetric stretching, and the asymmetric bending of SO_4^{2-}, it was not possible to specify if the bands belong to the A_u or B_u.

Two strong bands are expected for the ν_1 mode of NO_3^- and SO_4^{2-} and they belong to the symmetry species A_g. Taking into account the Raman activities shown in Table 1, we observed two strong bands assigned to NO_3^- and SO_4^{2-} ν_1 (A_g) at 1059 and 993 cm^{-1}, respectively, in polarized Raman spectra xx, yy, zz, and yz, and weak signals in polarized Raman spectra xy and xz. According to the character table for C_{2h} presented by Fateley et al.,[50] the Raman spectra xx, yy, zz, and xy show bands of species A_g while xz and yz show bands of species B_g. This apparent inconsistence observed in the xy and yz spectra can be

Table 1. Vibrational analysis of darapskite, $Na_3(NO_3)(SO_4) \cdot H_2O$

C_{2h}	N	T_A	T	R	SO_4^{2-}				W	NO_3^-				Activity[a]
					ν_1	ν_2	ν_3	ν_4		ν_1	ν_2	ν_3	ν_4	
A_g	27	0	11	3	1	1	2	2	2	1	0	2	2	$\alpha_{xx}, \alpha_{yy}, \alpha_{zz}, \alpha_{yz}$
B_g	18	0	7	6	0	1	1	1	1	0	1	0	0	α_{xy}, α_{xz}
A_u	18	1	6	6	0	1	1	1	1	0	1	0	0	T_z
B_u	27	2	9	3	1	1	2	2	2	1	0	2	2	T_x, T_y

N, total number of vibrations; T_A, acoustic modes; T, translational modes; R, rotational modes; W, internal H_2O modes; ν_i, internal SO_4^{2-} and NO_3^- modes.
[a]More details in the text.

Table 2. Vibrational spectra data and band assignments (cm^{-1}) of darapskite, $Na_3(NO_3)(SO_4) \cdot H_2O$

	Raman[a]					IR[a]	Assignments
xx	*yy*	*zz*	*xy*	*yz*	*xz*		
						1429 s	NO_3^- ν_3 (B_u)
1418 vw	1417 w	1417 vw		1417 w			NO_3^- ν_3 (A_g)
						1384 vs	NO_3^- ν_3 (B_u)
	1353 w	1353 vw		1353 w			NO_3^- ν_3 (A_g)
			1172 m		1172 w		SO_4^{2-} ν_3 (B_g)
						1160 vs	SO_4^{2-} ν_3 (A_u or B_u)
1123 m	1123 vw	1122 vw		1123 vw			SO_4^{2-} ν_3 (A_g)
						1117 vs	SO_4^{2-} ν_3 (A_u or B_u)
1085 vw	1084 w	1084 vw		1084 w			SO_4^{2-} ν_3 (A_g)
						1063 vw	NO_3^- ν_1 (B_u)
1060 m	1059 vs	1059 vs	1060*	1059 vs	1058*		NO_3^- ν_1 (A_g)
						997 w	SO_4^{2-} ν_1 (B_u)
993 vs	993 s	993 s	992*	992 s	992*		SO_4^{2-} ν_1 (A_g)
						831 m	NO_3^- ν_2 (A_u)
						732 vw	NO_3^- ν_4 (B_u)
	729 w	729 w		729 m			NO_3^- ν_4 (A_g)
	707 w	707 w		707 w			NO_3^- ν_4 (A_g)
640 m	640 w	640 vw		640 w			SO_4^{2-} ν_4 (A_g)
			638 m		637 w		SO_4^{2-} ν_4 (B_g)
						624 s	SO_4^{2-} ν_4 (A_u or B_u)
620 vw	620 w	620 w		619 w			SO_4^{2-} ν_4 (A_g)
						486 w	SO_4^{2-} ν_2 (A_u or B_u)
474 vw	473 vw	473 vw		473 w			SO_4^{2-} ν_2 (A_g)
						466 w	SO_4^{2-} ν_2 (A_u or B_u)
			456 m		457 w		SO_4^{2-} ν_2 (B_g)

[a] Relative intensities: vs, very strong; s, strong; m, medium; w, weak; vw, very weak.
* Weak bands assigned to symmetry species A_g

explained considering the orientation of the C_2 symmetry axis. The C_2 axis lies along the Z axis in the example presented by Fateley *et al.*[50] while, in case of darapskite, the C_2 axis is parallel to the X axis.

With these considerations, we propose the assignment of A_g species taking into account the activities in polarized Raman spectra *xx*, *yy*, *zz*, and *yz*; furthermore, B_g species are related with activities in polarized Raman spectra *xy* and *xz*. All polarized
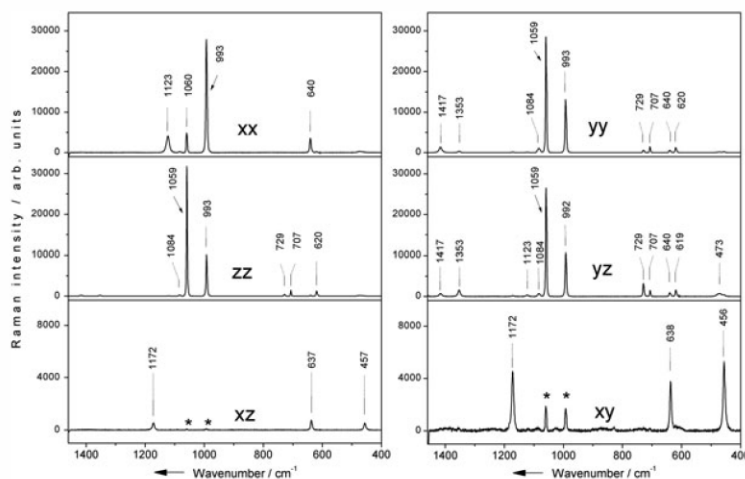
Figure 2. Polarized Raman spectra of darapskite, $Na_3(NO_3)(SO_4) \cdot H_2O$. (* Weak bands assigned to symmetry species A_g).

Origin of salt mixtures and mixed salts in atmospheric particulate matter

Journal of RAMAN SPECTROSCOPY

Raman spectra are shown in Fig. 2. The Raman and infrared spectra of darapskite powder are shown in Fig. S7. The infrared spectrum (Fig. S7) shows the same features as the spectrum reported earlier by Ericksen and Mrose.[30]

Conclusions

Using Raman spectroscopy, it was possible to monitor the crystallization process that takes place within a droplet of solution containing $NaNO_3$ and KNO_3, and to observe a phase transition from KNO_3 (III) to KNO_3 (II). The generated salt mixtures can have variable proportions of both salts, and their Raman spectra show clearly the characteristic bands of individual compounds.

Vaporization experiments of solutions containing $NaNO_3$ and Na_2SO_4 performed at room temperature show the occurrence of the mixed salt darapskite.

Synthetic darapskite has been obtained according to a previously reported method and the polarized Raman spectra were recorded. Using the Raman and infrared spectra of darapskite, the assignment of the detected bands was proposed.

Taking into account the occurrence of SO_4^{2-}, NO_3^-, Na^+, and K^+ reported several times in earlier works, we proposed the possible generation of both salt mixtures and mixed salts in atmospheric particulate matter considering water as the fundamental factor. Therefore, salt mixtures originating from the $NaNO_3$–KNO_3 system and the mixed salt darapskite, should be considered in future atmospheric studies.

Supporting Information

Supporting information may be found in the online version of this article.

References

[1] H. Bao, S. Yu, D. Q. Tong, *Nature* **2010**, *465*, 909.
[2] M. Y. Iwasaka, R. Imasu, A. Ono, *Tellus B* **1988**, *40*, 494.
[3] S. Rodríguez, X. Querol, A. Alastuey, G. Kallos, O. Kakaliagou, *Atmos. Environm.* **2001**, *35*, 2433.
[4] B. Artíñano, P. Salvador, D. G. Alonso, X. Querol, A. Alastuey, *Environ. Pollut.* **2003**, *125*, 453.
[5] X. Querol, A. Alastuey, S. Rodríguez, M. M. Viana, B. Artíñano, P. Salvador, E. Mantilla, S. García do Santos, R. Fernandez Patier, J. de La Rosa, A. Sanchez de la Campa, M. Menéndez, J. J. Gil, *Sci. Total. Environ.* **2004**, *334–335*, 359.
[6] G. G. C. Claridge, I. B. Campbell, *Nature* **1968**, *217*, 428.
[7] T. H. Misselbrook, T. J. Van Der Weerden, B. F. Pain, S. C. Jarvis, B. J. Chambers, K. A. Smith, V. R. Phillips, T. G. M. Demmers, *Atmos. Environm.* **2000**, *34*, 871.

[8] T. T. Canh, A. J. A. Aarnink, J. B. Schutte, A. Sutton, D. J. Langhout, M. W. A. Verstegen, *Livest. Prod. Sci.* **1998**, *56*, 181.
[9] I. Rodríguez, S. Gali, C. Marcos, *Environ. Geol.* **2009**, *56*, 1551.
[10] R. Voigt, K. H. Lieser, *Naturwissenschaften* **1984**, *71*, 377–378.
[11] R. M. Harrison, W. T. Sturges, *Atmos. Environm.* **1984**, *18*, 1829.
[12] D. W. Gunz, M. R. Hoffmann, *Atmos. Environm. A* **1990**, *24*, 1601.
[13] J. P. Lodge Jr., J. B. Pate, *Science* **1966**, *22*, 408.
[14] R. W. Boudel, D. L. Fox, D. B. Turner, A. C. Stern, Fundamentals of Air Pollution, Academic Press, U.S.A., **1973**.
[15] S. S. Abdalmogith, R. M. Harrison, *Atmos. Environm.* **2005**, *39*, 6686.
[16] D. Sopauskiene, D. Budvytyte, *Atmos. Environm.* **1994**, *28*, 1291.
[17] G. Wang, H. Wang, Y. Yu, S. Gao, J. Feng, S. Gao, L. Wang, *Atmos. Environm.* **2003**, *37*, 2893.
[18] M. O. Andreae, C. D. Jones, P. M. Cox, *Nature* **2005**, *435*, 1187.
[19] A. Arneth, N. Unger, M. Kulmala, M. O. Andreae, *Science* **2009**, *326*, 672.
[20] D. T. Shindell, G. Faluvegi, D. M. Koch, G. A. Schmidt, N. Unger, S. E. Bauer, *Science* **2009**, *326*, 716.
[21] E. E. Gard, M. J. Kleeman, D. S. Gross, L. S. Hughes, J. O. Allen, B. D. Morrical, D. P. Fergenson, T. Dienes, M. E. Gälli, R. J. Johnson, G. R. Cass, K. A. Prather, *Science* **1998**, *279*, 1184.
[22] G. Schweiger, *J. Aerosol Sci.* **1989**, *20*, 1621.
[23] K. H. Fung, D. G. Imre, I. N. Tang, *J. Aerosol Sci.* **1994**, *25*, 479.
[24] M. Trunk, J. Popp, I. Hartmann, M. Lankers, E. Urlaub, W. Kiefer, *Fresenius J. Anal. Chem.* **1996**, *355*, 354.
[25] M. Trunk, J. Popp, W. Kiefer, *Chem. Phys. Lett.* **1998**, *284*, 377.
[26] J. Musick, J. Popp, M. Trunk, W. Kiefer, *Appl. Spectrosc.* **1998**, *52*: 692.
[27] J. Musick, J. Popp, W. Kiefer, *J. Raman Spectrosc.* **2000**, *31*, 217.
[28] Y. Batonneau, S. Sobanska, J. Laureyns, C. Bremard, *Environ. Sci. Technol.* **2006**, *40*, 1300.
[29] W. Schumacher, M. Kühnert, P. Rösch, J. Popp, *J. Raman Spectrosc.* **2011**, *42*, 383.
[30] G. E. Ericksen, M. E. Mrose, *Am. Mineralogist* **1970**, *55*, 1500.
[31] R Development Core Team, R: A language and environment for statistical computing, R Foundation for Statistical Computing, Vienna, **2009**.
[32] T. Dörfer, T. Bocklitz, N. Tarcea, M. Schmitt, J. Popp, *Z. Phys. Chem.* **2011**, *225*, 753.
[33] Z.-M. Zhang, S. Chen, Y. Z. Liang, Z.-X. Liu, Q. M. Zhang, L. X. Ding, F. Ye, H. Zhou, *J. Raman Spectrosc.* **2010**, *41*, 659.
[34] A. T. Wilson, *Nature* **1959**, *184*, 99.
[35] M. P. Tolocka, T. D. Saul, M. V. Johnston, *J. Phys. Chem. A* **2004**, *108*, 2659.
[36] H. B. Singh, *Environ. Sci. Technol.* **1987**, *21*, 320.
[37] J. Dignon, *Atmos. Environm. A* **1992**, *26*, 1157.
[38] S. Li, J. Matthews, A. Sinha, *Science* **2008**, *319*, 1657.
[39] J. R. Sanghvi, *Int. J. Energy Environ.* **2008**, *2*, 16.
[40] B. J. M. Rajkumar, V. Ramakrishnan, R. K. Rajaram, *Spectrochim. Acta A* **1998**, *54*, 1527.
[41] K. L. Teo, Z. X. Shen, M. H. Kuok, S. H. Tang, *J. Mol. Struct.* **1993**, *294*, 163.
[42] D. L. Rousseau, R. E. Miller, *J. Chem. Phys.* **1968**, *48*, 3409.
[43] M. H. Brooker, *J. Phys.Chem. Solids* **1978**, *39*, 657.
[44] M. Balkanski, M. K. Teng, M. Nusimovici, *Phys. Rev.* **1968**, *176*, 1098.
[45] Z. X. Shen, W. F. Sherman, *J. Mol. Struct.* **1991**, *247*, 397.
[46] R. Murugan, P. J. Huang, A. Ghule, H. Chang, *Thermochim. Acta* **2000**, *346*, 83.
[47] B. Xu, G. Schweiger, *J. Aerosol Sci.* **1999**, *30*, S379.
[48] M. H. P. C. Holtkamp, W. M. M. Heijnen, *Stud. Conserv.* **1991**, *36*, 175.
[49] M. J. Redden, The crystal structure of darapskite, Master Thesis, Massachusetts Institute of Technology, U.S.A., **1968**.
[50] W. G. Fateley, F. R. Dollish, N. T. McDevitt, F. F. Bentley, Infrared and Raman selection rules for molecular and lattice vibrations: The Correlation Method, Wiley-Interscience, U.S.A., **1972**.

519

2.3 Raman spectroscopic study of calcium mixed salts of atmospheric importance [PV3]

Authorship of Publication

Paul Vargas Jentzsch: concept development

mixed salts preparation

experiments of crystallization within droplets

factor group analysis and bands assigment

writing of manuscript

Ralph Michael Bolanz: X-ray diffraction measurements

discussion of results

Valerian Ciobotă: Raman and infrared measurements

discussion of experimental concept and results

Bernd Kampe: Raman spectra processing

Petra Rösch: discussion of experimental concept and results

proofreading of manuscript

Juraj Majzlan: discussion of results

proofreading of manuscript

Jürgen Popp: project management

discussion of concepts and results

discussion and proofreading of manuscript

Raman spectroscopic study of calcium mixed salts of atmospheric importance

Paul Vargas Jentzsch[a], Ralph Michael Bolanz[b], Valerian Ciobotă[a], Bernd Kampe[a], Petra Rösch[a], Juraj Majzlan[b], Jürgen Popp[a,c,*]

[a] Institut für Physikalische Chemie, and Abbe Center of Photonics, Friedrich-Schiller-Universität Jena, D-07743 Jena, Germany
[b] Institut für Geowissenschaften, Friedrich-Schiller-Universität Jena, D-07749 Jena, Germany
[c] Institut für Photonische Technologien e.V. (IPHT), D-07745 Jena, Germany

ARTICLE INFO

ABSTRACT

The atmospheric particulate matter contains organic and inorganic components of both natural and anthropogenic origin. It is well-known that ions such as Na$^+$, K$^+$, Ca^{2+}, Mg^{2+}, NH$_4^+$, and SO$_4^{2-}$, occur in atmosphere, therefore the formation of simple and mixed salts as a consequence of dissolution–precipitation processes within water droplets, e.g., in fog or haze, is also possible. Considering the known occurrence in atmosphere of mixed salts such as K$_2$Ca(SO$_4$)$_2$·H$_2$O (syngenite), (NH$_4$)$_2$Ca(SO$_4$)$_2$·H$_2$O (koktaite), Na$_2$Ca(SO$_4$)$_2$ (glauberite), and K$_2$Ca$_2$Mg(SO$_4$)$_4$·2H$_2$O (polyhalite), more specific studies should elucidate their origin and environmental implications. This contribution presents the Raman spectroscopic study of the mentioned calcium-mixed salts. Based on experiments using single solution droplets, the atmospheric origin of syngenite and koktaite are postulated. The atmospheric origin of glauberite and polyhalite are discussed considering the characteristics of atmosphere as well as some principles usually used to explain the precipitation of minerals in evaporite deposits.

© 2012 Elsevier B.V. All rights reserved.

1. Introduction

At present, topics regarding atmospheric pollution are acquiring growing importance worldwide. Special concern is focused on atmospheric particles, because they can not only be inhaled and retained by the human respiratory system, but they have also a climate impact. It is recognized by many authors that atmospheric particles affect the weather and climate by direct and indirect influence on the incoming solar radiation (radiation absorption of particles and cloud droplets generated by condensation on particles), as well as their influence on the cloud lifetime [1,2]. Therefore, it is necessary to analyze the chemical composition of the atmospheric particulate matter, in order to know the associated implications.

The well-known occurrence of ions in atmosphere is attributed to both natural and anthropogenic sources. Many researchers reported variable concentrations of ions in the atmosphere of urban and rural areas using different methods [3–9]. Other authors studied not only the elemental composition, but also the chemical form in which these elements occur in atmospheric particles, reporting the occurrence of mixed salts in atmospheric particles [10–13], but the atmospheric origin of these compounds still remains unclear. The oceans are important contributors of ions to atmosphere;

according to values published by Preining [14], the sea salt emissions represent around 25% of the global production of aerosols. Most of the researchers agree that the observed composition of atmospheric particles (specially in coastal areas) is the result of the interaction of ocean-born ions with terrigenous material as well as some anthropogenic compounds [12,13,15], therefore the salts containing the ions Ca^{2+}, Mg^{2+}, Na$^+$, K$^+$, NH$_4^+$, and SO$_4^{2-}$ are of special importance and the implications of their atmospheric occurrence should be evaluated. Na$_2$Ca(SO$_4$)$_2$ (glauberite), K$_2$Ca(SO$_4$)$_2$·H$_2$O (syngenite), (NH$_4$)$_2$Ca(SO$_4$)$_2$·H$_2$O (koktaite), and K$_2$Ca$_2$Mg(SO$_4$)$_4$·2H$_2$O (polyhalite) have been reported in atmospheric particles by many studies [10,12,15–18]. Only a few attempts have been made to explain the origin of these specific mixed salts in atmospheric particles. Xie et al. [17,18] postulated that airborne K$_2$Ca(SO$_4$)$_2$·H$_2$O (syngenite) particles may be formed during coal combustion and/or as a consequence of cement production. Mori et al. [19] presented evidence of the reaction of an Asian dust particle (kosa) with (NH$_4$)$_2$SO$_4$ to produce (NH$_4$)$_2$Ca(SO$_4$)$_2$·H$_2$O (koktaite), and afterwards Ca(SO$_4$)$_2$·2H$_2$O (gypsum).

Taking into account that water is one of the most important tropospheric components, it is also expected to interact with other natural or anthropogenically generated compounds released to the atmosphere. Can water (liquid or vapor) participate in the formation process of some mixed salts? Apparently, this is possible, since Del Monte and Rossi [20] showed that (NH$_4$)$_2$Ca(SO$_4$)$_2$·H$_2$O and other mixed salts crystallized from fog water collected under

controlled laboratory vaporization conditions. We believe that similar vaporization processes can take place in airborne droplets and thus originate mixed salts depending on the specific ion composition.

Most of the published investigations of mixed salts in atmospheric particles were based on the analytical method of X-ray diffractometry, but Raman spectroscopy can also be used. In fact, several investigations using Raman spectroscopy reported the suitability of this technique for chemical characterization of atmospheric particles [21–30], and even the possibility to distinguish between organic and inorganic material [31].

In this contribution, we postulate the formation of syngenite and koktaite in atmosphere on the basis of our vaporization experiments of single solution droplets. Taking into account that Na^+ and Mg^{2+} are also usually found in atmospheric liquid water, the formation of $Na_2Ca(SO_4)_2$ (glauberite) and $K_2Ca_2Mg(SO_4)_4 \cdot 2H_2O$ (polyhalite) is discussed. The Raman spectra of these compounds are presented and the band assignment for each case is proposed.

2. Materials and methods

2.1. Chemicals and mixed salts synthesis

Sodium sulfate anhydrous, Na_2SO_4 ($\geq$99.0%), sodium chloride, NaCl (min. 99.5%), potassium sulfate, K_2SO_4 ($\geq$99.0%), ammonium sulfate, $(NH_4)_2SO_4$ ($\geq$99.0%), and calcium sulfate dihydrate, $CaSO_4 \cdot 2H_2O$ were purchased from Sigma–Aldrich, while calcium carbonate, $CaCO_3$ ($\geq$99.0%) was purchased from Merck. These reactants were used without further purification. Magnesium sulfate anhydrous (min. 99.5%) purchased from VWR was dried in an oven at 250 °C during 2 h before use, due to its high hygroscopicity.

Syngenite, $K_2Ca(SO_4)_2 \cdot H_2O$ was crystallized at room temperature (20 °C) by evaporation of a solution containing $CaSO_4$ and K_2SO_4 in a molar ratio of 1:50. Koktaite, $(NH_4)_2Ca(SO_4)_2 \cdot H_2O$ was obtained by two methods: (1) crystallization at 100 °C from a solution containing $CaSO_4$ and $(NH_4)_2SO_4$ in a molar ratio of 1:92, which is in agreement with the equilibrium data reported by Hill and Yanick [32]; and (2) method reported by Mori et al. [19], consisting of the exposition of a powder mixture containing 2.00 g of $CaCO_3$ and 2.64 g of $(NH_4)_2SO_4$ (molar ratio 1:1) to humid air (relative humidity 70%) at 23 °C during one day. Glauberite, $Na_2Ca(SO_4)_2$ was crystallized at 70 °C by controlled evaporization of a solution containing 28.39 g of Na_2SO_4, 0.10 g of $CaSO_4 \cdot 2H_2O$ and 8.18 g of NaCl in 120 ml of distilled water. The vaporization of this mixture generates a solution with salt concentrations within the expected range for glauberite crystallization [33].

Polyhalite, $K_2Ca_2Mg(SO_4)_4 \cdot 2H_2O$ was crystallized at 100 °C by controlled evaporation of a solution containing 5 g of $MgSO_4$, 5 g of K_2SO_4 and 0.2 g of $CaSO_4 \cdot 2H_2O$ in 250 ml of distilled water.

2.2. Crystallization within a droplet: the systems $CaSO_4$–K_2SO_4 and $CaSO_4$–$(NH_4)_2SO_4$

Individual saturated solutions containing $CaSO_4$ and K_2SO_4 (molar ratio 1:50), and $CaSO_4$ and $(NH_4)_2SO_4$ (molar ratio 1:50), respectively, were prepared and a droplet (diameter $\leq$1 mm) of these solutions was placed on separated microscope slides. In order to induce the crystallization, the droplet on the microscope slide was vaporized for a few minutes under room conditions (20 °C and $\sim$50% relative humidity). In each case, the Raman spectrum of the first crystal occurring in the solution was recorded and the following spectra were obtained during the water vaporization process until the droplet was dry.

2.3. Spectroscopic instrumentation and data processing

The Raman spectra were recorded with a micro-Raman setup (HR LabRam inverse system, Jobin Yvon Horiba). Raman scattering was excited by a frequency-doubled Nd:YAG laser at a wavelength of 532 nm with a laser power incident on the sample of about 2 mW. The laser beam was focused on individual crystals or particles using Olympus 50× (0.5 NA) and Zeiss 100× (0.75 NA) microscope objectives, for the crystallization study within the droplet and to record the Raman spectra of the synthetic mixed salts, respectively. The dispersive spectrometer has an entrance slit of 100 μm and a focal length of 800 mm and is equipped with a grating of 600 or 1200 lines mm^{-1} (spectral resolution $\sim$3 or $\sim$1.5 cm^{-1}, respectively), depending on the case. For the Raman spectroscopic study within droplets, the grating used was 600 lines mm^{-1}. The measurements of individual particles of synthetic mixed salts were performed using unpolarized radiation and the grating of 1200 lines mm^{-1}, in order to evaluate the bands (wavenumbers) in their spectra. The Raman scattered light was detected by a CCD camera operating at 220 K. The acquisition time per spectrum of 5 s and 10 s, when the gratings of 600 and 1200 lines mm^{-1}, respectively, were used. For the calibration procedure, titanium dioxide (anatase) and 4-acetamidophenol (4AAP) were measured daily as a reference control for subsequent data pre-processing.

All spectroscopic data were processed using the "R" software [34]. A minimum of 50 Raman spectra of each mixed salt (syngenite, koktaite, glauberite and polyhalite) were collected and the average spectra obtained. For all spectra, a background reduction was performed using R package baselineWavelet, and the calibration procedure was completed performing a shift correction with 4AAP using an R script [35,36].

2.4. FT-IR measurements

The infrared spectroscopic measurements were carried out using a Bruker IFS66 FTIR spectrometer. The spectra were registered with a spectral resolution of 4 cm^{-1} within the 400–6000 cm^{-1} range. The transmission measurements at normal incidence were performed on a pellet of the milled mixed salt (syngenite and koktaite) dispersed in a KBr host matrix.

2.5. XRD

X-ray diffractometry was carried out with a Bruker D8 Advance DaVinci diffractometer, employing Cu Kα radiation ($\lambda = 1.54060$ Å) and a LYNXEYE 1-D detector. The patterns were collected at room temperature between 5 and 90°2θ, with a step size of 0.02°2θ and a time per step of 0.2 s.

3. Results and discussion

3.1. Preparation aspects and identity of calcium mixed salts

The obtained $K_2Ca(SO_4)_2 \cdot H_2O$ showed a texture similar to glass-wool, while $(NH_4)_2Ca(SO_4)_2 \cdot H_2O$ (from method 1) crystallized as fine needles of a few mm length. In both cases, the separation from the solution by decantation and/or using a spatula is easy. $K_2Ca(SO_4)_2 \cdot H_2O$ can be washed with small amounts of cold water and dried at room temperature, but $(NH_4)_2Ca(SO_4)_2 \cdot H_2O$ not. Any attempt to wash $(NH_4)_2Ca(SO_4)_2 \cdot H_2O$ with water results in the decomposition of the mixed salt to produce $(NH_4)_2SO_4$ and $CaSO_4 \cdot 2H_2O$, and even the exposition of this mixed salt during a few hours to environmental humid air may result in its decomposition. For the specific case of the separation of $(NH_4)_2Ca(SO_4)_2 \cdot H_2O$ from its mother liquor, we recommend the removal of crystals with a

spatula and the fast and careful drying of those needle-shaped crystals with an absorbent paper tissue. The identity of the obtained $K_2Ca(SO_4)_2 \cdot H_2O$ and $(NH_4)_2Ca(SO_4)_2 \cdot H_2O$ (method 1) was confirmed by powder X-ray diffraction measurements. The recorded X-ray diffraction patterns are shown in Figs. S1 and S2 (Supplementary data).

We used method 2 for the $(NH_4)_2Ca(SO_4)_2 \cdot H_2O$ preparation for comparative purposes; the resulting bulk substance is a mixture of $(NH_4)_2Ca(SO_4)_2 \cdot H_2O$ with unreacted $CaCO_3$ and $(NH_4)_2SO_4$. In this mixture, small elongated crystals of just a few μm were identified as $(NH_4)_2Ca(SO_4)_2 \cdot H_2O$ and their Raman spectra show the same features observed in the Raman spectra of the crystals obtained by method 1.

Both $Na_2Ca(SO_4)_2$ and $K_2Ca_2Mg(SO_4)_4 \cdot 2H_2O$ crystallize as a white powder. The identity of the obtained $Na_2Ca(SO_4)_2$ and $K_2Ca_2Mg(SO_4)_4 \cdot 2H_2O$ was confirmed by powder X-ray diffraction measurements (the recorded X-ray diffraction patterns are shown in Figures S3 and S4 of Supplementary data). Nevertheless, in the case of these two mixed salts, small amounts of an impurity identified as $CaSO_4 \cdot 2H_2O$ were detected in the bulk substance, probably produced during the separation of these compounds from the mother liquor. The separation of $Na_2Ca(SO_4)_2$ and $K_2Ca_2Mg(SO_4)_4 \cdot 2H_2O$ from their hot mother liquor is critical because a washing step with a small amount of cold water is required, otherwise important amounts of soluble sulfate salts like Na_2SO_4, K_2SO_4 and $MgSO_4 \cdot 7H_2O$ can remain as impurities in the final solid dried material. The case of $K_2Ca_2Mg(SO_4)_4 \cdot 2H_2O$ is specially sensible, since solutions containing high concentrations of $MgSO_4$ tend to form a "gel" [37] of high viscosity at room temperature; therefore, high amounts of solution can be incorporated to the mixed salt powder during the separation. Soluble salt residues can be efficiently removed by washing $Na_2Ca(SO_4)_2$ and $K_2Ca_2Mg(SO_4)_4 \cdot 2H_2O$ powders, but small amounts of the mixed salts are dissolved as well. Considering the fact that these salts have incongruent solubility, the observed $CaSO_4 \cdot 2H_2O$ can be explained and expected as a consequence of the washing and drying steps. In order to verify the stability of $Na_2Ca(SO_4)_2$ and $K_2Ca_2Mg(SO_4)_4 \cdot 2H_2O$, Raman measurements were performed in the obtained mixed salts after five months' storage in sealed flasks; the Raman spectra in both cases showed no changes.

3.2. Vibrational study: factor group analysis

In order to understand the formation of the calcium mixed salts, first the Raman spectrum of each pure mixed salt has to be studied, since the characteristic signals observed in these spectra are the basis of the Raman spectroscopic analysis.

The most intense bands expected in the Raman spectra of sulfate salts are related with vibrations of the sulfate ion (SO_4^{2-}). Considering the free ion symmetry of SO_4^{2-} (T_d), there are four normal modes of vibration: ν_1 (A_1) symmetric stretching, ν_2 (E) symmetric bending, ν_3 (F_2) asymmetric stretching, and ν_4 (F_2) asymmetric bending, all of them are Raman active. The stretching modes usually occur in the 950–1200 cm^{-1} region, and the bending modes appear in the 400–650 cm^{-1} region [38]. The feature produced by the ν_1 (A_1) mode is expected to be the most intense. As a consequence of the elimination of degeneration, a splitting of the SO_4^{2-} modes is expected in the Raman spectrum of sulfate crystals.

$K_2Ca(SO_4)_2 \cdot H_2O$ is present in nature as a mineral called syngenite, which crystallizes in a monoclinic system with the space group $P2_1/m$ (C^2_{2h}) and has two molecules in the unit cell [39]. Syngenite has also been found as a component of efflorescent salts on buildings, as in the case of the efflorescence found at the "Deutscher Dom" (German Cathedral) in Berlin during restoration works [40]. From the engineering point of view, syngenite was considered for a long time as an important industrial chemical because it is

an intermediate in the production process of potassium sulfate as well as fertilizers from polyhalite [41,42]. With regard to the cement industry, Smillie and coworkers have postulated that the presence and formation of syngenite can affect the freshness of stored cement [43]. In addition, the formation of syngenite was observed by Kloprogge and coworkers during the treatment of manure with sulfuric acid [44,45].

According to the crystal structure data of syngenite reported by Corazza and Sabelli [39], all K$^+$ ions occupy general positions. Ca^{2+} and SO_4^{2-} ions, as well as H_2O molecules, occupy special positions. The correlation for the fundamental modes of the SO_4^{2-} ion (T_d) and the H_2O molecule (C_{2v}) with the site of symmetry C_s and the unit-cell symmetry C_{2h}, are shown in Fig. S5 (Supplementary data).

Considering the results obtained for syngenite using the Correlation Method [46], 96 fundamental modes (including the acoustic modes) are expected and split into

$$\Gamma_{96} = 28A_g + 20B_g + 20A_u + 28B_u$$

The species with subscript g are Raman active, while the species with subscript u are infrared active. According to this analysis, the four fundamental modes of the free ion SO_4^{2-} split into the following 18 fundamental Raman active modes, due to factor group interactions: two for ν_1 (A_g), four for ν_2 (2 A_g and 2 B_g), six for ν_3 (4 A_g and 2 B_g), and six for ν_4 (4 A_g and 2 B_g). However, not necessarily all components are expected to appear. The average spectrum of syngenite (Fig. 1a) shows two strong bands at 1003 and 979 cm^{-1}, which are assigned to SO_4^{2-} ν_1. However, if all SO_4^{2-} ions in the unit cell are in the site of symmetry C_s, and the two calculated modes of ν_1 belong both to the symmetry species A_g, why does ν_1 split into two bands in the Raman spectra? The explanation seems to be in the "nature" of the complexes generated by the sulfur tetrahedra. The sulfur tetrahedra occupy two different crystallographic sites, and this is why two bands appear in the Raman spectrum. The other bands observed in the average Raman spectrum of syngenite (Fig. 1a) are listed in Table 1 and all these wavenumbers are in good agreement with the values reported previously by Kloprogge et al. for syngenite obtained by reaction of manure with sulfuric acid [44]. The bands observed in the infrared spectrum of syngenite (Fig. S6, Supplementary data) are listed in Table 1 and are in good agreement with the values previously reported for synthetic syngenite [47].

$(NH_4)_2Ca(SO_4)_2 \cdot H_2O$ is present in nature as a mineral called koktaite, which crystallizes in a monoclinic system with the space group $P2_1/m$ (C^2_{2h}) and has two molecules in the unit cell [48]. It is also commonly referred to as "ammonium syngenite" due to its structural similarities with syngenite; this compound has important applications in the fertilizing industry [49,50].

Taking into account that koktaite is isostructural with syngenite [48], the SO_4^{2-} and Ca^{2+} ions, as well as H_2O molecules occupy special positions, while NH$_4^+$ ions occupy general positions. The correlation for the fundamental modes of the SO_4^{2-} ion (T_d), NH$_4^+$ ion (T_d), and the H_2O molecule (C_{2v}) with the site of symmetry (C_s for SO_4^{2-} ions and H_2O molecules, C_1 for NH$_4^+$ ions) and the unit-cell symmetry C_{2h}, are shown in Fig. S7 (Supplementary data).

Considering the results obtained for koktaite using the Correlation Method [46], 144 fundamental modes (including the acoustic modes) are expected and split into

$$\Gamma_{144} = 40A_g + 32B_g + 32A_u + 40B_u$$

As for the case of syngenite, the four fundamental modes of the free ion SO_4^{2-} split into 18 fundamental Raman active modes and two strong bands (996 and 980 cm^{-1}) for ν_1 are expected to appear in the Raman spectrum. According to the factor group analysis, the four fundamental modes of the free ion NH$_4^+$ split into the following 18 fundamental Raman active modes, due to factor

Table 1
Raman and infrared signals (cm^{-1}) of syngenite, koktaite, glauberite and polyhalite.

Syngenite[a]		Koktaite		Glauberite	Polyhalite[b]	Assignment
Raman	IR	Raman	IR	Raman	Raman	
					3437	H_2O sym. and asym. stretching
3388	3336(3377)	3353				
3310	3319(3248)				3288	
		3149	3192			NH_4^+ stretching (for the case of koktaite)[c]
			3125			
		2852	2922sh			
			2857			
		1723	1733			NH_4^+ bending (ν_2)
	1676	1677	1662sh			H_2O bending (ν_2)
	1632(1631)		1636			
	1452 ?	1453	1457sh			NH_4^+ bending (ν_4)
		1419	1402			
	1192(1193)				1181	SO_4^{2-} asym. stretching (ν_3)
1164(1166)			1177	1167	1165	
1140(1138)	1140(1148)	1153		1154	1144	
		1132	1131	1138	1130	
1117(1117)	1126(1125)					
	1106(1110)	1104	1108	1104	1094	
1081		1087				
					1069	
1003(1004)	1002(999)				1014(1017)	SO_4^{2-} sym. stretching (ν_1)
		996	998	998		
979(981)	982(980)	980	981		987(991)	
	752(754)		749			OH-lib.
659	658(657)	656	656	647	652	SO_4^{2-} asym. bending (ν_4)
641(641)	644(644)	642	646	642	641	
631	615(617)	625	614	632	626	
619	604(604)	616	602	621	620sh	
607		603		616		
492(491)	438(439)	487	483	484	477sh	SO_4^{2-} sym. bending (ν_2)
472(471)		474	471	469	464	
441(441)		437	438	452	448	
428(424)		423	425		436	

[a] The Raman and IR signals in parenthesis were observed by Kloprogge et al. [44].
[b] The Raman signals in parenthesis were observed by Wollmann et al. [69].
[c] The stretching modes of NH_4^+ may be superposed by stretching modes of H_2O.

group interactions: two for ν_1 (1 A_g and 1 B_g), four for ν_2 (2 A_g and 2 B_g), six for ν_3 (3 A_g and 3 B_g), and six for ν_4 (3 A_g and 3 B_g). Fig. 1b shows the average Raman spectrum of koktaite. The bands observed in the average Raman and infrared spectra of koktaite (Fig. S8, Supplementary data) are listed in Table 1.

$Na_2Ca(SO_4)_2$ is present in nature as a mineral called glauberite, which crystallizes in a monoclinic system with the space group $C2/c$ (C_{2h}^6) and has four molecules in the unit cell [51,52]. According to the data reported by Araki and Zoltai [52], the Na^+ and SO_4^{2-} ions occupy general positions, while Ca^{2+} ions occupy special positions. The correlation for the fundamental modes of the SO_4^{2-} ion (T_d) with the site of symmetry C_1 and the unit-cell symmetry C_{2h}, is shown in Fig. S9 (Supplementary data).

Considering the results obtained for glauberite using the Correlation Method [46], 78 fundamental modes (including the acoustic modes) are expected and split into

$$\Gamma_{78} = 19A_g + 20B_g + 19A_u + 20B_u$$

According to this analysis, the four fundamental modes of the free ion SO_4^{2-} split in 18 fundamental Raman active modes due to factor group interactions: two for ν_1 (1 A_g and 1 B_g), four for ν_2 (2 A_g and 2 B_g), six for ν_3 (3 A_g and 3 B_g), and six for ν_4 (3 A_g and 3 B_g). The average spectrum of glauberite shows one strong band at 998 cm^{-1}, which is assigned to SO_4^{2-} ν_1. Fig. 1c shows the average Raman spectrum of glauberite and the observed bands are listed in Table 1.

$K_2Ca_2Mg(SO_4)_4 \cdot 2H_2O$ is present in nature as a mineral called polyhalite, which crystallizes in a triclinic system with the space group $P\bar{1}$ (C_i^1) and has one molecule in the unit cell [53]. All the ions and water molecules except Mg^{2+} ion are in general position. Mg^{2+} ions occupy the site of symmetry C_i. The correlation for the fundamental modes of the SO_4^{2-} ion (T_d) and the H_2O molecule (C_{2v}) with the site of symmetry C_1 and the unit-cell symmetry C_i, are shown in Fig. S10 (Supplementary data). Considering the results obtained for polyhalite using the Correlation Method [46], 93 fundamental modes (including the acoustic modes) are expected and split into

$$\Gamma_{93} = 45A_g + 48A_u$$

According to this analysis, the four fundamental modes of the free ion SO_4^{2-} split in 18 fundamental Raman active modes due to the factor group interactions: two for ν_1, four for ν_2, six for ν_3, and six for ν_4. Although all SO_4^{2-} ions occupy general positions and the two modes for ν_1 are A_g, two bands (at 1014 and 987 cm^{-1}) are observed in the Raman spectrum of polyhalite. Apparently this is due to the fact that the sulfur tetrahedra form two different complexes with the surrounding ions and molecules (H_2O). Fig. 1d shows the average Raman spectrum of polyhalite and the observed bands are listed in Table 1.

Despite the mentioned impurity detected in the synthetic glauberite and polyhalite, the Raman spectra of both substances were recorded by means of micro Raman spectroscopy, which allows to record the Raman spectrum of individual micrometric particles (or microcrystals). Unfortunately, the pellet necessary to record the infrared spectrum is prepared using the bulk substance, so the resulting spectrum is not of a pure substance. This is the reason why we decided not to include the infrared spectra of glauberite and polyhalite in this work.

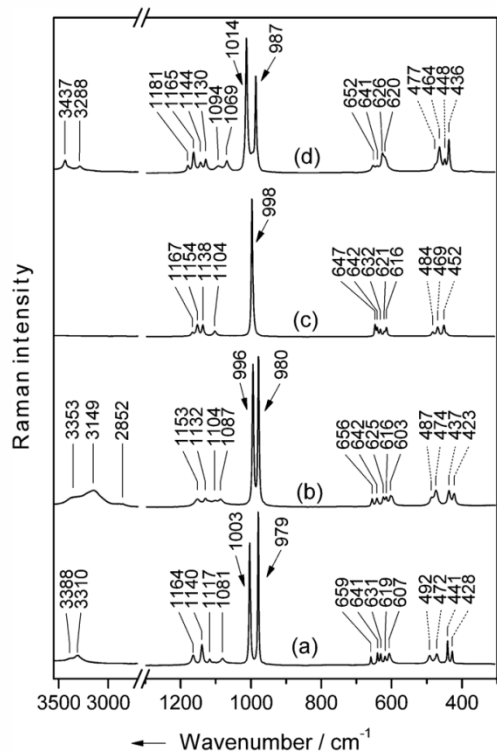**Fig. 1.** Average Raman spectra of mixed salts (spectral resolution $\sim$1.5 cm^{-1}): (a) K$_2$Ca(SO$_4$)$_2$·H$_2$O (syngenite), (b) (NH$_4$)$_2$Ca(SO$_4$)$_2$·H$_2$O (koktaite), (c) Na$_2$Ca(SO$_4$)$_2$ (glauberite), and (d) K$_2$Ca$_2$Mg(SO$_4$)$_4$·2H$_2$O (polyhalite).

In summary, from the Raman spectroscopic data of the four calcium mixed salts (Fig. 1), it is easy to note the similarities between the spectra of syngenite and koktaite; the number of bands observed for each SO$_4^{2-}$ mode is equal and only small differences in the wavenumbers of the SO$_4^{2-}$ bands can be observed. Apparently the Raman spectra of these mixed salts also reveal the structural relationships among them. Despite these similarities, the unambiguous differentiation between these mixed salts is possible using the broad bands of NH$_4^+$ (ν_2 and ν_4), as these are absent in the spectra of syngenite. As expected from the crystal structure of glauberite and polyhalite, the Raman spectra of these mixed salts are clearly different compared to the spectra of syngenite and koktaite.

3.3. Crystallization studies within droplets and environmental considerations

When a saturated solution containing CaSO$_4$ and K$_2$SO$_4$ evaporates, a process which can be expected in small water droplets of fog or haze, the successive crystallization of salts is expected according to their individual solubilities. The solubility in water (25 °C) of CaSO$_4$, CaSO$_4$·2H$_2$O, syngenite, and K$_2$SO$_4$ are 3.11, 2.08, 23.68, and 120.53 g/kg H$_2$O, respectively [54]. There is no solubility data available for koktaite, nevertheless, according to Yoder and Rowand [55], its solubility is expected to be similar to CaSO$_4$·2H$_2$O, or to lie between solubility values of CaSO$_4$·2H$_2$O and (NH$_4$)$_2$SO$_4$ ($\sim$750 g/kg H$_2$O at 25 °C [32]). Therefore, the mixed

salts syngenite and koktaite will always crystallize earlier than K$_2$SO$_4$ and (NH$_4$)$_2$SO$_4$.

In order to perform the droplet crystallization experiments for the systems CaSO$_4$–K$_2$SO$_4$ and CaSO$_4$–(NH$_4$)$_2$SO$_4$, many different molar ratios for each case were evaluated. We finally chose the molar ratio of 1:50 for both systems, as this ratio allowed the crystallization of syngenite and koktaite to be observed.

The experiment for the system CaSO$_4$–K$_2$SO$_4$ was performed within a droplet using a molar ratio of 1:50. Fig. 2a shows microphotographs of the crystal formation at different time points and their respective Raman spectra. Fig. 2b shows the Raman spectra of the pure substances involved in the system CaSO$_4$–K$_2$SO$_4$. The Raman spectrum of the crystal at t = 0 shows two strong bands at 1001 and 978 cm^{-1}, which clearly belong to the SO$_4^{2-}$ ν_1. In addition, there are signals in the region of the SO$_4^{2-}$ ν_3 (1163, 1138, and 1115 cm^{-1}), SO$_4^{2-}$ ν_4 (659, 639, 632, 618, and 607 cm^{-1}), and SO$_4^{2-}$ ν_2 (493, 472, 442, and 430 cm^{-1}). These values were observed in the Raman spectrum of pure syngenite with a spectral resolution of $\sim$3 cm^{-1} (see Table S1, Supplementary data). At t = 102 s, the Raman spectrum of the crystal formation shows the emergence of bands at 1143, 625, and 455 cm^{-1}, which are in good agreement with the values reported in an earlier spectroscopic study of K$_2$SO$_4$ [56], as well as the values of the Raman spectrum we recoded of K$_2$SO$_4$ (see Table S2, Supplementary data). Furthermore, the relation of intensities of the strongest signals is different than the observed a t = 0, clearly the band at 978 cm^{-1} is much stronger than the one at 1001 cm^{-1}. This difference in intensity can be explained by an overlapping effect of the signals of syngenite and K$_2$SO$_4$. At t = 234 s, the droplet was dry and the predominant signals in the Raman spectrum were those of K$_2$SO$_4$.

The experiment for the system CaSO$_4$–(NH$_4$)$_2$SO$_4$ was performed within a droplet using a molar ratio of 1:50. Fig. 3a shows microphotographs of the crystal formation at different time points and their respective Raman spectra. Fig. 3b shows the Raman spectra of the pure substances involved in the system CaSO$_4$–(NH$_4$)$_2$SO$_4$. The Raman spectrum recorded of the crystal at t = 0 shows two strong bands at 994 and 978 cm^{-1}, which belong to SO$_4^{2-}$ ν_1. In addition, there are signals in the region of SO$_4^{2-}$ ν_3 (1130 and 1085 cm^{-1}), SO$_4^{2-}$ ν_4 (657, 641, 624, 615, and 603 cm^{-1}), and SO$_4^{2-}$ ν_2 (489, 477, 439, and 424 cm^{-1}). These values were observed in the Raman spectrum of pure koktaite with a spectral resolution of $\sim$3 cm^{-1} (see Table S3, Supplementary data). At t = 140 s, the characteristic features of koktaite are still observable in the Raman spectrum, but no Raman signals of (NH$_4$)$_2$SO$_4$ can be observed. However, the microphotograph at this time point shows small amounts of liquid solution remainder surrounding the main needle-shaped crystal formation. By this point, a major portion of the water was already vaporized, but due to the high solubility of (NH$_4$)$_2$SO$_4$ no crystallization took place. Only when the water was completely vaporized, at t = 210 s, a strong band at 971 cm^{-1} emerged, which is in good agreement with the value reported in earlier spectroscopic studies of (NH$_4$)$_2$SO$_4$ [57,58], as well as the values of the Raman spectrum of (NH$_4$)$_2$SO$_4$ (see Table S4, Supplementary data) recorded by us. The band at 994 cm^{-1} persists, and a shoulder can be observed at 978 cm^{-1}.

It is important to note that for these specific solutions used in the droplet crystallization experiments no characteristic bands of CaSO$_4$·2H$_2$O (gypsum) (see Table S5, Supplementary data) were observed during the whole vaporization process. On the other hand, crystallization of gypsum is definitely expected for solutions containing higher proportions of the Ca^{2+} ion.

The droplet crystallization experiments demonstrate not only that the respective mixed salt of each system (CaSO$_4$–K$_2$SO$_4$ and CaSO$_4$–(NH$_4$)$_2$SO$_4$) can crystallize during evaporation at room temperature, but also that the result is a mixture of compounds and thus this kind of mixtures may be expected in atmosphere.
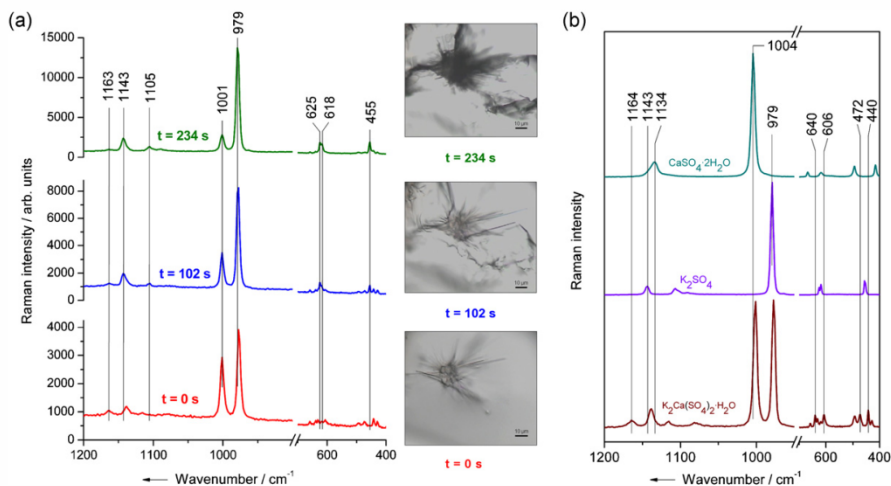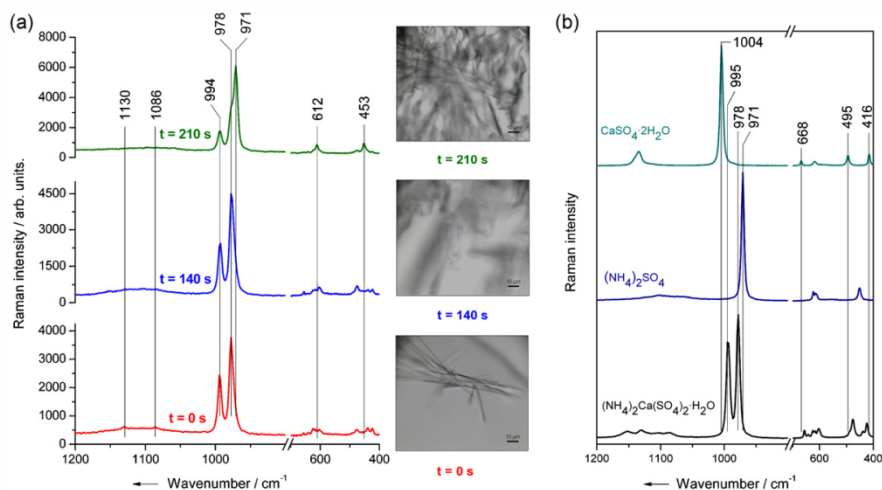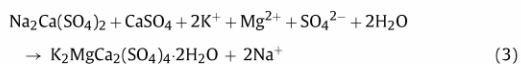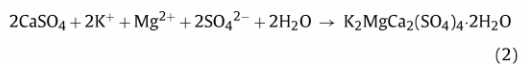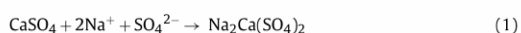
Fig. 2. (a) Microphotographs of the crystal formation at di×fferent time points, obtained by evaporation at 20 °C from a solution containing $CaSO_4$ and K_2SO_4 molar ratio 1:50, and their respective Raman spectra. (b) Raman spectra (resolution $\sim$3 cm^{-1}) of pure $K_2Ca(SO_4)_2 \cdot H_2O$ (syngenite), K_2SO_4, and $CaSO_4 \cdot 2H_2O$.

As a matter of fact, the reported works about composition of atmospheric particulate matter, in which syngenite has been found, show also the presence of K_2SO_4 [17,18]. The same holds true for the case of koktaite, i.e., when koktaite was present in atmospheric particles, $(NH_4)_2SO_4$ has been found, too [10,11].

Our attempts to crystallize glauberite and polyhalite at room temperature (20 °C) were unsuccessful. Using different solutions containing $CaSO_4$ and Na_2SO_4 (molar ratio 1:50 and higher) in the droplet crystallization experiments, we observed the formation of gypsum or Na_2SO_4 in phase III, but not glauberite. This seems to confirm the results reported by Block and Waters Jr. [33] with respect to solutions containing only $CaSO_4$ and Na_2SO_4 at 25 °C.

These authors claimed that in absence of NaCl, the only solid phases in equilibrium with the solution are gypsum and/or $Na_2SO_4 \cdot 10H_2O$. Furthermore, they concluded that the crystallization of glauberite requires the presence of NaCl and/or higher temperatures. The crystallization of Na_2SO_4 in phase III from solutions containing Na$^+$ and SO_4^{2-} ions and its relatively high stability at room temperature was earlier reported by Xu and Schweiger [59], and its environmental occurrence should be considered and evaluated in future studies on atmospheric particles.

Evaluating the vaporization of different solutions containing $CaSO_4$, K_2SO_4 and $MgSO_4$ ($CaSO_4$ in smaller proportions compared to K_2SO_4 and $MgSO_4$) at room temperature, we found that in most

Fig. 3. (a) Microphotographs of the crystal formations at different time points, obtained by evaporation at 20 °C from a solution containing $CaSO_4$ and $(NH_4)_2SO_4$ molar ratio 1:50, and their respective Raman spectra. (b) Raman spectra (resolution $\sim$3 cm^{-1}) of pure $(NH_4)_2Ca(SO_4)_2 \cdot H_2O$ (koktaite), $(NH_4)_2SO_4$, and $CaSO_4 \cdot 2H_2O$.

P. Vargas Jentzsch et al. / Vibrational Spectroscopy 61 (2012) 206–213

cases syngenite undergoes crystallization, whereas polyhalite does not crystallize. It seems that the polyhalite crystallization requires higher temperatures. In one of his articles, Jänecke [60] presented a phase diagram for the $MgSO_4$–K_2SO_4–$CaSO_4$ system at 83 °C, in which a region for polyhalite precipitation was identified. Other authors suggested that polyhalite may precipitate together with halite at temperatures >30 °C, when explaining the composition of certain salt deposits [61].

If glauberite and polyhalite do not crystallize from solutions containing the constituent ions at 20 °C, and the temperatures required for their crystallization from solutions are even higher than the normal atmospheric (tropospheric) temperature, how should the reported occurrence of these minerals in atmospheric particles [12,15,16] be explained? The answer may be found analyzing the geological processes, since glauberite and polyhalite are well-known minerals in evaporite deposits [54,61–64].

The formation of evaporite minerals is dictated by the principle of "chemical divides", which explains the origin of the three major compositional types of brines and, considering the relative concentrations of ions, predicts the precipitation of minerals [65]. However, there is an additional consideration referred to the back-reaction of early-formed minerals. Harvie and co-workers [66], based on computer calculations, suggested back-reactions of early-formed $CaSO_4$ (anhydrite) or gypsum and glauberite, in order to explain the formation of glauberite and polyhalite. Today these back-reactions of early formed minerals are recognized by the scientific community and allows to explain the existence of glauberite and polyhalite in many evaporite deposits around the World [54,67]. Some of the proposed reactions [66] were:

$$CaSO_4 + 2Na^+ + SO_4^{2-} \rightarrow Na_2Ca(SO_4)_2 \qquad (1)$$

$$2CaSO_4 + 2K^+ + Mg^{2+} + 2SO_4^{2-} + 2H_2O \rightarrow K_2MgCa_2(SO_4)_4 \cdot 2H_2O \qquad (2)$$

$$Na_2Ca(SO_4)_2 + CaSO_4 + 2K^+ + Mg^{2+} + SO_4^{2-} + 2H_2O$$
$$\rightarrow K_2MgCa_2(SO_4)_4 \cdot 2H_2O + 2Na^+ \qquad (3)$$

Basically, the anhydrite reacts with the brine and the products are glauberite and polyhalite (Eqs. (1) and (2)). Harvie and co-workers [66] also suggested that glauberite can be replaced in part by anhydrite, and then both generate polyhalite (Eq. (3)).

Analyzing the available data, glauberite and polyhalite in atmospheric particulate matter was found associated with gypsum and those samples were collected in regions with a recognized sea salt contribution to atmosphere [12,15,16]. Gypsum is a mineral usually found in atmosphere; its atmospheric occurrence can be attributed to blow dust, sea salt contribution and chemical reactions in the atmosphere (e.g., reaction of calcite with H_2SO_4) [15].

Atmospheric particles interact with water; according to estimations, during the residence and transport of particles in atmosphere, they undergo around ten condensation–evaporation cycles [68], which are likely to produce important changes in their chemical composition. During the condensation the soluble portion of a particle tends to dissolve, leaving behind a solid core of insoluble material surrounded by a "brine". The composition of this atmospheric brine can change not only due to the evaporation process, but also by coagulation (when two particles combine to form one particle).

As mentioned above, gypsum has a low solubility in water. If a particle of gypsum (which can also evolute to anhydrite depending

on the atmospheric humidity during the transport) acts as a condensation nucleus and the surrounding water contains ions such as Na^+, K^+, Mg^{2+}, Cl^- and SO_4^{2-}, which are also present in marine and non-marine brines responsible of evaporite deposits, it is feasible that similar processes to those taking place in evaporite systems may be involved in the mineral formation of the atmospheric particulate matter. Apparently the mechanisms described by Eqs. (1)–(3) might occur in atmosphere due to the well-known presence of gypsum and can explain the occurrence of glauberite and polyhalite in atmospheric particles.

Taking into account the physical and chemical properties of syngenite, koktaite, glauberite and polyhalite, the presence of these compounds in atmosphere can provide information not only of the reactivity involved in their origin, but also about the "age" of the particulate matter. For instance, koktaite is a mixed salt with a relatively low stability in contact with water; Del Monte and Rossi [20] demonstrate that as a consequence of this low stability, the koktaite generated by vaporization of fog water degrades easily to gypsum and it is this compound which deposits on buildings (the also resulting $(NH_4)_2SO_4$ is washed and run-off due to its high water solubility). In fact, during our attempts to isolate pure koktaite, we tried to wash the crystallized koktaite with water resulting in its complete and immediate degradation to the constituent simple salts.

It is also important to note that all these four mixed salts have incongruent solubility, this means that it is not possible to recrystallize the mixed salts from the solutions resulting from their dissolution.

4. Conclusion

Synthetic $K_2Ca(SO_4)_2 \cdot H_2O$ (syngenite), $(NH_4)_2Ca(SO_4)_2 \cdot H_2O$ (koktaite), $Na_2Ca(SO_4)_2$ (glauberite), and $K_2Ca_2Mg(SO_4)_4 \cdot 2H_2O$ (polyhalite) were obtained and their purity confirmed by X-ray diffractometry.

The Raman and infrared spectra of the synthetic minerals were recorded and a band assignment for each case was proposed. The number of bands observed in the Raman spectra of the synthetic minerals as well as their wavenumbers were discussed, taking into account the results obtained applying the "Correlation Method" and other crystal structure criteria.

Regarding the atmospheric origin of calcium mixed salts in atmosphere, by means of the droplet crystallization experiments we confirmed that it is possible to crystallize syngenite and koktaite at 20 °C by evaporation of solutions containing the constituent ions. A similar vaporization process is expected to occur in atmosphere producing atmospheric particles containing syngenite, koktaite, as well as K_2SO_4 and $(NH_4)_2SO_4$.

A theory to explain the atmospheric formation of glauberite and polyhalite was proposed, in which $CaSO_4 \cdot 2H_2O$ (gypsum) and $CaSO_4$ (anhydrite) particles must be early-formed and then back-react with water and ions deposited on them.

Some characteristics of the mixed salts of this study, such as incongruent solubility, crystallization conditions and chemical stability, can be used in future atmospheric studies not only to evaluate the atmospheric reactivity, but also the "age" of the atmospheric particles and further implications.

Appendix A. Supplementary data

Supplementary data associated with this article can be found, in the online version, at http://dx.doi.org/10.1016/j.vibspec.2012.03.007.

References

[1] R.J. Charlson, S.E. Schwartz, J.M. Hales, R.D. Cess, J.A. Coakley Jr., J.E. Hansen, D.J. Hofmann, Science 255 (1992) 423–430.
[2] M.O. Andreae, C.D. Jones, P.M. Cox, Nature 435 (2005) 1187–1190.
[3] W.Z. De Mello, Environ. Pollut. 114 (2001) 235–242.
[4] D. Migliavacca, E.C. Teixeira, M. Pires, J. Fachel, Atmos. Environ. 38 (2004) 1641–1656.
[5] D. Sopauskiene, D. Budvytyte, Atmos. Environ. 28 (1994) 1291–1296.
[6] G. Wang, H. Wang, Y. Yu, S. Gao, J. Feng, S. Gao, L. Wang, Atmos. Environ. 37 (2003) 2893–2902.
[7] V. Ariola, A. D'Alessandro, F. Lucarelli, G. Marcazzan, F. Mazzei, S. Nava, I. Garcia-Orellana, P. Prati, G. Valli, R. Vecchi, A. Zucchiatti, Chemosphere 62 (2006) 226–232.
[8] M. Amodio, P. Bruno, M. Caselli, G. De Gennaro, P.R. Dambruoso, B.E. Daresta, P. Ielpo, F. Guncolo, C.M. Placentino, V. Paolillo, M. Tutino, Atmos. Res. 90 (2008) 313–325.
[9] J.N. Galloway, G.E. Likens, Tellus 30 (1978) 71–82.
[10] R. Voigt, K.H. Lieser, Naturwissenschaften 71 (1984) 377–378.
[11] X. Querol, A. Alastuey, J.A. Puicercus, E. Mantilla, C.R. Ruiz, A. Lopez-Soler, F. Plana, R. Juan, Atmos. Environ. 32 (1998) 719–731.
[12] A. Chabas, R.A. Lefèvre, Atmos. Environ. 34 (2000) 225–238.
[13] I. Rodríguez, S. Gali, C. Marcos, Environ. Geol. 56 (2009) 1551–1561.
[14] O. Preining, Atmos. Environ. A 25 (1991) 2443–2444.
[15] G. Zhou, K. Tazaki, Atmos. Environ. 30 (1996) 3301–3308.
[16] M. Derbez, R. Lefèvre, Pollut. Atmos. 177 (2003) 103–125.
[17] R.K. Xie, H.M. Seip, J.R. Leinum, T. Winje, J.S. Xiao, Sci. Total Environ. 343 (2005) 261–272.
[18] R.K. Xie, H.M. Seip, L. Liu, D.S. Zhang, Air Qual. Atmos. Health 2 (2009) 123–131.
[19] I. Mori, M. Nishikawa, Y. Iwasaka, Sci. Total Environ. 224 (1998) 87–91.
[20] M. Del Monte, P. Rossi, Atmos. Environ. 31 (1997) 1637–1646.
[21] G. Schweiger, J. Aerosol Sci. 20 (1989) 1621–1624.
[22] K.H. Fung, D.G. Imre, I.N. Tang, J. Aerosol Sci. 25 (1994) 479–485.
[23] M. Trunk, J. Popp, I. Hartmann, M. Lankers, E. Urlaub, W. Kiefer, Fresenius J. Anal. Chem. 355 (1996) 354–356.
[24] M. Trunk, J. Popp, W. Kiefer, Chem. Phys. Lett. 284 (1998) 377–381.
[25] J. Musick, J. Popp, M. Trunk, W. Kiefer, Appl. Spectrosc. 52 (1998) 692–701.
[26] J. Musick, J. Popp, W. Kiefer, J. Raman Spectrosc. 31 (2000) 217–219.
[27] Y. Batonneau, S. Sobanska, J. Laureyns, C. Bremard, Environ. Sci. Technol. 40 (2006) 1300–1306.
[28] W. Schumacher, M. Kühnert, P. Rösch, J. Popp, J. Raman Spectrosc. 42 (2011) 383–392.
[29] P. Vargas Jentzsch, B. Kampe, P. Rösch, J. Popp, J. Phys. Chem. A 115 (2011) 5540–5546.

[30] P. Vargas Jentzsch, V. Ciobotă, B. Kampe, P. Rösch, J. Popp, J. Raman Spectrosc. (2011), http://dx.doi.org/10.1002/jrs.3064.
[31] V. Ciobotă, W. Salama, N. Tarcea, P. Rösch, M.E. Aref, R. Gaupp, J. Popp, J. Raman Spectrosc. 43 (2012) 405–410.
[32] A.E. Hill, N.S. Yanick, J. Am. Chem. Soc. 57 (1935) 645–651.
[33] J. Block, O.B. Waters Jr., J. Chem. Eng. Data 13 (1968) 336–344.
[34] R Development Core Team, R: A Language and Environment for Statistical Computing, R Foundation for Statistical Computing, Vienna, 2009.
[35] Z.-M. Zhang, S. Chen, Y.-Z. Liang, Z.-X. Liu, Q.-M. Zhang, L.-X. Ding, F. Ye, H. Zhou, J. Raman Spectrosc. 41 (2010) 659–669.
[36] T. Dörfer, T. Bocklitz, N. Tarcea, M. Schmitt, J. Popp, Z. Phys. Chem. 225 (2011) 753–764.
[37] C.K. Chan, Z. Ha, M.Y. Choi, Atmos. Environ. 34 (2000) 4795–4803.
[38] V. Ramakrishnan, V.U. Nayar, G. Aruldhas, Infrared Phys. 25 (1985) 607–610.
[39] E. Corazza, C. Sabelli, Z. Kristallogr. 124 (1967) 398–408.
[40] J. Riederer, Bautenschutz Bausanierung 15 (1992) 54–56.
[41] L. Clarke, E.P. Partridge, Ind. Eng. Chem. 26 (1934) 897–903.
[42] J. Dankiewicz, K. Wieczorek-Ciurowa, J. Therm. Anal. Calorim. 13 (1978) 543–552.
[43] S. Smillie, E. Moulin, D.E. Macphee, F.P. Glasser, Adv. Cement Res. 5 (1993) 93–96.
[44] J.T. Kloprogge, R.D. Schuiling, Z. Ding, L. Hickey, D. Wharton, R.L. Frost, Vib. Spectrosc. 28 (2002) 209–221.
[45] J.T. Kloprogge, Z. Ding, W.N. Martens, R.D. Schuiling, L.V. Duong, R.L. Frost, Thermochim. Acta 417 (2004) 143–155.
[46] W.G. Fateley, F.R. Dollish, N.T. McDevitt, F.F. Bentley, Infrared and Raman Selection Rules for Molecular and Lattice Vibrations: The Correlation Method, Wiley-Interscience, USA, 1972.
[47] P. Ballirano, G. Belardi, A. Maras, N. Jb. Miner. Abh. 182 (2005) 15–21.
[48] G.B. Bokii, N.A. Pal'chik, M.Y. Antipin, Trudy Instituta Geologii i Geofiziki 487 (1981) 4–8.
[49] J. Ando, S. Matsuno, Bull. Chem. Soc. Jpn. 34 (1961) 678–683.
[50] W. Von Maessenhausen, V. Czikkely, J. Jung, US Patent 4,883,530 (1988).
[51] G. Cocco, E. Corazza, C. Sabelli, Z. Kristallogr. 122 (1965) 175–186.
[52] T. Araki, T. Zoltai, Am. Mineral. 52 (1967) 1272–1277.
[53] L. Bindi, Acta Crystallogr., Sect. E: Struct. Rep. Online 61 (2005) i135–i136.
[54] R.J. Spencer, Rev. Mineral. Geochem. 40 (2000) 173–192.
[55] C.H. Yoder, J.P. Rowand, Am. Mineral. 91 (2006) 747–752.
[56] F. Meserole, J.C. Decius, R.E. Carlson, Spectrochim. Acta 30 (1974) 2179–2195.
[57] P. Venkateswarlu, H.D. Bist, Y.S. Jain, J. Raman Spectrosc. 3 (1975) 143–151.
[58] I.N. Tang, K.H. Fung, J. Aerosol Sci. 20 (1989) 609–617.
[59] B. Xu, G. Schweiger, J. Aerosol Sci. 30 (1999) S379–S380.
[60] E. Jänecke, Z. Anorg. Chem. 51 (1906) 132–157.
[61] T.M. Peryt, C. Pierre, S.P. Gryniv, Sedimentology 45 (1998) 565–578.
[62] H.P. Eugster, Ann. Rev. Earth Planet. Sci. 8 (1980) 35–63.
[63] I. Gündogan, C. Helvaci, Int. Geol. Rev. 43 (2001) 818–829.
[64] J.M. Salvany, J. García-Veigas, F. Ortí, Sedimentology 54 (2007) 443–467.
[65] L.A. Hardie, H.P. Eugster, Mineral. Soc. Am., Spec. Pap. 3 (1970) 273–290.
[66] C.E. Harvie, J.H. Weare, L.A. Hardie, H.P. Eugster, Science 208 (1980) 498–500.
[67] L. Ma, T.K. Lowenstein, B. Li, P. Jiang, C. Liu, J. Zhong, J. Sheng, H. Qiu, H. Wu, Appl. Geochem. 25 (2010) 1770–1782.
[68] H.R. Pruppacher, R. Jaenicke, Atmos. Res. 38 (1995) 283–295.
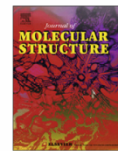[69] G. Wollmann, D. Freyer, W. Voigt, Monatsh. Chem. 139 (2008) 739–745.

2.4 Raman and infrared spectroscopic study of synthetic ungemachite, $K_3Na_8Fe(SO_4)_6(NO_3)_2 \cdot 6H_2O$ [PV4]

Authorship of Publication

Paul Vargas Jentzsch: concept development

                                      ungemachite preparation

                                      Raman measurements

                                        factor group analysis and bands assigment

                                        writing of manuscript

Valerian Ciobotă: Raman and infrared measurements

                                        discussion of experimental concept and results

Ralph Michael Bolanz: X-ray diffraction measurements

                                        discussion of results

Bernd Kampe: Raman spectra processing

Petra Rösch: discussion of experimental concept and results

                                        proofreading of manuscript

Juraj Majzlan: discussion of results

                                        proofreading of manuscript

Jürgen Popp: project management

                                        discussion of concepts and results

                                        discussion and proofreading of manuscript

Raman and infrared spectroscopic study of synthetic ungemachite, $K_3Na_8Fe(SO_4)_6(NO_3)_2 \cdot 6H_2O$

Paul Vargas Jentzsch [a], Valerian Ciobotă [a], Ralph Michael Bolanz [b], Bernd Kampe [a], Petra Rösch [a], Juraj Majzlan [b], Jürgen Popp [a,c,*]

[a] Institut für Physikalische Chemie, and Abbe Center of Photonics, Friedrich-Schiller-Universität Jena, D-07743 Jena, Germany
[b] Institut für Geowissenschaften, Friedrich-Schiller-Universität Jena, D-07749 Jena, Germany
[c] Institut für Photonische Technologien e.V. (IPHT), D-07745 Jena, Germany

HIGHLIGHTS

▶ We found that ungemachite crystallizes from acidic aqueous solution at 20 °C.
▶ The Raman and IR spectra of synthetic ungemachite were recorded and bands assigned.
▶ The atmospheric formation of ungemachite is postulated.

ARTICLE INFO

ABSTRACT

Iron is an important element usually found in atmospheric particulate matter, and its occurrence can be attributed to both natural and anthropogenic sources. It is an accepted fact that the atmospheric particles interact with water and other atmospheric components, therefore dissolution–crystallization processes can be expected. In this work, considering specially that low pH values are characteristic of aerosol solutions, we postulate that the rare mineral ungemachite, $K_3Na_8Fe(SO_4)_6(NO_3)_2 \cdot 6H_2O$ can crystallize in atmosphere. The Raman and infrared spectra of synthetic ungemachite are presented and the band assignments are proposed and discussed. This is the first time that a synthetic method for ungemachite is reported.

© 2012 Elsevier B.V. All rights reserved.

1. Introduction

The study of mineral deposits and their subsequent exploitation requires adequate and reliable analytical methods. Fast analysis of mineral samples is important to identify the composition of mineral deposits and also to investigate geological processes. X-ray diffractometry is probably the most popular of the analytical methods for these purposes, but in the last years, Raman spectroscopy has also been considered for this kind of studies [1].

At this point, it is important to mention that the study of minerals is not only related to processes on the terrestrial crust. Many authors, generally using X-ray diffractometry, reported the occurrence of some minerals in atmospheric particulate matter, specifically this is the case of $Na_2Mg(SO_4)_2 \cdot 4H_2O$ (bloedite),

$(NH_4)_2Mg(SO_4)_2 \cdot 6H_2O$ (boussingaultite), $(NH_4)_2Ca(SO_4)_2 \cdot H_2O$ (koktaite), $(NH_4)_2Fe(SO_4)_2 \cdot 6H_2O$ (mohrite), $Na_3(NO_3)(SO_4) \cdot H_2O$ (darapskite) and others [2–4]. Again, as an alternative technique, the suitability of Raman spectroscopy for chemical characterization of this kind of material was discussed by many researchers [5–13].

The origin of minerals in atmospheric particles can be attributed to the suspension/transport of soil and rock material (dust) by wind, but apparently this is not the only source. For the specific case of the mineral darapskite, Harrison and Sturges attributed its atmospheric occurrence to acid attack upon airborne marine NaCl [3]. However, in a recent work, we have postulated that the formation mechanism of darapskite may be a consequence of simple dissolution–crystallization processes [14]. Furthermore, these dissolution–crystallization processes can explain the formation not only of darapskite but also of other minerals in the atmosphere. The necessary conditions for crystallization of minerals in atmosphere are the existence of liquid water and the specific ions for each case. Liquid water is present in atmosphere as fog, cloud droplets and wet aerosols; clouds cover ~60% of the Earth's surface

* Corresponding author at: Institut für Physikalische Chemie, and Abbe Center of Photonics, Friedrich-Schiller-Universität Jena, D-07743 Jena, Germany. Tel.: +49 3641 9 48320; fax: +49 3641 9 48302.
E-mail address: juergen.popp@uni-jena.de (J. Popp).

and occupy about 7% of the tropospheric total volume [15]. Also, the occurrence of ions in atmosphere is a well-known fact, a large proportion of salt being injected into atmosphere as aerosol by breaking waves and bursting bubbles on the ocean surface [16]. Many researchers reported variable concentrations of Na^+, K^+, SO_4^{2-}, NO_3^- and other ions in atmospheric particulate matter of urban and rural areas, using different methods [17–20], and the presence of these ions in atmospheric precipitation (wet and bulk precipitation) has also been reported and discussed by many authors [21,22].

The long-range transport of dust has been considered as one of the most important sources of particulate matter to atmosphere. Seasonal dust events like the so-called "Kosa", which takes place yearly in Asia [23,24], and the transport of Saharan mineral dust to remote areas [25–27], not only have a significant effect on the air quality, but also represent an important movement of mineral material. A remarkable characteristic of those dust materials is the presence of iron in their composition. As these Fe-rich dust particles are usually smaller in size than the median size particles in dust, they can be transported for longer distances and remain suspended for a longer period [28]. In general, according to estimations, during the residence and transport of aerosols in atmosphere, they undergo around ten condensation–evaporation cycles [29], which are likely to produce important changes in their chemical composition.

Considering that Na^+, K^+, Fe^{3+}, NO_3^- and SO_4^{2-} ions (in different forms and from different sources) occur in atmosphere together with water, and the characteristic pH value of aerosol solutions is acidic [30], the crystallization in atmosphere of the mineral ungemachite could be expected.

Ungemachite, $K_3Na_8Fe(SO_4)_6(NO_3)_2 \cdot 6H_2O$ has been found and reported for the first time by Peacock and Bandy. In the original collected samples, they recognized two polymorphs, a rhombohedral one (ungemachite) and a monoclinic one (clino-ungemachite) [31,32]. The mineral ungemachite occurs in massive iron sulfate "veins" mainly formed of jarosite and metasideronatrite in association with metavoltine, fibroferrite and sodium alum, and its origin is usually linked to the oxidation of primary pyrite [33], probably because the first specimens were found in an oxidized zone of a copper deposit [34].

In this article we present evidence which suggest that ungemachite can be formed as aerosol in atmosphere by dissolution–crystallization processes. Furthermore, the Raman and infrared spectra of ungemachite are presented and the assignment of the bands observed in both Raman and IR spectra is proposed and discussed. This is the first time that a synthetic method for ungemachite is reported.

2. Materials and methods

2.1. Chemicals and ungemachite synthesis

Sodium sulfate anhydrous, Na_2SO_4 ($\geqslant 99.0\%$), potassium sulfate, K_2SO_4 ($\geqslant 99.0\%$), potassium nitrate, KNO_3 ($\geqslant 99.0\%$), iron (III) sulfate hydrate, $Fe_2(SO_4)_3 \cdot xH_2O$ (Fe 21–23%) and sulfuric acid, H_2SO_4 (95.0–98.0%) were purchased from Sigma–Aldrich, while sodium nitrate, $NaNO_3$ (min 99%) was purchased from VWR. These reactants were used without further purification.

Ungemachite crystallized from a solution containing stoichiometric amounts of each ion. About 200 ml of a solution containing 8.15 g Na_2SO_4, 1.25 g K_2SO_4, 2.90 g KNO_3, 3.64 g $Fe_2(SO_4)_3 \cdot xH_2O$ and 0.3 ml H_2SO_4 (95.0–98.0%), was slowly evaporated at room temperature during two weeks. A white efflorescent salt identified as ungemachite crystallized on the walls and bottom of the beaker. In order to remove the acid and remainder residues of the other salts, the obtained crude ungemachite was washed with small amounts of distilled water and dried at room temperature.

An additional experiment to evaluate the possible crystallization of ungemachite in atmospheric conditions was performed. In this experiment we modified the ratio of K^+ and Na^+ ions to get a weight ratio K^+/Na^+ of 0.29, which is considered representative of the atmospheric environment (find more details in the section Environmental Implications). About 200 ml of a solution containing 7.51 g Na_2SO_4, 2.00 g K_2SO_4, 2.44 g $NaNO_3$, 3.64 g $Fe_2(S-O_4)_3 \cdot xH_2O$ and 0.3 ml H_2SO_4 (95.0–98.0%), was slowly evaporated at room temperature during two weeks. The crystallized solid material on the walls and bottom of the vessel was washed and dried under the same conditions as mentioned above.

2.2. Spectroscopic instrumentation and data processing

The Raman spectra in this study were recorded in the range 310–3550 cm^{-1} with a micro-Raman setup (HR LabRam inverse system, Jobin Yvon Horiba). Raman scattering was excited by a frequency-doubled Nd/YAG laser at a wavelength of 532 nm with a laser power incident on the sample of about 2 mW. The laser beam was focused on individual crystals or particles using a Zeiss 100× microscope objective. The dispersive spectrometer has an entrance slit of 100 μm and a focal length of 800 mm and is equipped with a grating of 1200 lines mm^{-1} (spectral resolution ∼1.5 cm^{-1}). The spectra were recorded using unpolarized radiation and the Raman scattered light was detected by a CCD camera operating at 220 K. The acquisition time per spectrum was 10 s. For the calibration procedure, titanium dioxide (anatase) and 4-acetamidophenol (4AAP) were measured daily as a reference control for subsequent data pre-processing.

All spectroscopic data were processed using the "R" software [35]. Fifty Raman spectra of synthetic ungemachite were collected and an average spectrum obtained. For all spectra, a background reduction was performed using R package baselineWavelet, and the calibration procedure was completed performing a shift correction with 4AAP using an R script [36,37].

2.3. FT-IR measurements

The infrared spectroscopic measurements were carried out using a Bruker IFS66 FTIR spectrometer. The spectra were registered with a spectral resolution of 4 cm^{-1} within the 400–6000 cm^{-1} range. The transmission measurements at normal incidence were performed on a pellet of the milled ungemachite dispersed in a KBr host matrix.

2.4. XRD

X-ray diffractometry was carried out with a Bruker D8 Advance DaVinci diffractometer, using Cu Kα radiation ($\lambda = 1.54060$ Å) with a LYNXEYE 1-D detector. The patterns were collected at room temperature between 5° and 90° 2θ, with a step size of 0.02° 2θ and a time per step of 0.2 s.

3. Results and discussion

3.1. Raman and IR spectroscopy

Although natural samples of ungemachite have been described in the past by researchers as a yellowish material, the synthetic ungemachite obtained for this work was white. As a consequence of the slow evaporation process of the solution containing the required ions, the synthetic ungemachite crystallized on the walls and the bottom of the vessel. The identity of the synthetic ungemachite was confirmed by powder X-ray diffraction measurements.

The recorded X-ray diffraction pattern of the synthetic ungemachite is shown in Fig. 1.

Ungemachite crystallizes in a hexagonal system with the space group $R\bar{3}$ (C_{3i}^2) and has three molecules in the unit cell [33]. The reported structural data indicate that all SO_4^{2-} ions as well as 18 Na^+ ions occupy general positions, while the remaining 6 Na^+ ions as well as all NO_3^- and Fe^{3+} ions occupy special positions. These positions within the crystal unit cell affect the observed vibrational spectra, due to the factor group interactions. The factor group analysis links the structural characteristics of the unit cell of a specific substance to its vibrational spectrum. Thus the symmetries and numbers of the predicted vibrational bands are solely a function of the number of atoms and the symmetry of the unit cell [38].

For ungemachite, strong Raman and infrared signals of SO_4^{2-} and NO_3^- ions are expected. The four normal modes of the free SO_4^{2-} ion (T_d) are: v_1 (A_1) symmetric stretching, v_2 (E) symmetric bending, v_3 (F) asymmetric stretching, and v_4 (F) asymmetric bending, all of them are Raman active. These modes occur at 981 cm^{-1} (v_1), 451 cm^{-1} (v_2), 1104 cm^{-1} (v_3) and 613 cm^{-1} (v_4) [39]. The four normal modes of the free NO_3^- ion (D_{3h}) are: v_1 (A_1') symmetric stretching, v_2 (A_2'') symmetric bending, v_3 (E') asymmetric stretching, and v_4 (E') asymmetric bending; only v_2 is not Raman active. These modes occur at 1049 cm^{-1} (v_1), 830 cm^{-1} (v_2), 1355 cm^{-1} (v_3) and 690 cm^{-1} (v_4) [40]. The factor group analysis applying the Correlation Method [41] shows that 108 and 24 vibrational fundamental modes are expected for SO_4^{2-} and NO_3^-, respectively, and they split down as shown in Table 1. However, not necessarily all components predicted by the factor group analysis are expected to appear. The correlation for the fundamental modes of the SO_4^{2-} ion (T_d), NO_3^- ion (D_{3h}) and the H_2O molecule (C_{2v}) with the site of symmetry (C_1 for SO_4^{2-} and H_2O, and C_3 for NO_3^-) and the unit-cell symmetry C_{3i} are shown in Fig. 2.

The average Raman spectrum of ungemachite (Fig. 3a) shows four bands in the region where SO_4^{2-} and NO_3^- symmetric stretching modes are expected (950–1070 cm^{-1}). The band at 1047 cm^{-1} is assigned to NO_3^- v_1 (A_g), while the bands at 1035, 1011 and 952 cm^{-1} are assigned to SO_4^{2-} v_1 (A_g and E_g). Wavenumbers as high as 1035 cm^{-1} for SO_4^{2-} v_1 have been found before for other sulfate minerals, e.g., paracoquimbite, $Fe_2(SO_4)_3 \cdot 9H_2O$. With respect to a Raman spectrum of paracoquimbite, Ling and Wang [42] reported bands at 1037.0, 1025.4, and 1012.3 cm^{-1} for SO_4^{2-} v_1. The crystal structure data reported for ungemachite [33] show: (1) one of the S–O bond distances is significantly longer as compared to the

Table 1
Vibrational analysis of ungemachite, $K_3Na_8Fe(SO_4)_6(NO_3)_2 \cdot 6H_2O$.

C_{3i}	SO_4^{2-}				NO_3^-				H_2O			Activity
	v_1	v_2	v_3	v_4	v_1	v_2	v_3	v_4	v_1	v_2	v_3	
A_g	3	6	9	9	3	3	0	0	3	3	3	Raman
E_g	3	6	9	9	0	0	3	3	3	3	3	Raman
A_u	3	6	9	9	0	0	3	3	3	3	3	IR
E_u	3	6	9	9	3	3	0	0	3	3	3	IR

other three (S–O(1) is 1.512 Å, while S–O(2), S–O(3), and S–O(4) are 1.457, 1.465, and 1.461 Å, respectively), and (2) the O–S–O angles vary in the range of 105.4° to 112.0°. It is evident that the SO_4^{2-} ions within the crystal of ungemachite are slightly distorted, and probably this fact and the interatomic interactions responsible for the distortion, are the reasons for the occurrence of three bands in the symmetrical stretching mode of SO_4^{2-}. On the other hand, the crystal structure [33] shows no distortion of the NO_3^- ions within the crystal; considering that all the N–O bond distances are 1.249 Å and all O–N–O angles are 120°, there is no reason to expect more than one band for the NO_3^- v_1.

The average Raman spectrum of ungemachite (Fig. 3a) shows only one band for both NO_3^- v_3 (E_g) and NO_3^- v_4 (E_g), at 1383 and 721 cm^{-1}, respectively. The asymmetric stretching and bending of SO_4^{2-} can be unambiguously assigned; the bands at 1192, 1163 and 1144 cm^{-1} are assigned to SO_4^{2-} v_3 (A_g and E_g), while the bands at 655, 645, 619 and 600 cm^{-1} are assigned to SO_4^{2-} v_4 (A_g and E_g). Not only the bands of the symmetric bending mode of SO_4^{2-} are expected to appear in the region 400–500 cm^{-1}, but also a fundamental mode related to the Fe–O coordinations (see below for more details); therefore the bands at 472, 464 and 446 cm^{-1} are assigned to SO_4^{2-} v_2 (A_g and E_g) + FeO_6 v_2. According the results of the vibrational analysis of ungemachite (Table 1), the split of the H_2O modes can be observed in both Raman and infrared spectra. Two broad and overlapped bands are observed at 3420 and 3370 cm^{-1}, which are assigned to the stretching modes of H_2O (v_1 and v_3). For the H_2O bending mode (v_2) two broad and weak bands centered at 1711 and 1663 cm^{-1} are observed.

The infrared spectrum of ungemachite (Fig. 3b) shows a strong band for NO_3^- v_1 (E_u) at 1046 cm^{-1} and another one for SO_4^{2-} v_1 (A_u and E_u) at 964 cm^{-1}. Unambiguous assignment of the remaining three fundamental modes of SO_4^{2-} and NO_3^- is possible. Two bands are observed for NO_3^- v_3 (A_u) at 1402 and 1384 cm^{-1}, one band for
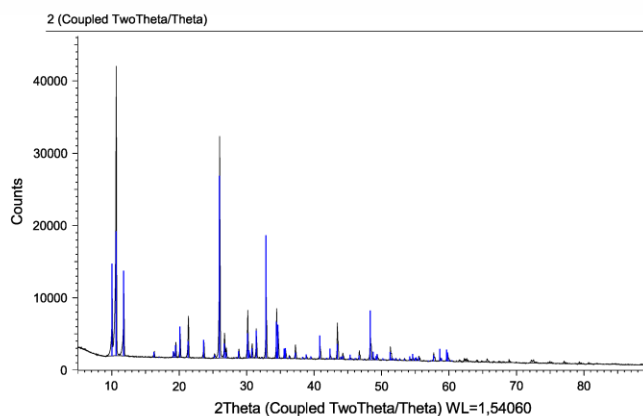
Fig. 1. X-ray diffraction pattern of synthetic ungemachite.

Fig. 2. Correlation scheme for the vibrational modes of SO_4^{2-}, NO_3^-, FeO_6 octahedron, and H_2O.

Fig. 3. (a) Average Raman spectrum of ungemachite; (b) infrared spectrum of ungemachite.

NO_3^- v_4 (A_u) at 735 cm^{-1}, and one band for NO_3^- v_2 (E_u) at 829 cm^{-1}. For the SO_4^{2-} ion, four bands at 1215, 1195, 1166, and 1131 cm^{-1} are assigned to the SO_4^{2-} v_3 (A_u and E_u). Four bands are observed for the SO_4^{2-} v_4 (A_u and E_u) at 661, 649, 617, and 604 cm^{-1}, while a weak band at 466 cm^{-1} is assigned to SO_4^{2-} v_2 (A_u and E_u). One band centered at 3422 cm^{-1} is observed and assigned to the stretching modes of H_2O (v_1 and v_3). Usually the H_2O bending mode is expected to appear at ~1500 cm^{-1}, nevertheless for some iron sulfate minerals it was also observed at values as high as ~1700 cm^{-1} [42]. This is the reason why the bands at 1769, 1698 and 1635 cm^{-1} are assigned to the H_2O bending mode (v_2). However, the unusual high value of the band at 1769 cm^{-1} should be taken carefully.

Although for ungemachite the strongest Raman and infrared signals are those generated by SO_4^{2-}, NO_3^- ions and H_2O vibrations, other crystal structure characteristics may contribute with weaker but specific signals. An important structural feature to be considered is that Fe^{3+} ions are octahedrally coordinated by six oxygen atoms and all six Fe–O bonds are equivalent [33,43], therefore the resulting FeO_6 octahedron belongs to the point group symmetry O_h. The fundamental modes to be observed under a O_h symmetry are v_1 (A_{1g}), v_2 (E_g), v_3 (F_{1u}), v_4 (F_{1u}), v_5 (F_{2g}), and v_6 (F_{2u}), where v_1, v_2 and v_5 are Raman active, v_3 and v_4 are infrared active, and v_6 is inactive in both infrared and Raman spectra [44]. The correlation

for the modes of the FeO_6 octahedron (O_h) with the site of symmetry C_{3i} and the unit-cell symmetry C_{3i} are shown in Fig. 2.

The octahedron coordination of a trivalent metal and oxygen is also observed in a group of compounds known as "alums", $Me^IMe^{III}(SO_4)_2 \cdot 12H_2O$ (where Me^I is a monovalent and Me^{III} is a trivalent metal). The vibrational spectra of "alums" with special attention focused on the trivalent metal–oxygen complex formed in the crystal, were the subject of both theoretical and experimental studies performed and published in the past [45,38,46–49]. Considering these studies, the expected wavenumber ranges for each Raman active fundamental mode of the $Me^{III}O_6$ octahedron in the crystal are well known; in the case of the FeO_6 octahedron the values expected are: ~523 cm^{-1} for v_1, ~475 cm^{-1} for v_2, and ~306–332 cm^{-1} for v_5 [46,47]. In the Raman spectrum of ungemachite (Fig. 3a), a broad band appears centered at 534 cm^{-1} and we assigned it to FeO_6 v_1. As the other FeO_6 octahedron bands may even be weaker than FeO_6 v_1, they may not necessarily appear. No bands were found in the region of FeO_6 v_5. The three bands in the region 400–500 cm^{-1} are assigned to SO_4^{2-} v_2 + FeO_6 v_2, as it was impossible to distinguish the modes from each other.

The infrared spectrum of ungemachite (Fig. 3b) also shows a band related to the FeO_6 octahedron; the band centered at 511 cm^{-1} is assigned to the FeO_6 v_3, since this fundamental mode was observed at 505 cm^{-1} in the infrared spectrum of $CsFe(SO_4)_2 \cdot 12H_2O$ [49].

3.2. Environmental implications

Ungemachite is a rare mineral which has only been identified in a copper deposit in Atacama (Chile) and – a single specimen – in the New Cobar copper–gold deposit, New South Wales (Australia) [34]. Probably the reason why ungemachite does not often occur in mineral deposits is the same which explains why nitrate deposits can only be found in a few regions in the world. As Claridge and Campbell [50] postulated, nitrate deposits can only be found in specific regions where arid conditions preserve the nitrate minerals from being washed out by rainwater or consumed by biological activity. The crystallization of ungemachite also requires the presence of sulfate; therefore the natural occurrence of this mineral depends on more specific conditions than the simple presence of nitrate minerals.

Although the occurrence of ungemachite in mineral deposits is strongly conditioned, we believe that this mineral may have important implications in another environmental compartment: air (atmosphere).

The formation of acidic aqueous solutions containing Na^+, K^+, NO_3^-, SO_4^{2-} and Fe^{3+} ions and their subsequent evaporization are the conditions required for the generation of ungemachite, conditions which can be achieved in atmosphere, since all those chemical species are usually present in the troposphere. A value of pH = 4.7 usually is considered as characteristic of atmospheric conditions, [51–54] but under certain circumstances the pH of the aerosol solution could even be lower than 1.0 [30]. The origin of these extreme low pH values is imaginable considering that nitrogen oxides (NO_x = NO + NO_2) and sulfur oxides (SO_x) – precursors of atmospheric HNO_3 and H_2SO_4, respectively – can be taken up by small droplets of fog and haze. The subsequent water vaporization process of the droplets not only produces an increase of diluted ions, but also provides adequate acid concentrations resulting in the decrease of the pH value.

The most important anthropogenic sources of nitrogen compounds in atmosphere are the agricultural activities and the livestock, in both cases the emissions are in the form of ammonia [55], but there are also natural sources such as the oceans. Wilson [56] postulated that the oceans are an important input of albuminoid nitrogen (proteinaceous nitrogen derived from animal and plant life) to the atmosphere, contributing in this way to the nitrogen cycle. Oxidation processes in atmosphere, involving ozone, O_3 and the hydroxyl radical $HO^·$, transform the ammonia as well as the albuminoid nitrogen to NO_3^-. There are also important emissions of NO_x, which are between 70% and 90% of anthropogenic origin [57].

On the other hand, there are important emissions of SO_x, that originate predominantly from volcanoes as natural source, but also from fossil fuel burning and industry [58].

The photochemical reactions of NO_x and SO_x with O_3 or $HO^·$ to produce NO_3^- and SO_4^{2-}, respectively, are well known [59,60]. In fact, by ^{17}O enrichment studies, Michalski et al. [60] confirmed that the main source of NO_3^- and SO_4^{2-} in the Atacama Desert (Chile) is the accumulation of these anions produced by the referred photochemical reactions, showing the great importance of these pathways in atmosphere and the impact on the terrestrial crust.

Na^+ and K^+ ions are present in ocean water and therefore their incorporation to the atmosphere by breaking waves and bursting bubbles on the ocean surface is expected; in fact, these ions are usually found in atmospheric particulate matter, especially in coastal areas. Ungemachite contains 0.375 mol K^+ per mol of Na^+ compared to 0.022 mol K^+ per mol of Na^+ (weight ratio K^+/Na^+ of 0.037) typically found in ocean water, [56] so the question is: is there enough K^+ ion in atmosphere (in relation to the Na^+ ion content) to produce ungemachite? Assuming that the weight ratio K^+/Na^+ in atmosphere is the same as the value observed in ocean

water, probably the weight ratio K^+/Na^+ would be too low to produce ungemachite, but this is not the case. On the basis of analysis done in ocean water, ocean foam, rainwater and snow, Wilson [56] reported that the same process which incorporates albuminoid nitrogen to atmosphere, is responsible for an enrichment of the K^+ ion with respect to the Na^+ ion concentration, increasing the weight ratio K^+/Na^+ in one order of magnitude. Furthermore, it is well known that biomass burning incorporates additional amounts of K^+ ion to atmosphere, to the extent that the concentration of this ion can be used as an indicator of burned biomass [61].

Our attempt to crystallize ungemachite from a solution with a weight ratio K^+/Na^+ of 0.29 (lower than the stoichiometric value according to the molecular formula of ungemachite) was successful. Therefore, considering the atmospheric occurrence of NO_3^- and SO_4^{2-} ions, and the possibility to achieve an adequate ratio of K^+ and Na^+ ions concentration in atmosphere as well as the common low pH values in aerosol droplets, the only factor which could limit the atmospheric formation of ungemachite would be an insufficient availability of Fe^{3+} ion.

The occurrence of iron in atmosphere as well as its transport has been intensively studied in the past [52,62,63], due to the biological implications in oceanic systems. In oceans, iron is an important micronutrient which restricts the growth of phytoplankton [64]. One of the most important pathways for iron to enter in the ocean is the deposition of atmospheric iron (transported from continental areas) [30]. The dust material suspended in atmosphere and transported over long distances following seasonal dust events, contains iron in different chemical forms, therefore the study of the relative amount of iron capable to dissolve under atmospheric conditions has been the subject of many works [30,65–70]. However, it is important to remark that the iron-rich atmospheric particulate matter is not only composed of dust, but also of aerosol material originated from biomass burning [71] and even fuel combustion [72].

The solubility of the iron contained in atmospheric particulate matter is variable and depends on the mineralogy (origin), size of particles, the formation of organic complexes (e.g., with oxalate), and specially the pH [30,51,54,63,65,66,69,73]. Common iron minerals on the terrestrial crust have low solubilities in water (e.g., hematite, goethite, etc.), nevertheless the solubilities of iron minerals in general increase drastically at low pH values like those typically found in aerosol solutions. The solubility of iron originated from crystalline matrix like alumino–silicated mineral is lower (with likewise lower dissolution rates) than the iron coming from carbonaceous matrix (fuel combustion) [66]. In fact, a specific study carried out by Huffman and coworkers [74] on fine particulate matter produced by combustion of fuel oil, showed that iron is found in this kind of particulate matter as $Fe_2(SO_4)_3$, a compound with a relatively high solubility in water. Therefore, it is common that soluble iron in atmospheric particulate matter is related to anthropogenic activities [62,75]. Biomass burning was also identified as a source of soluble iron in atmospheric aerosols, hence the iron contained in biomass burning aerosols is significantly more soluble in water than the iron in mineral dust [63,71].

It is generally accepted that higher iron solubility is linked with smaller particles, because smaller particles have a larger surface area to volume ratio; [67] in fact, iron from combustion sources (more soluble than iron in dust material) is found frequently in smaller particles [62].

If atmospheric particles containing iron interact with atmospheric water under the mentioned condition of low pH values, the dissolution of important amounts of iron is expected. Taking into account that smaller particles remain suspended for longer periods, and the fact that iron-rich particles are found in smaller particles, the dissolution chances of iron can increase significantly. Furthermore, particles originated from combustion (generally

linked to human activities), which contain a more soluble iron, can add this more soluble iron to the atmosphere.

Considering all the mentioned aspects, there are enough arguments to consider the atmospheric formation of ungemachite feasible.

4. Conclusions

Synthetic ungemachite, $K_3Na_8Fe(SO_4)_6(NO_3)_2 \cdot 6H_2O$ was obtained for the first time and its purity was confirmed by X-ray diffractometry. The Raman and infrared spectra of synthetic ungemachite were recorded and band assignments proposed. In addition to the fundamental modes of SO_4^{2-} and NO_3^- ions, the Raman spectrum of ungemachite shows a band at 534 cm^{-1}, which was assigned to the stretching mode, v_1, of the FeO$_6$ octahedron, an important structural feature observed earlier in the crystal of ungemachite.

Considering that atmospheric materials of natural and anthropogenic origin contain Fe as well as K$^+$ and Na$^+$ ions and that atmospheric conditions support the formation of NO$_3^-$ and SO$_4^{2-}$ ions, the atmospheric generation of ungemachite by condensation-evaporation cycles has been postulated. The characteristic low pH value of the aerosol solution is considered a key factor not only to dissolve the iron present in atmospheric particles, but also to allow the crystallization of ungemachite.

Acknowledgments

References

[1] V. Ciobotă, W. Salama, N. Tarcea, P. Rösch, M.E. Aref, R. Gaupp, J. Popp, J. Raman Spectrosc. 43 (2012) 405.
[2] R. Voigt, K.H. Lieser, Naturwissenschaften 71 (1984) 377.
[3] R.M. Harrison, W.T. Sturges, Atmos. Environ. 18 (1984) 1829.
[4] I. Rodríguez, S. Gali, C. Marcos, Environ. Geol. 56 (2009) 1551.
[5] G. Schweiger, J. Aerosol Sci. 20 (1989) 1621.
[6] K.H. Fung, D.G. Imre, I.N. Tang, J. Aerosol Sci. 25 (1994) 479.
[7] M. Trunk, J. Popp, I. Hartmann, M. Lankers, E. Urlaub, W. Kiefer, Fresenius J. Anal. Chem. 355 (1996) 354.
[8] M. Trunk, J. Popp, W. Kiefer, Chem. Phys. Lett. 284 (1998) 377.
[9] J. Musick, J. Popp, M. Trunk, W. Kiefer, Appl. Spectrosc. 52 (1998) 692.
[10] J. Musick, J. Popp, W. Kiefer, J. Raman Spectrosc. 31 (2000) 217.
[11] Y. Batonneau, S. Sobanska, J. Laureyns, C. Bremard, Environ. Sci. Technol. 40 (2006) 1300.
[12] W. Schumacher, M. Kühnert, P. Rösch, J. Popp, J. Raman Spectrosc. 42 (2011) 383.
[13] P. Vargas Jentzsch, B. Kampe, P. Rösch, J. Popp, J. Phys. Chem. A 115 (2011) 5540.
[14] P. Vargas Jentzsch, V. Ciobotă, B. Kampe, P. Rösch, J. Popp, J. Raman Spectrosc. 43 (2012) 514.
[15] S. Myriokefalitakis, K. Tsigaridis, N. Mihalopoulos, J. Sciare, A. Nenes, K. Kawamura, A. Segers, M. Kanakidou, Atmos. Chem. Phys. 11 (2011) 5761.
[16] M.P. Tolocka, T.D. Saul, M.V. Johnston, J. Phys. Chem. A 108 (2004) 2659.
[17] D. Sopauskiene, D. Budvytyte, Atmos. Environ. 28 (1994) 1291.
[18] G. Wang, H. Wang, Y. Yu, S. Gao, J. Feng, S. Gao, L. Wang, Atmos. Environ. 37 (2003) 2893.
[19] V. Ariola, A. D'Alessandro, F. Lucarelli, G. Marcazzan, F. Mazzei, S. Nava, I. Garcia-Orellana, P. Prati, G. Valli, R. Vecchi, A. Zucchiatti, Chemosphere 62 (2006) 226.
[20] M. Amodio, P. Bruno, M. Caselli, G. De Gennaro, P.R. Dambruoso, B.E. Daresta, P. Ielpo, F. Guncolo, C.M. Placentino, V. Paolillo, M. Tutino, Atmos. Res. 90 (2008) 313.
[21] J.N. Galloway, G.E. Likens, Tellus 30 (1978) 71.
[22] W.Z. De Mello, Environ. Poll. 114 (2001) 235.
[23] M.Y. Iwasaka, R. Imasu, A. Ono, Tellus B 40 (1988) 494.
[24] I. Mori, M. Nishikawa, Y. Iwasaka, Sci. Total Environ. 224 (1998) 87.
[25] S. Rodríguez, X. Querol, A. Alastuey, G. Kallos, O. Kakaliagou, Atmos. Environ. 35 (2001) 2433.
[26] B. Artíñano, P. Salvador, D.G. Alonso, X. Querol, A. Alastuey, Environ. Pollut. 125 (2003) 453.
[27] G. Kallos, A. Papadopoulos, P. Katsafados, S. Nickovic, J. Geophys. Res. 111 (2006) D09204.
[28] D.M. Cwiertny, J. Baltrusaitis, G.J. Hunter, A. Laskin, M.M. Scherer, V.H. Grassian, J. Geophys. Res. 113 (2008) D05202.
[29] H.R. Pruppacher, R. Jaenicke, Atmos. Res. 38 (1995) 283.
[30] X. Zhu, J.M. Prospero, F.J. Millero, D.L. Savoie, G.W. Brass, Mar. Chem. 38 (1992) 91.
[31] M.A. Peacock, M.C. Bandy, Am. Mineralogist 22 (1937) 207.
[32] M.A. Peacock, M.C. Bandy, Am. Mineralogist 23 (1938) 314.
[33] L.A. Groat, F.C. Hawthorne, Am. Mineralogist 71 (1986) 826.
[34] R.L. Frost, K.L. Erickson, M.L. Weier, P. Leverett, P.A. Williams, Spectrochim. Acta A 61 (2005) 607.
[35] R Development Core Team, R: A Language and Environment for Statistical Computing, R Foundation for Statistical Computing; Vienna, 2009.
[36] T. Dörfer, T. Bocklitz, N. Tarcea, M. Schmitt, J. Popp, Z. Phys. Chem. 225 (2011) 753.
[37] Z.-M. Zhang, S. Chen, Y.-Z. Liang, Z.-X. Liu, Q.-M. Zhang, L.-X. Ding, F. Ye, H. Zhou, J. Raman Spectrosc. 41 (2010) 659.
[38] S.P. Best, R.S. Armstrong, J.K. Beattie, J. Chem. Soc. Dalton Trans. (1982) 1655.
[39] V.S. Jayakumar, G. Sekar, P. Rajagopal, G. Aruldhas, Phys. Stat. Sol. (a) 109 (1988) 635.
[40] B.J.M. Rajkumar, V. Ramakrishnan, R.K. Rajaram, Spectrochim. Acta A 54 (1998) 1527.
[41] W.G. Fateley, F.R. Dollish, N.T. McDevitt, F.F. Bentley, Infrared and Raman selection rules for molecular and lattice vibrations: The Correlation Method, Wiley-Interscience, USA, 1972.
[42] Z.C. Ling, A. Wang, Icarus 209 (2010) 422.
[43] F.C. Hawthorne, S.V. Krivovichev, P.C. Burns, Rev. Mineral. Geochem. 40 (2000) 1.
[44] A.M. Heyns, Spectrochim. Acta A 33 (1977) 315.
[45] H.H. Eysel, J. Eckert, Z. Anorg. Allg. Chem. 424 (1976) 68.
[46] S.P. Best, J.K. Beattie, R.S. Armstrong, J. Chem. Soc. Dalton Trans. (1984) 2611.
[47] A.A. Jarzęcki, A.D. Anbar, T.G. Spiro, J. Phys. Chem. A 108 (2004) 2726.
[48] M. Boujelbene, T. Mhiri, Int. J. Spectrosc. (2011), http://dx.doi.org/10.1155/2011/128401.
[49] S.P. Best, R.S. Armstrong, J.K. Beattie, Inorg. Chem. 19 (1980) 1958.
[50] G.G.C. Claridge, I.B. Campbell, Nature 217 (1968) 428.
[51] K.V. Desboeufs, R. Losno, J.L. Colin, Atmos. Environ. 35 (2001) 3529.
[52] G. Sarthou, A.R. Baker, S. Blain, E.P. Achterberg, M. Boye, A.R. Bowie, P. Croot, P. Laan, H.J.W. De Baar, T.D. Jickells, P.J. Worsfold, Deep-Sea Res. Pt I (50) (2003) 1339.
[53] A.R. Baker, T.D. Jickells, M. Witt, K.L. Linge, Mar. Chem. 98 (2006) 43.
[54] R. Paris, K.V. Desboeufs, E. Journet, Atmos. Environ. 45 (2011) 6510.
[55] T.H. Misselbrook, T.J. Van Der Weerden, B.F. Pain, S.C. Jarvis, B.J. Chambers, K.A. Smith, V.R. Phillips, T.G.M. Demmers, Atmos. Environ. 34 (2000) 871.
[56] A.T. Wilson, Nature 184 (1959) 99.
[57] H.B. Singh, Environ. Sci. Technol. 21 (1987) 320.
[58] J. Dignon, Atmos. Environ. A 26 (1992) 1157.
[59] B.J. Finlayson-Pitts, J.N. Pitts Jr., Chemistry of the upper and lower atmosphere: Theory, experiments, and applications, Academic Press, USA, 2000.
[60] G. Michalski, J.K. Böhlke, M. Thiemens, Geochim. Cosmochim. Acta 68 (2004) 4023.
[61] M.O. Andreae, Science 220 (1983) 1148.
[62] E.R. Sholkovitz, P.N. Sedwick, T.M. Church, Geochim. Cosmochim. Acta 73 (2009) 3981.
[63] R. Paris, K.V. Desboeufs, P. Formenti, S. Nava, C. Chou, Atmos. Chem. Phys. 10 (2010) 4273.
[64] J.H. Martin, S.E. Fitzwater, Nature 331 (1988) 341.
[65] L.J. Spokes, D. Jickells, B. Lim, Geochim. Cosmochim. Acta 58 (1994) 3281.
[66] K.V. Desboeufs, A. Sofikitis, R. Losno, J.L. Colin, P. Ausset, Chemosphere 58 (2005) 195.
[67] A. Ito, Y. Feng, Atmos. Chem. Phys. 10 (2010) 9237.
[68] F. Solmon, P.Y. Chuang, N. Meskhidze, Y. Chen, J. Geophys. Res. 114 (2009) D02305.
[69] A.R. Baker, T.D. Jickells, Geophys. Res. Lett. 33 (2006) L17608.
[70] Z. Shi, S. Bonneville, M.D. Krom, K.S. Carslaw, T.D. Jickells, A.R. Baker, L.G. Benning, Atmos. Chem. Phys. 11 (2011) 995.
[71] C. Guieu, S. Bonnet, T. Wagener, M.-D. Loÿe-Pilot, Geophys. Res. Lett. 32 (2005) L19608.
[72] R.D. Smith, Prog. Energy Combust. Sci. 6 (1980) 53.
[73] R.M. Cornell, P.W. Schindler, Clays Clay Miner. 35 (1987) 347.
[74] G.P. Huffman, F.E. Huggins, N. Shah, R. Huggins, W.P. Linak, C.A. Miller, R.J. Pugmire, H.L.C. Meuzelaar, M.S. Seehra, A. Manivannan, J. Air Waste Manage. Assoc. 50 (2000) 1106.
[75] P.Y. Chuang, R.M. Duvall, M.M. Shafer, J.J. Schauer, Geophys. Res. Lett. 32 (2005) L07813.

2.5 Inorganic salts in atmospheric particulate matter: Raman spectroscopy as an analytical tool [PV5]

Authorship of Publication

Paul Vargas Jentzsch: concept development

salts preparation

Raman measurements

writing of manuscript

Bernd Kampe: Raman spectra processing

classification and identification using chemometric methods

Valerian Ciobotă: Raman measurements

discussion of experimental concept and results

Petra Rösch: discussion of experimental concept and results

proofreading of manuscript

Jürgen Popp: project management

discussion of concepts and results

discussion and proofreading of manuscript

Submitted to *Spectrochimica Acta A*

INORGANIC SALTS IN ATMOSPHERIC PARTICULATE MATTER: RAMAN SPECTROSCOPY AS AN ANALYTICAL TOOL

Paul Vargas Jentzsch[a§]; Bernd Kampe[a§]; Valerian Ciobotă[a]; Petra Rösch[a]; Jürgen Popp[a,b*]

[a] Institut für Physikalische Chemie, and Abbe Center of Photonics,
Friedrich-Schiller-Universität Jena,
D-07743 Jena, Germany
[b] Institut für Photonische Technologien e.V. (IPHT),
D-07745 Jena, Germany

Atmospheric particulate matter is composed of inorganic and organic components of natural and anthropogenic origin. Wind-transport is probably the most important process responsible for the emission of solid particulate matter into the troposphere, but there are also important contributions from chemical reactions due to the interaction of different atmospheric components in presence of water and solar radiation. Sulfate, nitrate and carbonate salts can be both reactants and products in this complex dynamic system, and there is no doubt about their important impact on the climate. Both simple and mixed salts can be produced in atmosphere by dissolution-crystallization processes. The Raman spectra of 45 representative salts of the atmospheric environment were recorded and the bands assigned. The chemometric analysis of the spectroscopic data of these 45 salts demonstrates the suitability of Raman spectroscopy to classify and identify sulfate, nitrate and carbonate salts of atmospheric importance. Salts were classified into three groups: "sulfates", "nitrates or carbonates" and "sulfate-nitrates or sulfate-carbonate". This kind of information is relevant in atmospheric studies because specific characteristics of the salts can provide valuable information about the origin of the salts, the atmospheric chemistry and climate forcing, thus contributing to the evaluation of environmental impacts.

Keywords: Atmospheric particles, Raman spectroscopy, chemometric methods, minerals, simple salts, mixed salts.

1 Introduction

The existence of several dynamic processes on the planet Earth is a well-known fact for a long time, but the interest in these processes is growing as mankind is becoming aware that their activities can affect and even modify them. Some general aspects of the environmental impacts caused by human activities were exposed by Crutzen [1].

At present, environmental topics such as the global warming have importance worldwide, as there may be dramatic consequences to human future. A complete study of the weather includes the investigation of its changes over the time, i.e. the development of weather conditions through different eras and their possible trends. Researchers can use geologic information to identify climate changes in ancient times [2] and the occurrence in soil of a specific kind of ions is an indicator of the precipitation pattern of a specific region, e.g., nitrate salts are characteristic of arid soils [3,4]. However, the study of minerals seems not to be limited to the lithosphere, but also comprises the atmosphere, as huge amounts of particulate matter (aerosols) are not only released to the atmosphere, but they are also produced by chemical reactions within the atmosphere. About two decades ago, Preining [5] estimated that the annual global aerosol production totaled approx. 2 Pg (1 Pg = 10^{15} g), whereof 40% was attributed to direct natural emissions (sea salt, mineral dust and volcanic material), 40% to natural gas emissions converted to aerosols (sulfates, nitrates and hydrocarbons), and 20% to anthropogenic emissions (direct and gas-to-particle conversion). A few years later, Tegen and coworkers [6,7] demonstrated by using model calculations that not all mineral dust has a natural origin, in fact more than 50% of the total atmospheric dust mass originates from disturbed soils, in other words, it is produced by human activities.

Atmospheric particles are important for heterogeneous reactions which can alter the atmospheric composition; as an example the reaction between gaseous nitric acid, $HNO_3(g)$, and solid sodium chloride, $NaCl(s)$, is

---

§ These authors contributed equally to this work.
* Corresponding author. Tel.: +49-3641/9-48320; Fax: +49-3641/9-48302;
E-mail address: juergen.popp@uni-jena.de.

reported by Gard et al. [8]. Photochemical reactions of mineral dust have been the subject of different investigations on the daytime chemistry [9]. Atmospheric particles affect also the weather conditions and climate, since they influence the cloud lifetime and the Earth radiation budget [10,11].

Many authors, generally using X-ray diffractometry, reported the occurrence in atmospheric particle samples of minerals such as $Na_2Mg(SO_4)_2 \cdot 4H_2O$ (bloedite), $(NH_4)_2Mg(SO_4)_2 \cdot 6H_2O$ (boussingaultite), $(NH_4)_2Ca(SO_4)_2 \cdot H_2O$ (koktaite), $(NH_4)_2Fe(SO_4)_2 \cdot 6H_2O$ (mohrite), $Na_3(NO_3)(SO_4) \cdot H_2O$ (darapskite), $K_2Ca(SO_4)_2 \cdot H_2O$ (syngenite), $Na_2Ca(SO_4)_2$ (glauberite), $K_2Ca_2Mg(SO_4)_4 \cdot 2H_2O$ (polyhalite) among others [12-22]. While these minerals partly originate from blown dust, the atmospheric formation of particles cannot be ruled out. It is well known that salts containing characteristic aerosol ions are released to atmosphere by breaking waves and bursting bubbles on the ocean surface [23]; NO_3^- (especially as HNO_3) and SO_4^{2-} (as H_2SO_4) ions are produced in atmosphere by oxidation processes [24], and certain human activities release specific ions to atmosphere [19,25]. According to estimations these materials interact with atmospheric water, during the residence and transport of aerosols in atmosphere, undergoing around ten condensation-evaporation cycles [26], which are likely to produce important changes in their chemical composition. Based on these considerations we postulated in earlier articles [27-29] that mixed salts are formed in atmosphere as a result of dissolution-precipitation processes.

As mentioned, X-ray diffractometry is probably the most popular analytical method for mineral analysis, but infrared spectroscopy has also been proposed as a complementary analytical tool [30,31]. Recently, Raman spectroscopy is acquiring growing importance in mineral analysis; it has already been used to elucidate the composition of mineral deposits when studying geological processes [32] and is proposed for mineralogical studies in the planetary exploration [33,34]. In addition, several investigations reported the suitability of this technique for chemical characterization of atmospheric particles [27,28,35-42].

In this article we evaluate the Raman spectra of the most representative salts expected to be produced in atmosphere by the interaction of atmospheric material with water. It is known that sulfate and nitrate salts can be found in atmospheric particulate matter, and we believe that carbonate and bicarbonate salts (generally of terrigenous origin) can also play an important role in atmospheric chemistry; accordingly we selected representative salts for this study. The spectroscopic information is analyzed using chemometric methods to classify the atmospheric salts and to determine whether this kind of salts can be identified adequately using Raman spectroscopy.

2 Materials and methods

2.1 Chemicals and salt synthesis

Ammonium bicarbonate, NH_4HCO_3 ($\geq 99.0\%$), ammonium nitrate, NH_4NO_3 ($\geq 99.0\%$), ammonium sulfate, $(NH_4)_2SO_4$ ($\geq 99.0\%$), calcium nitrate tetrahydrate, $Ca(NO_3)_2 \cdot 4H_2O$ ($\geq 99.0\%$), calcium sulfate dihydrate, $CaSO_4 \cdot 2H_2O$ ($\geq 99\%$), iron (III) sulfate hydrate, $Fe_2(SO_4)_3 \cdot xH_2O$ (Fe 21-23%), iron (II) sulfate heptahydrate, $FeSO_4 \cdot 7H_2O$ ($\geq 99.0\%$), sodium bicarbonate, $NaHCO_3$ ($\geq 99.5\%$), sodium carbonate decahydrate, $Na_2CO_3 \cdot 10H_2O$ ($\geq 99.0\%$), sodium chloride, NaCl (min 99.5%), sodium sulfate anhydrous, Na_2SO_4 ($\geq 99.0\%$), magnesium nitrate hexahydrate, $Mg(NO_3)_2 \cdot 6H_2O$ ($\geq 99.0\%$), manganese (II) sulfate monohydrate, $MnSO_4 \cdot H_2O$ ($\geq 99\%$), potassium nitrate, KNO_3 ($\geq 99.0\%$), potassium sulfate, K_2SO_4 ($\geq 99.0\%$), hydrochloric acid, HCl ($\geq 37\%$), and sulphuric acid, H_2SO_4 (95.0-98.0%), were purchased from Sigma-Aldrich. Calcium carbonate, $CaCO_3$ ($\geq 99.0\%$), copper (II) sulfate pentahydrate, $CuSO_4 \cdot 5H_2O$ ($\geq 99\%$) and zinc sulfate heptahydrate, $ZnSO_4 \cdot 7H_2O$ ($\geq 99\%$) were purchased from Merck. Sodium nitrate, $NaNO_3$ (min. 99%) was purchased from VWR. These reactants were used without further purification. Magnesium sulfate anhydrous, $MgSO_4$ (min. 99.5%) purchased from VWR was dried in an oven at 250 °C during 2 hours before use, due to its high hygroscopicity.

$(NH_4)Fe(SO_4)_2 \cdot 12H_2O$ (lonecreekite) was crystallized at room temperature (20°C) by slow evaporation of an acidic solution (pH < 2) containing $Fe_2(SO_4)_3$ and $(NH_4)_2SO_4$ in a molar ratio of 1:1. $(NH_4)_2Fe(SO_4)_2 \cdot 6H_2O$ (mohrite) was crystallized at room temperature by slow evaporation of a slightly acidic solution containing $FeSO_4$ and $(NH_4)_2SO_4$ in a molar ratio of 1:1. In both cases, H_2SO_4 was used to acidify the solutions.

Considering that the commercial $FeSO_4 \cdot 7H_2O$ can contain impurities (Fe^{3+}), this salt was recrystallized. A slightly acidic saturated aqueous solution of the commercial $FeSO_4 \cdot 7H_2O$ ($\geq 99.0\%$) was prepared and vaporized at room temperature (20°C). The resulting flat green crystals (a few millimeters long) were washed with small amounts of distilled water and dried carefully with a piece of absorbent paper.

$FeSO_4 \cdot H_2O$ (szomolnokite) was obtained using three methods: 1) heating crystals of $FeSO_4 \cdot 7H_2O$ at 40°C during 2 h; 2) exposition of $FeSO_4 \cdot 7H_2O$ crystals to a very low humidity air environment (in a desiccator) overnight; and 3) recrystallization of the heptahydrate using a 50% v/v solution of H_2SO_4. [43] In all three cases the resulting product was grey and the Raman spectra showed the same features.

$FeSO_4 \cdot 4H_2O$ (rozenite) was obtained by exposition of $FeSO_4 \cdot H_2O$ powder to humid air (relative humidity 70%) during 10 minutes. The resulting powder was light yellow.

$K_3Na(SO_4)_2$ (aphthitalite) was obtained by slow vaporization of a saturated solution containing K_2SO_4 and Na_2SO_4, molar ratio 1:1.

For the preparation of Na_2SO_4 in phase III, a saturated solution of Na_2SO_4 at 100°C was fast vaporized on a hot glass surface at 100°C. Na_2SO_4 in phase III crystallized as tiny, less than 1 mm long needles.

$(NH_4)_2Fe(SO_4)_2 \cdot 6H_2O$ (mohrite) was crystallized at room temperature (20 °C) by slow evaporation of a slightly acidic solution containing $FeSO_4$ and $(NH_4)_2SO_4$ in a molar ratio of 1:1.

$Na_3(CO_3)(HCO_3) \cdot 2H_2O$ (trona) was crystallized from a solution containing Na_2CO_3 and $NaHCO_3$. To prepare this solution, about 16.42 g of $Na_2CO_3 \cdot 10H_2O$ were dissolved in 100 ml of water and 1 ml of a 25% HCl solution was added for partial neutralization. The resulting solution was slowly evaporated at 40°C (evaporation rate ~ 0.3 ml/h) until elongated translucent crystals were formed. The resulting amounts of Na_2CO_3 and $NaHCO_3$ in solution are in agreement with the equilibrium data reported by Hill and Bacon [44] for $Na_3(CO_3)(HCO_3) \cdot 2H_2O$ crystallization. The temperature was selected using the phase diagram as a function of the CO_2 content published by Datta et al. [45] and considering the region of CO_2 content of air.

$Na_2CO_3 \cdot H_2O$ (thermonatrite) was prepared by heating crystals of $Na_2CO_3 \cdot 10H_2O$ at 32°C during 12 h.

$Na_6(CO_3)(SO_4)_2$ (burkeite) was crystallized at 75°C from a solution containing Na_2CO_3 and Na_2SO_4 in a molar ratio of 1:2.

$Na_2Mn(SO_4)_2 \cdot 2H_2O$ and $Na_2Zn(SO_4)_2 \cdot 4H_2O$ (changoite) were crystallized at room temperature by slow evaporation of equimolar solutions containing Na_2SO_4 and $MnSO_4$, and Na_2SO_4 and $ZnSO_4$, respectively. The crystallization of $Na_2Mn(SO_4)_2 \cdot 2H_2O$ and $Na_2Zn(SO_4)_2 \cdot 4H_2O$ from the mentioned solutions is in good agreement with the equilibrium data for $ZnSO_4$-Na_2SO_4-H_2O and $MnSO_4$-Na_2SO_4-H_2O systems published by Caven and Johnston [46].

$MgSO_4 \cdot 7H_2O$ (epsomite), $(NH_4)_2Ca(SO_4)_2 \cdot H_2O$ (koktaite), $(NH_4)_2Cu(SO_4)_2 \cdot 6H_2O$, $(NH_4)_2Mg(SO_4)_2 \cdot 6H_2O$ (boussingaultite), $(NH_4)_2Mn(SO_4)_2 \cdot 6H_2O$, $(NH_4)NaSO_4 \cdot 2H_2O$ (lecontite), $(NH_4)_2Zn(SO_4)_2 \cdot 6H_2O$, $K_2Ca(SO_4)_2 \cdot H_2O$ (syngenite), $K_2Ca_2Mg(SO_4)_4 \cdot 2H_2O$ (polyhalite), $K_2Cu(SO_4)_2 \cdot 6H_2O$, $K_2Mg(SO_4)_2 \cdot 6H_2O$ (picromerite), $K_2Zn(SO_4)_2 \cdot 6H_2O$, $Na_2Ca(SO_4)_2$ (glauberite), $Na_2Cu(SO_4)_2 \cdot 2H_2O$ (krohnkite), $Na_2Mg(SO_4)_2 \cdot 5H_2O$ (konyaite), $K_3Na_8Fe(SO_4)_6(NO_3)_2 \cdot 6H_2O$ (ungemachite), $(NH_4)_2SO_4 \cdot 3NH_4NO_3$, and $Na_3(SO_4)(NO_3) \cdot H_2O$ (darapskite) were obtained according to earlier reported methods [28,29,47-57].

2.2 Spectroscopic instrumentation and data processing

The Raman spectra were recorded with a micro-Raman setup (HR LabRam inverse system, Jobin Yvon Horiba). Raman scattering was excited by a frequency-doubled Nd:YAG laser at a wavelength of 532 nm with a laser power incident on the sample of about 2 mW. The laser beam was focused on individual particles using a Zeiss 100x/0.75NA microscope objective. The dispersive spectrometer has an entrance slit of 100 μm and a focal length of 800 mm and is equipped with a grating of 1200 lines mm^{-1} (spectral resolution ~1.5 cm^{-1}). The Raman scattered light was detected by a CCD camera operating at 220 K. The measurements of individual particles of the different salts were performed using unpolarized radiation and the total acquisition time was 100 s per spectrum. For the calibration procedure, titanium dioxide (anatase) and 4-acetamidophenol (4AAP) were measured daily as a reference control for subsequent data pre-processing.

The Raman spectrum of a minimum of 50 individual particles (diameter ~2-20 μm) of each salt were collected and the average spectra obtained. All spectroscopic data were processed using the "R" software [58]. For all spectra a calibration procedure was performed by a shift correction with 4AAP using an R script [59].

2.3 XRD

X-ray diffractometry was carried out with a Bruker D8 Advance DaVinci diffractometer, employing Cu Kα radiation (λ = 1.54060 Å) and a LYNXEYE 1-D detector. The patterns were collected at room temperature between 5 and 90° 2θ, with a step size of 0.02° 2θ and a time per step of 0.2 seconds.

3 Results and discussion

3.1 Raman spectroscopic data

The average Raman spectra of the selected forty-five salts (simple and mixed) and the proposed band assignments are presented in the Supporting Information (Figures S1-S45 and Tables S1-6). The interquartile range in the Figures S1-S45 shows some variations between Raman spectra of the same salt, probably due to crystal grains of different orientations. The identity of the synthetic salts was confirmed using X-ray diffractometry and the X-ray patterns are presented in the Supporting Information (Figures S46-S76).

For crystalline solids the Raman spectrum is determined by the space group, therefore different crystal forms (polymorphs) generally give different spectra. Depending on the crystal structure of the solid and the positions (general or special) occupied by the sulfate, nitrate, carbonate and/or bicarbonate ions in the unit cell, some shifts as well as splits of the normal modes are expected in the Raman spectra of the crystalline solids. Most of the salts considered in this study are monoclinic, but orthorhombic, triclinic, trigonal and cubic salts are considered as well. In order to assign the observed bands in the Raman spectra of sulfate, nitrate, carbonate and bicarbonate salts, the normal modes of the "free ions" should be known.

Specific details of the band assignments, some characteristics of the salts related to the observed Raman spectrum (e.g., the crystal structure) and the comparison of salts to each other are presented and discussed in the following subsections.

3.1.1 Sulfates

This study considers thirty-one sulfate salts containing Na^+, K^+, NH_4^+, Mg^{2+}, Ca^{2+}, Fe^{3+}, Fe^{2+}, Mn^{2+}, Cu^{2+} and Zn^{2+} ions, twenty of which are monoclinic, seven orthorhombic, three triclinic and one cubic. The strongest bands in the Raman spectra of sulfate salts are related to the SO_4^{2-} ion. The four normal modes of the free SO_4^{2-} ion (T_d) are: ν_1 (A_1) symmetric stretching, ν_2 (E) symmetric bending, ν_3 (F) asymmetric stretching and ν_4 (F) asymmetric bending, all of them are Raman active. These modes occur at 981 cm^{-1} (ν_1), 451 cm^{-1} (ν_2), 1104 cm^{-1} (ν_3) and 613 cm^{-1} (ν_4) [51]. The positions of the SO_4^{2-} ions within the crystal unit cell affect the observed vibrational spectra due to the factor group interactions. When Raman spectra of isomorphous sulfate salts are compared, the presence of one specific cation (instead of another one in the same position) has a notorious effect. In these cases, the SO_4^{2-} ions occupy the same position, but there may be changes in the interatomic distances as well as distortions in the bond angles, resulting in variations in the vibrational spectra. Some comparisons of this kind are considered in this subsection.

Crystalline $(NH_4)_2SO_4$ and K_2SO_4 at room temperature belong both to the orthorhombic system (D^{16}_{2h} factor group). The SO_4^{2-} symmetric stretching (ν_1), which is the strongest signal in the Raman spectra of sulfate salts, appears as a single band at 972 and 980 cm^{-1} for $(NH_4)_2SO_4$ and K_2SO_4, respectively (Figure S1 and S2). The differences observed between the Raman spectra of $(NH_4)_2SO_4$ and K_2SO_4 can be explained in terms of structural details; in both cases the SO_4^{2-} ions occupy the site of symmetry C_s, but the presence of K^+ or NH_4^+ ions modifies the unit-cell dimensions and therefore the interatomic distances and bond angles in each case. For instance, the interatomic distances S-O for K_2SO_4 are between 1.459 and 1.473 Å compared to 1.49 Å for $(NH_4)_2SO_4$ [60,61]. A shorter interatomic distance implies a higher force constant and therefore higher wavenumbers for the bands of the stretching modes. The presence of NH_4^+ ions contributes additional wide bands to the Raman spectrum of $(NH_4)_2SO_4$; the NH_4^+ stretching modes appear at 3303, 3145 and 2826 cm^{-1}, while the NH_4^+ bending modes appear at 1690, 1667 and 1414 cm^{-1}.

Crystalline Na_2SO_4 exhibits phase transitions when heated; the orthorhombic phases V and III can be expected to occur and persist at room temperature. Phase V (D^{24}_{2h} factor group) is the stable phase at room temperature, while the metastable phase III (D^{17}_{2h} factor group) tends to transform slowly to phase V [62,63]. Both phases are considered in this study; the commercial Na_2SO_4 was found to be in phase V, and the recrystallization of this salt by fast vaporization at 100°C produced phase III. The average Raman spectra of Na_2SO_4 in phase V (Figure S3) and III (Figure S4) show the strongest band (SO_4^{2-} ν_1) at 990 and 994 cm^{-1}, respectively.

Both $MgSO_4 \cdot 7H_2O$ and $ZnSO_4 \cdot 7H_2O$ belong to the orthorhombic system (D^4_2 factor group) [64,65]. As expected, the average Raman spectra of these isomorphous salts show important similarities; the most notorious differences can be observed in the SO_4^{2-} asymmetric stretching (ν_3), SO_4^{2-} asymmetric bending (ν_4) and in the shape of the broad H_2O stretching bands, as shown in Figure 1a. The shape of the H_2O stretching bands (overlapped) is important, because it can be used to distinguish between two different hydrated salts, for instance, $MgSO_4 \cdot 7H_2O$ and $MgSO_4 \cdot 6H_2O$. Wang et al. [65] showed that the wavenumber difference in the SO_4^{2-} ν_1 between $MgSO_4 \cdot 7H_2O$ and $MgSO_4 \cdot 6H_2O$ is less than 1 cm^{-1}, which is a value considerably low and most of

the times below the spectral resolution of routine measurements, but the characteristic shape of the H_2O bands in the region ~3000-3700 cm^{-1} allows to distinguish the salts from each other. The same criterion can be used to distinguish between $MgSO_4 \cdot 7H_2O$ and $ZnSO_4 \cdot 7H_2O$, since the SO_4^{2-} ν_1 for these salts appears with a difference of ~1 cm^{-1}. The average Raman spectra of $MgSO_4 \cdot 7H_2O$ and $ZnSO_4 \cdot 7H_2O$ show the strongest band at 982 and 981 cm^{-1}, respectively. The bands for $MgSO_4 \cdot 7H_2O$ are in good agreement with the spectroscopic data previously reported by Wang et al. [65], but for $ZnSO_4 \cdot 7H_2O$ important wavenumber differences are observed with respect to the work of Shantakumari [66], e.g., the band of the SO_4^{2-} ν_1 observed in this work at 981 cm^{-1}, was observed before at 990 cm^{-1}. This kind of differences may be attributed to instrumental and technical variations.

The Raman spectrum of $CuSO_4 \cdot 5H_2O$, which crystallizes in the triclinic system (C_i^l factor group), was previously reported by Liu and Ullman [67]. The features observed in our average Raman spectrum of this salt (Figure S7) are in good agreement with those previously reported data. Among the different features observed in the Raman spectrum, it is important to note that a weak broad band centered at 872 cm^{-1} and assigned to an H_2O libration mode, as well as a band at 466 cm^{-1} assigned to a stretching mode of the $(Cu^{2+}(H_2O)_4)$ complex, can be observed.

The "hydration" of iron (II) sulfates is conditioned by the temperature and the relative humidity in contact with the crystals. In this context, the monoclinic salts $FeSO_4 \cdot H_2O$ (C_{2h}^6 factor group), $FeSO_4 \cdot 4H_2O$ (C_{2h}^5 factor group) and $FeSO_4 \cdot 7H_2O$ (C_{2h}^5 factor group) are commonly found as minerals. They belong to the same crystal system but there are packing differences closely related to the number of H_2O molecules in the molecular formula. Within the crystal structure of these three salts it is possible to observe that the Fe^{2+} ion coordinates with six oxygen atoms, which belong to either the H_2O molecules or the SO_4^{2-} ions. The crystal structure data of $FeSO_4 \cdot 7H_2O$ [68] show that Fe^{2+} ions are octahedrally coordinated by H_2O molecules producing two FeO_6 octahedra (with different average interatomic distances Fe-O) within the unit cell. The crystal structure data of $FeSO_4 \cdot 4H_2O$ [69] show that Fe^{2+} ions coordinate with four oxygen atoms of H_2O molecules and two oxygen atoms of SO_4^{2-} ions. The crystal structure data of $FeSO_4 \cdot H_2O$ [70] shows that Fe^{2+} ions coordinate with two oxygen atoms of H_2O molecules and four oxygen atoms of SO_4^{2-} ions. Considering earlier spectroscopic studies [43,71-73], weak bands related to the three mentioned FeO_6 octahedron complexes are expected to appear at wavenumbers <400 cm^{-1}. However, the coordination of Fe^{2+} ions with oxygen atoms of SO_4^{2-} ions can have effects on the wavenumbers of the SO_4^{2-} fundamental modes. In the average Raman spectra of these salts (Figures S8-S10) the SO_4^{2-} ν_1 appears at 1015, 987, and 974 cm^{-1} for $FeSO_4 \cdot H_2O$, $FeSO_4 \cdot 4H_2O$, and $FeSO_4 \cdot 7H_2O$, respectively (in good agreement with values observed by Chio et al. [43]), showing that when the Fe^{2+} ion has a lower influence on the oxygen atoms of SO_4^{2-} ions, there are less energy requirements for the S-O stretching, thus resulting in a lower wavenumber for the SO_4^{2-} ν_1.

$MnSO_4 \cdot H_2O$ and $FeSO_4 \cdot H_2O$ are isomorphous, therefore their Raman spectra are expected to have similarities. These similarities can be observed in Figure 1b, which shows the average spectra of $MnSO_4 \cdot H_2O$ and $FeSO_4 \cdot H_2O$; the bands of the SO_4^{2-} ν_1 are centered at 1016 and 1015 cm^{-1}, for $MnSO_4 \cdot H_2O$ and $FeSO_4 \cdot H_2O$, respectively, and the bands belonging to the other SO_4^{2-} modes also show similarities. Analogously to other isomorphous salts, the presence of different ions in the same position modifies the unit-cell dimensions and therefore the interatomic distances and bond angles. Considering the interatomic distances, the average S-O distance is slightly longer for $FeSO_4 \cdot H_2O$ than for $MnSO_4 \cdot H_2O$ [70], which explains a slightly higher wavenumber for the SO_4^{2-} ν_1 of $MnSO_4 \cdot H_2O$ (compared to $FeSO_4 \cdot H_2O$).

Although it is possible to compare Raman spectra of salts belonging to the same crystal system (monoclinic, orthorhombic, triclinic, etc.) it should be noted that this is not always applicable. $MnSO_4 \cdot H_2O$, $FeSO_4 \cdot H_2O$ and $CaSO_4 \cdot 2H_2O$ all crystallize in the monoclinic system, and belong to the C_{2h}^6 factor group having four molecules in their unit cells, but $CaSO_4 \cdot 2H_2O$ is not isomorphous to $MnSO_4 \cdot H_2O$ and $FeSO_4 \cdot H_2O$. Since $CaSO_4 \cdot 2H_2O$ has one additional H_2O molecule in its molecular formula (four more in its unit cell), the packing of all ions and molecules in the unit cell is considerably different compared to $MnSO_4 \cdot H_2O$ and $FeSO_4 \cdot H_2O$. The average Raman spectrum of $CaSO_4 \cdot 2H_2O$ shows the band of the SO_4^{2-} ν_1 at 1005 cm^{-1}, which is a value considerably different compared to the values observed for $MnSO_4 \cdot H_2O$ and $FeSO_4 \cdot H_2O$ (Figure 1b).

In an earlier work we studied the Raman spectra of $K_2Ca(SO_4)_2 \cdot H_2O$, $(NH_4)_2Ca(SO_4)_2 \cdot H_2O$, $Na_2Ca(SO_4)_2$ and $K_2Ca_2Mg(SO_4)_4 \cdot 2H_2O$ [29]. Both $K_2Ca(SO_4)_2 \cdot H_2O$ and $(NH_4)_2Ca(SO_4)_2 \cdot H_2O$ are monoclinic (C_{2h}^2 factor group) [74,75] and their Raman spectra (Figures S13 and S14) show certain similarities in the number of the observed bands. For instance, the SO_4^{2-} ν_1 is observed as two strong bands: 1003 and 979 cm^{-1} for $K_2Ca(SO_4)_2 \cdot H_2O$, while 996 and 980 cm^{-1} are observed for $(NH_4)_2Ca(SO_4)_2 \cdot H_2O$). Analogically to the cases mentioned before, those similarities may be attributed to the fact that $K_2Ca(SO_4)_2 \cdot H_2O$ and $(NH_4)_2Ca(SO_4)_2 \cdot H_2O$ are both isomorphous, in other words, the crystal structure of $(NH_4)_2Ca(SO_4)_2 \cdot H_2O$ can be interpreted as the structure of $K_2Ca(SO_4)_2 \cdot H_2O$ replacing the K^+ ions by NH_4^+ ions. Obviously these replacements modify the unit-cell dimensions, but SO_4^{2-} ions still occupy the same special positions, therefore the same number of SO_4^{2-} bands but

with different wavenumbers are expected for $K_2Ca(SO_4)_2·H_2O$ and $(NH_4)_2Ca(SO_4)_2·H_2O$. As expected, the average Raman spectra of these two salts are clearly different compared to the average Raman spectrum of $K_2Ca_2Mg(SO_4)_4·2H_2O$ (Figure S15), which belongs to the triclinic system (C^l_i factor group) [76]. In contrast to the other three calcium mixed salts, the average Raman spectrum of the monoclinic salt $Na_2Ca(SO_4)_2$ (C^6_{2h} factor group) [77] shows only one strong band at 998 cm^{-1} for the SO_4^{2-} ν_1, as it is shown in Figure S16.

Tutton's salts have the general formula $M^I_2M^{II}(SO_4)_2·6H_2O$ (where M^I and M^{II} are a monovalent and a divalent cation, respectively) and belong to the monoclinic system (C^5_{2h} factor group). The Tutton's salts considered in this study are: $(NH_4)_2Cu(SO_4)_2·6H_2O$, $(NH_4)_2Fe(SO_4)_2·6H_2O$, $(NH_4)_2Mg(SO_4)_2·6H_2O$, $(NH_4)_2Mn(SO_4)_2·6H_2O$, $(NH_4)_2Zn(SO_4)_2·6H_2O$, $K_2Cu(SO_4)_2·6H_2O$, $K_2Mg(SO_4)_2·6H_2O$, and $K_2Zn(SO_4)_2·6H_2O$. Obviously, the unit-cell dimensions in each case depend on the cations (monovalent and/or divalent). The average Raman spectra of these salts show the band of the SO_4^{2-} ν_1 at wavenumbers ranging between 979 and 984 cm^{-1}, as shown in Figures S17-S24 and Table S1 (Supporting Information). The NH_4^+ ions in the crystal structure contribute to the Raman spectra of the salts additional bands which belong to the NH_4^+ stretching modes (>2800 cm^{-1}) and are overlapping the H_2O stretching modes, and the NH_4^+ bending modes (~1600 cm^{-1} and ~1400 cm^{-1}). The bands of the NH_4^+ bending modes are weak and broad making their observation difficult. A comparison of the Raman spectra of four Tutton's salts is shown in Figure 1c.

$(NH_4)Fe(SO_4)_2·12H_2O$ belongs to a group of compounds known as "alums", $Me^IMe^{III}(SO_4)_2·12H_2O$ (where Me^I is a monovalent and Me^{III} is a trivalent metal), which crystallize in the cubic system (T^6_h factor group) [78]. The NH_4^+ and SO_4^{2-} bands as well as the bands of the H_2O stretching modes are relatively easy to identify in the average Raman spectrum of $(NH_4)Fe(SO_4)_2·12H_2O$ (Figure S25), but an additional specific particularity should be considered. "Alums" have a $Me^{III}O_6$ octahedron in their crystal structure and this structural characteristic contributes some additional bands to both Raman and infrared spectra [73,79-81]. The band at 518 cm^{-1} is assigned to the stretching mode of FeO_6 ν_1, while the bands in the region 400-500 cm^{-1} are assigned to SO_4^{2-} ν_2 + FeO_6 ν_2, as it is not possible to distinguish the modes from each other.

The average Raman spectrum of the orthorhombic salt $(NH_4)NaSO_4·2H_2O$ (Figure S26) shows the strongest band (SO_4^{2-} ν_1) at 982 cm^{-1}, which is in good agreement with the data reported by Kloprogge et al. [56]. A remarkable feature observed in the Raman spectrum of this salt is the complex series of overlapping bands in the region of the H_2O and NH_4^+ stretching modes (2700-3500 cm^{-1}).

Both $Na_2Cu(SO_4)_2·2H_2O$ and $Na_2Mn(SO_4)_2·2H_2O$ crystals belong to the monoclinic system (C^5_{2h} factor group) [82,83]. As mentioned before, the Raman spectra of two salts with the same crystal structure show similarities. The strongest band (SO_4^{2-} ν_1) in the Raman spectrum of $Na_2Cu(SO_4)_2·2H_2O$ (Figure S27) appears at 987 cm^{-1}, while for $Na_2Mn(SO_4)_2·2H_2O$ (Figure S28) appears at 985 cm^{-1}. Also it should be noted that the Raman spectra of $Na_2Cu(SO_4)_2·2H_2O$ and $Na_2Mn(SO_4)_2·2H_2O$ show bands of the H_2O libration modes, which could not be observed consistently in the spectra of other hydrated salts; while $Na_2Cu(SO_4)_2·2H_2O$ shows three bands of H_2O libration modes (859, 741 and 562 cm^{-1}), only one band (577 cm^{-1}) is observed for $Na_2Mn(SO_4)_2·2H_2O$, probably because the others are too weak.

Crystalline $Na_2Zn(SO_4)_2·4H_2O$ (also known as "Zn-bloedite" because it is isostructural to bloedite), $Na_2Mg(SO_4)_2·4H_2O$ and $Na_2Mg(SO_4)_2·5H_2O$ belong all to the monoclinic system (C^5_{2h} factor group) [48,84], but there are important structural differences between them. As we explained before in an earlier work [27], although $Na_2Mg(SO_4)_2·5H_2O$ and $Na_2Mg(SO_4)_2·4H_2O$ differ from each other by only one H_2O molecule, as shown in the molecular formula, the crystal unit cell of $Na_2Mg(SO_4)_2·5H_2O$ has a much more densely packed sheet arrangement accommodating more molecules per unit cell than $Na_2Mg(SO_4)_2·4H_2O$, and therefore the Raman spectra of these two mixed salts are notoriously different. As expected, the average Raman spectrum of $Na_2Zn(SO_4)_2·4H_2O$ (Figure S29) shows only one strong band at 985 cm^{-1} attributed to the SO_4^{2-} ν_1 (as in the case of the $Na_2Mg(SO_4)_2·4H_2O$ Raman spectrum), while the $Na_2Mg(SO_4)_2·5H_2O$ average spectrum (Figure S30) shows two strong bands (1003 and 981 cm^{-1}) for this mode.

$K_3Na(SO_4)_2$ crystallizes in the trigonal system (D^3_{3d} factor group) [85]. The average Raman spectrum of $K_3Na(SO_4)_2$ (Figures S31) shows clearly the characteristic bands of the SO_4^{2-} modes, highlighting the strong band of the SO_4^{2-} ν_1 at 990 cm^{-1}. To our knowledge, there is no Raman spectroscopic data for $K_3Na(SO_4)_2$ in literature, but our average Raman spectrum seems to be in agreement with the infrared spectroscopic data reported by Natarajan and Secco [85]. Figure 2a shows the Raman spectra of $K_3Na(SO_4)_2$ and Na_2SO_4 in phase V, which belong to different crystal systems. It is important to note that the SO_4^{2-} ν_1 for both $K_3Na(SO_4)_2$ and Na_2SO_4 in phase V appears at 990 cm^{-1}, however there are remarkable differences as to the number of bands, relative intensity and wavenumbers of the remaining three SO_4^{2-} modes, obviously due to the crystal structure of these salts. To illustrate the effect of the crystal structure, the Raman spectra of K_2SO_4 and Na_2SO_4 in phase V are also included in Figure 2a.

3.1.2 Nitrates

There are five nitrate salts considered in this study: $Ca(NO_3)_2 \cdot 4H_2O$, KNO_3, $Mg(NO_3)_2 \cdot 6H_2O$, NH_4NO_3, and $NaNO_3$. The four normal modes of the free NO_3^- ion (D_{3h}) are: ν_1 (A_1') symmetric stretching, ν_2 (A_2'') symmetric bending, ν_3 (E') asymmetric stretching, and ν_4 (E') asymmetric bending; only ν_2 is not Raman active. These modes occur at 1049 cm^{-1} (ν_1), 830 cm^{-1} (ν_2), 1355 cm^{-1} (ν_3) and 690 cm^{-1} (ν_4) [86].

Crystalline $Ca(NO_3)_2 \cdot 4H_2O$ belongs to the monoclinic system (C_{2h}^5 factor group) [87]. The average Raman spectrum of $Ca(NO_3)_2 \cdot 4H_2O$ (Figure S32) shows clearly the three Raman active normal modes of NO_3^-; a strong band at 1047 cm^{-1} assigned to the NO_3^- symmetric stretching (ν_1) and the overlapped bands belonging to the H_2O stretching modes (> 3100 cm^{-1}) are observed as the most noticeable feature. Similar is the case of the monoclinic $Mg(NO_3)_2 \cdot 6H_2O$ (C_{2h}^5 factor group) [88,89], which shows in its Raman spectrum (Figure S33) a sharp strong band at 1058 cm^{-1} (NO_3^- ν_1) and broad overlapped bands for the stretching modes of H_2O. Although both $Ca(NO_3)_2 \cdot 4H_2O$ and $Mg(NO_3)_2 \cdot 6H_2O$ belong to the same factor group, remarkable differences can be observed in the unit-cell dimensions as well as the package of the ions and molecules. ($Ca(NO_3)_2 \cdot 4H_2O$ has four molecules per unit cell, while $Mg(NO_3)_2 \cdot 6H_2O$ has only two). These differences affect the N-O distances; the N-O distances for $Ca(NO_3)_2 \cdot 4H_2O$ range between 1.227 and 1.273 Å [87], while for $Mg(NO_3)_2 \cdot 6H_2O$ the N-O distances range between 1.196 and 1.264 Å [88], resulting in a higher average distance for $Ca(NO_3)_2 \cdot 4H_2O$ than for $Mg(NO_3)_2 \cdot 6H_2O$. This seems to explain (at least partially) why the NO_3^- ν_1 for $Mg(NO_3)_2 \cdot 6H_2O$ appears at higher wavenumbers than $Ca(NO_3)_2 \cdot 4H_2O$.

Depending on the temperature and the thermal process, KNO_3 exists in three different phases (I, II and III), with their respective Raman spectroscopic characteristics discussed in detail by Balkanski et al. [90] and Murugan et al. [91]. As expected, the commercial KNO_3 is in phase II (orthorhombic, D_{2h}^{16} factor group), which is the room temperature phase. The average Raman spectrum of KNO_3 (Figure S34) shows the strongest band (NO_3^- ν_1) at 1048 cm^{-1}, which is similar to earlier reported values [90-92].

NH_4NO_3 has six stable solid phases under normal pressure. Starting from the melting point, there is a succession of solid phases with characteristic temperatures of transition: I, II, III, IV, V and VII [93]. The average Raman spectrum of the commercial product (Figure S35) shows the NO_3^- ν_1 at 1040 cm^{-1}. In earlier studies [93-95], this band was observed at 1043 and 1044 cm^{-1} for the phase IV, while for phases III, II and I (higher temperature phases) values of 1047, 1054 and 1050 cm^{-1}, respectively, were reported. Phases V and VII are low-temperature phases [93] with temperatures of transition below 0°C, therefore their occurrence at room temperature is highly unlikely. Considering these aspects, it is reasonable to conclude that the commercial NH_4NO_3 is in phase IV (orthorhombic, factor group D_{2h}^{13}) and this salt can be found in atmosphere mostly in this phase.

$NaNO_3$ crystallizes at room temperature in the trigonal system (D_{3d}^6 factor group), also known as phase II, and undergoes the phase transition at ~275°C [96]. The average Raman spectrum of $NaNO_3$ (Figure S36) shows the strongest band at 1066 cm^{-1}, is in good agreement with the spectroscopic data reported previously for $NaNO_3$ in phase II by Brooker [96].

3.1.3 Carbonates and/or bicarbonates

This study considers five carbonate and/or bicarbonate salts: NH_4HCO_3, $NaHCO_3$, $Na_3(CO_3)(HCO_3) \cdot 2H_2O$, $CaCO_3$ and $Na_2CO_3 \cdot H_2O$.

The nine normal modes of the free HCO_3^- ion (C_s) are: ν_1 (A') OH stretching, ν_2 (A') CO asymmetric stretching, ν_3 (A') CO symmetric stretching, ν_4 (A') HOC bending, ν_5 (A') C-OH stretching, ν_6 (A') CO_2 bending, ν_7 (A') OC-(OH) wagging, ν_8 (A'') CO_2 out-of-plane deformation, and ν_9 (A'') H torsion, all of them are both Raman and infrared active. Using infrared spectroscopy, Bernitt et al. [97] observed the normal modes of the HCO_3^- ion in solid solution in different matrixes (KCl, KBr and KI). The normal modes of the HCO_3^- ion in a KBr matrix at liquid-N_2 temperature reported by these authors are: 3390 cm^{-1} (ν_1), 1697 cm^{-1} (ν_2), 1338 cm^{-1} (ν_3), 1211 cm^{-1} (ν_4), 960 cm^{-1} (ν_5), 712 cm^{-1} (ν_6), 579 cm^{-1} (ν_7), 835 cm^{-1} (ν_8), and 600 cm^{-1} (ν_9). Of course, these values can change depending on the specific conditions affecting the HCO_3^- ions; Davis and Oliver [98] observed Raman signals of the HCO_3^- ion in aqueous solution at 2650 cm^{-1} (ν_1), 1630 cm^{-1} (ν_2), 1360 cm^{-1} (ν_3), 1302 cm^{-1} (ν_4), 1017 cm^{-1} (ν_5), 672 cm^{-1} (ν_6), 632 cm^{-1} (ν_7), and 841 cm^{-1} (ν_8), while ν_9 was not observed.

Both $NaHCO_3$ and $Na_3(CO_3)(HCO_3) \cdot 2H_2O$ crystallize in the monoclinic system and belong to the C_{2h}^5 and C_{2h}^6 factor group, respectively [99,100]. The crystal structure of these salts is characterized by strong hydrogen bonds; it consists of infinite chains of HCO_3^- ions linked by hydrogen bonds in the case of $NaHCO_3$ and of dimers (a dimer contains two CO_3^{2-} ions linked by a hydrogen bond) linked to each other by two H_2O molecules in the case of $Na_3(CO_3)(HCO_3) \cdot 2H_2O$. Therefore, the assumption that the main features in the Raman spectra of these salts are related to the HCO_3^- ion seems plausible. In fact, eight of the nine expected modes are observed

in the average Raman spectrum of $NaHCO_3$ (Figure S37), while seven modes are observed in the average Raman spectrum of $Na_3(CO_3)(HCO_3)\cdot2H_2O$ (Figure S38). The H torsion (ν_9) is not observed in neither case, because this mode probably appears at wavenumbers < 400 cm^{-1}. The HOC bending (ν_4) is not observed either in the Raman spectrum of $Na_3(CO_3)(HCO_3)\cdot2H_2O$, probably due to a certain rigidity in the O--H--O section of the dimer, which limits the HOC bending. The strongest band in the average Raman spectra of $NaHCO_3$ and $Na_3(CO_3)(HCO_3)\cdot2H_2O$ is observed at 1058 and 1042 cm^{-1}, respectively (1064 and 1047 cm^{-1}, respectively, according to Bertoluzza et al. [101]).

The average Raman spectrum of NH_4HCO_3 (Figure S39), which crystallizes in the monoclinic system (C^5_{2h} factor group) [102], shows bands that can be assigned to eight of the nine modes expected for the HCO_3^- ion; again, ν_9 seems to appear at wavenumbers < 400 cm^{-1}. An additional complication for the band assignment arises from the presence of the NH_4^+ ion in the structure; the NH_4^+ bending modes ν_2 and ν_4 appear at 1680 and 1400 cm^{-1}, respectively [103], and therefore these modes seem to appear superposed by the bands of the CO asymmetric stretching (ν_2) and CO symmetric stretching (ν_3). The NH_4^+ stretching modes ν_1 and ν_3 were unambiguously assigned. A weak but noticeable band at 1026 cm^{-1} was assigned to the COH out-of-plane bending mode (γ_{COH}). With respect to this band, the bands at 1941 and 1840 cm^{-1} were assigned to an overtone and a combination of γ_{OH}. The band at 2137 cm^{-1} was assigned to a combination.

Like the free NO_3^- ion, the free CO_3^{2-} ion has also four modes: ν_1 (A_1') symmetric stretching at 1063 cm^{-1}, ν_2 (A_2'') symmetric bending at 879 cm^{-1}, ν_3 (E') asymmetric stretching at 1415 cm^{-1}, and ν_4 (E') asymmetric bending at 680 cm^{-1} [104]. Only ν_2 is not Raman active.

$CaCO_3$ crystallizes as calcite, aragonite or vaterite. Behrens et al. [105] demonstrate that these three polymorphs can be distinguished from each other using Raman spectroscopy. Calcite belongs to the trigonal system (D^6_{3d} factor group) [106] and is the most thermodynamically stable polymorph [107]. The average Raman spectrum of the commercial $CaCO_3$ (Figure S40) shows the strongest band (CO_3^{2-} ν_1) at 1083 cm^{-1}, which is in good agreement with the spectroscopic data reported by Behrens et al. [105] for calcite.

The average Raman spectrum of the orthorhombic $Na_2CO_3\cdot H_2O$ (Figure S41) shows a strong band at 1067 cm^{-1} and weak signals for the CO_3^{2-} asymmetric stretching (ν_3) and asymmetric bending (ν_4). One band at 1535 cm^{-1} is observed for the H_2O bending mode, while the H_2O stretching modes are observed as overlapped broad bands. Figure 2b shows the similarities between the Raman spectra of NH_4HCO_3 and $NaHCO_3$, and the differences observed when they are compared to the spectra of $Na_3(CO_3)(HCO_3)\cdot2H_2O$ and $Na_2CO_3\cdot H_2O$.

3.1.4 Sulfate-nitrates and sulfate-carbonate

There are three sulfate-nitrates and one sulfate-carbonate considered in this study: $(NH_4)_2SO_4\cdot3NH_4NO_3$, $Na_6(CO_3)(SO_4)_2$, $K_3Na_8Fe(SO_4)_6(NO_3)_2\cdot6H_2O$ and $Na_3(SO_4)(NO_3)\cdot H_2O$. Figure 2c shows the Raman spectra of these salts illustrating the differences.

$(NH_4)_2SO_4\cdot3NH_4NO_3$, which is one of the two known double salts of ammonium nitrate and ammonium sulfate, crystallizes in the monoclinic system (C^2_2 factor group) [108]. Ling and Chang [109] studied the formation and evolution of ammonium nitrate sulfate salts in droplets, and they reported signals at 1053 and 980 cm^{-1} in the Raman spectrum of $(NH_4)_2SO_4\cdot3NH_4NO_3$. Our average Raman spectrum of $(NH_4)_2SO_4\cdot3NH_4NO_3$ presented in Figure 2c (1:3), shows two bands at 1048 and 977 cm^{-1}, corresponding to the NO_3^- ν_1 and SO_4^{2-} ν_1, respectively. The other nitrate and sulfate bands can be observed at 1345 cm^{-1} for the NO_3^- ν_3, 721, 712 and 703 cm^{-1} for the NO_3^- ν_4, 1122 and 1082 cm^{-1} for the SO_4^{2-} ν_3, 620 and 610 cm^{-1} for the SO_4^{2-} ν_4, and 456 and 445 cm^{-1} for the SO_4^{2-} ν_2. Weak and broad bands are observed for the fundamental modes of NH_4^+ ion; signals at 3144 and 2834 cm^{-1} were observed for the NH_4^+ stretching modes, 1695, 1668 and 1650 cm^{-1} for the NH_4^+ ν_2, and 1471 and 1420 cm^{-1} for the NH_4^+ ν_4.

$Na_6(CO_3)(SO_4)_2$, which crystallizes in the orthorhombic system (D^{13}_{2h} factor group) [110], has often been identified in mineral formations. In one of these mineralogical studies, Korsakov et al. [111] identified $Na_6(CO_3)(SO_4)_2$ using Raman spectroscopy and they reported bands at the following wavenumbers: 1065, 994, 644, 633, 620, 474 and 451 cm^{-1}. To our knowledge, this is the only report with Raman spectroscopic data of $Na_6(CO_3)(SO_4)_2$ and clearly some bands are missing. The strongest bands in our average Raman spectrum of $Na_6(CO_3)(SO_4)_2$ (Figure 2c (Bur.)) appear at 1059 cm^{-1}, assigned to the CO_3^{2-} ν_1, and at 989 cm^{-1} with a shoulder at 1005 cm^{-1}, both assigned to the SO_4^{2-} ν_1. Two bands at 1460 and 1408 cm^{-1} are assigned to the CO_3^{2-} ν_3 and one band at 702 cm^{-1} to the CO_3^{2-} ν_4. Four bands at 1192, 1160, 1119 and 1097 cm^{-1} are assigned to the SO_4^{2-} ν_3, three bands at 639, 630 and 617 cm^{-1} to the SO_4^{2-} ν_4 and two bands at 472 and 451 cm^{-1} to the SO_4^{2-} ν_2.

The average Raman spectra of the trigonal $K_3Na_8Fe(SO_4)_6(NO_3)_2\cdot6H_2O$ and the monoclinic $Na_3(SO_4)(NO_3)\cdot H_2O$ show bands related to both NO_3^- and SO_4^{2-} ions. We discussed the spectroscopic details in earlier works [28,57].

3.2 Classification and identification using chemometric methods

As already mentioned in section 3.1.1, spectra of specific groups might only differ in faint details that are hard to spot with the naked eye. Tutton's salt, as shown in Figure 1c, form such a group. In order to facilitate the identification of spectra and to get a better overview of the relationships between spectra, we opted for two different support vector machine models (SVMs).

As traditional SVMs solve two-class problems and the data set contains a large number of classes, the "all pairs" approach of the standard SVM leads to an excessive increase in computational time. It constructs all possible combinations and conducts a vote on all models. Each sample gets assigned to the class with the majority of votes. In our case there were $\binom{45}{2}$ = 990 SVM models to calculate. The results of those calculations were generally worse than those obtained with the other models used and are not shown here. Apart from the traditional SVM model, there exist native-multiclass models which offer speed advantages for the construction of a model in the face of a large amount of classes. Multicategory support vector machines (MC-SVMs) [112] have shown to be a reliable and competitive alternative to binary SVMs [113]. They are based on the alternative "one-vs-rest" (OVR) classification scheme, in which k SVMs are built that each distinguish between one of the k classes in the data set and the rest. By modifying how misclassified samples are penalized, it is possible to merge the inequalities that make up the individual SVMs into one model and compute them simultaneously. Instead of taking into account the penalties of all models, only the largest penalty exerts influence.

We used both MC-SVMs with linear and radial basis kernels. The estimate of the sigma parameter in the case of radial basis kernel was based on the work of Caputo [114]. SVMs with a linear kernel provided the best classification with an average error rate for cross-validation of 3-5 spectra (0.130-0.217%). The best result with a radial basis kernel was an error of 12-13 spectra. In the case of MC-SVM there was no feature selection applied.

According to our requirements of both a high-performance classification and a model with a structure that makes the result easy to interpret, we chose the "margin tree" [115], which is a combination of a binary decision tree and support vector machines (SVMs). Basically, it constructs a cluster dendrogram with SVMs with a linear kernel at the inner nodes. Instead of using the Euclidean distances or correlation of the spectra, as usually done with hierarchical cluster analysis, this clustering scheme operates on the class margins previously computed by the generation of all one-against-one SVM models. The models are discarded afterwards retaining only the margins to build a tree via complete linkage clustering [116].

Since a simpler model might be able to generalize better, we used the built-in feature selection capabilities of the "margintree" package [117], to find that the amount of wavenumbers in each model could be reduced from the original 4749 to at least 2950, and in four cases, e.g. Na_2SO_4 (phase III) against $Na_3(NO_3)(SO_4) \cdot H_2O$ or $CaCO_3$ against the whole subtree, down to 11. The range of misclassified spectra, which will appear due to the random nature of dataset splits in cross-validation, broadened from 0.043-0.130% to 0.0-0.174%, or 0 to 4 spectra out of 2302. Therefore the resulting reduced model has an improved generalization performance over the full model, while keeping the error rate of cross-validation the same for the average case.

To represent the data in the tree more clearly, we applied computer-aided selection of characteristic wavenumber ranges. This preselection step resulted in the clean separation into the groups of "sulfates", "nitrates or carbonates" and "sulfate-nitrates or sulfate-carbonate". In this subsection and only for classification purposes, we use the term "carbonates" to refer to both carbonate (CO_3^{2-}) and bicarbonate (HCO_3^-) salts. As the strongest Raman bands for nitrate and carbonate species can appear in the same spectral regions, it is normally not possible to assign the spectrum to the nitrate or carbonate ion only using the Raman spectra. However, sulfate salts can be distinguished from both nitrate and carbonate salts, because their strongest bands generally appear at lower wavenumbers. Concretely, the preselection step works as follows: if the maximum intensity in the range of 951 to 1030 cm^{-1} is 7 times higher than the average intensity of the mean spectrum of that mineral, then that spectrum is associated with a sulfate; on the contrary, if the spectrum shows a high intensity in the range of 1030 to 1102 cm^{-1}, above the threshold mentioned before, then it is assigned to the group of nitrates or carbonates. $Na_2Cu(SO_4)_2 \cdot 2H_2O$ proved to be a special case. The band of symmetric stretching at 1044 cm^{-1} of this mineral was so strong that we needed an additional restriction in the preselection process. It did not classify as a sulfate-nitrate or a sulfate-carbonate, because it did not show any of the smaller nitrate bands between 1280 and 1400 cm^{-1}.

The resulting classification trees for the salts without and with the preselection process are presented in Figures 3 and 4, respectively. For comparative purposes and the evaluation of the results, these Figures include also the wavenumbers of the strongest Raman bands (in cm^{-1}) and the crystal systems in which the salts crystallize. It is easy to observe that without the preselection process, sulfates, nitrates and carbonates are organized in the tree

without any specific pattern. Although the crystal system in which a salt crystallizes affects the position of the bands in the Raman spectrum, there are no defined wavenumber ranges for a specific band (e.g., SO_4^{2-} v_1) according to the crystal system of the salt. This is because the wavenumbers of the bands belonging to the stretching and bending modes are closely related to the interatomic distances (S-O for sulfate, N-O for nitrate, etc.), the bond angles and the influence of certain ions or molecules on the SO_4^{2-}, NO_3^-, CO_3^{2-} and HCO_3^- ions (depending on the case). These parameters may vary substantially depending on the unit-cell dimensions as well as the species involved.

As shown in Figure 4, the preselection process is used to classify the salts according to their anions. In some cases the crystal structure similarities among the different salts appear to be expressed in the classification tree, as in the cases of $Na_2Cu(SO_4)_2 \cdot 2H_2O$ and $Na_2Mn(SO_4)_2 \cdot 2H_2O$, $MgSO_4 \cdot 7H_2O$ and $ZnSO_4 \cdot 7H_2O$, $NaHCO_3$ and NH_4HCO_3, and most of the considered Tutton's salts.

In atmospheric scenarios, the classification of particles into one of the three groups (sulfates, nitrates or carbonates and sulfate-nitrates or sulfate-carbonate) can provide valuable information about the origin of these materials, the atmospheric chemistry and climate forcing. In the atmosphere, both sulfate and nitrate are fundamentally produced from SO_x and NO_x by oxidative atmospheric processes [3,118], thus the oxidants availability has a strong influence. Calculations performed by Shindell et al. [119] showed that variations in emissions of a given component can modify the concentration of others, e.g., an increase in the SO_2 emissions results in the formation of less nitrate aerosols and the increase of sulfate aerosols. Therefore, the observation of salts containing sulfate, nitrate or both together can be used to monitor the emissions of industrial areas and also to estimate changes in the global radiative forcing. Nitrate and carbonate salts cannot be classified separately from each other using only the Raman spectra, but other chemical and environmental criteria can be included in the data analysis for atmospheric purposes. While nitrate salts are produced in the atmosphere, carbonate salts in atmospheric particulate matter can be associated to wind-transported soil and sediment materials (terrigenous origin), as is the case with the dust emissions from playas in the Mojave desert [120]. In addition, it should be considered that the wind-transported carbonate salts can react with other atmospheric components during the transport, as we reported in a recent study [121]. Taking into account these aspects, it is possible to deduce that the atmospheric lifetime of carbonate salts may be considerably shorter than nitrate salts, and the observation of carbonate salts in atmospheric particulate matter is conditioned to the influence of sources of alkaline minerals (e.g., playas, alkaline soils, etc.). These two criteria can complement the evaluation of Raman spectroscopic data of particulate matter.

These forty-five salts are only some of the salts expected to occur in atmospheric particles; it is not difficult to imagine the great heterogeneity in the atmosphere, especially when considering the effects of different regional variables (natural or anthropogenic). The results of the application of chemometric methods to the Raman spectra of these representative salts shows that it is possible to classify the salts by groups and to distinguish them from each other.

4 Conclusions

The average Raman spectra of forty-five salts (sulfates, nitrates, carbonates, bicarbonates, sulfate-nitrates and sulfate-carbonate) were evaluated and the band assignments proposed and discussed. The chemometric analysis of the spectroscopic data of these forty-five salts shows that the Raman spectroscopy is a powerful tool for the chemical characterization of atmospheric particles, especially with regard to those salts expected to precipitate during the condensation-evaporation cycles. In some cases the crystal structure similarities among the different salts appear to be expressed in the classification tree.

The identification of salts in the atmospheric particulate matter can be useful not only to estimate the degree of pollution in specific areas and the sources of such pollution, but can also provide clues about processes taking place in the atmosphere. Considering the formation conditions of salts, the age of the atmospheric particulate matter can be estimated. Such indicators of atmospheric aging can be used for pollution monitoring purposes, the study of long-range transport of materials, and the evaluation of the environmental impacts caused by megacities as well as industrial areas in remote areas. Studies of this kind could be successfully carried out using Raman spectroscopy.

Although atmospheric water is normally acidic, alkaline salts can play an important role in atmospheric chemistry. Alkaline salts like calcite, thermonatrite, trona and burkeite can be released to the atmosphere by wind action and play an important role in the atmospheric chemistry. The reactivity of these salts should be considered in future works using Raman spectroscopy not only to identify the reaction products, but also to elucidate the chemical reactions themselves.

Some models successfully applied in the past to predict mineral solubilities (and precipitation sequences) of seawater may also be applicable for studies of atmospheric particulate matter with respect to possible climate implications. Hygroscopic properties of typical and well-known aerosol salts (e.g., $(NH_4)_2SO_4$ and NH_4NO_3) have been the subject of many studies in the past, but there are other salts that should be investigated considering their direct and indirect influence on the cloud formation and lifetime as well as the incoming solar radiation, as these aspects are important inputs in climate models.

References

[1]   P.J. Crutzen, Nature 415 (2002) 23.
[2]   J.A. Rech, B.S. Currie, G. Michalski, A.M. Cowan, Geology 34 (2006) 761-764.
[3]   G.G.C. Claridge, I.B. Campbell, Nature 217 (1968) 428-430.
[4]   G. Mueller, Nature 219 (1968) 1131-1134.
[5]   O. Preining Atmos. Environ. A 25 (1991) 2443-2444.
[6]   I. Tegen, I. Fung, J. Geophys. Res. 100 (1995) 18707-18726.
[7]   I. Tegen, A.A. Lacis, I. Fung, Nature 380 (1996) 419-422.
[8]   E.E. Gard, M.J. Kleeman, D.S. Gross, L.S. Hughes, J.O. Allen, B.D. Morrical, D.P. Fergenson, T. Dienes, M.E. Gälli, R.J. Johnson, G.R. Cass, K.A. Prather, Science 279 (1998) 1184-1187.
[9]   G. Rubasinghege, S. Elzey, J. Baltrusaitis, P.M. Jayaweera, V.H. Grassian, J. Phys. Chem. Lett. 1 (2010) 1729-1737.
[10]   R.J. Charlson, S.E. Schwartz, J.M. Hales, R.D. Cess, J.A. Coakley Jr., J.E. Hansen, D.J. Hofmann, Science 255 (1992) 423-430.
[11]   M.O. Andreae, C.D. Jones, P.M. Cox, Nature 435 (2005) 1187-1190.
[12]   R. Voigt, K.H. Lieser, Naturwissenschaften 71 (1984) 377-378.
[13]   R.M. Harrison, W.T. Sturges, Atmos. Environ. 18 (1984) 1829-1833.
[14]   W.T. Sturges, R.M. Harrison, L.A. Barrie, Atmos. Environ. 23 (1989) 1083-1098.
[15]   G. Zhou, K. Tazaki, Atmos. Environ. 30 (1996) 3301-3308.
[16]   X. Querol, A. Alastuey, J.A. Puicercus, E. Mantilla, C.R. Ruiz, A. Lopez-Soler, F. Plana, R. Juan Atmos. Environ. 32 (1998) 719-731.
[17]   A. Chabas, R.A. Lefèvre, Atmos. Environ. 34 (2000) 225-238.
[18]   M. Derbez, R. Lefèvre, Pollut. Atmos. 177 (2003) 103-125.
[19]   R.K. Xie, H.M. Seip, J.R. Leinum, T. Winje, J.S. Xiao, Sci. Total Environ. 343 (2005) 261-272.
[20]   R.K. Xie, H.M. Seip, L. Liu, D.S. Zhang, Air Qual. Atmos. Health 2 (2009) 123-131.
[21]   I. Rodríguez, S. Gali, C. Marcos, Environ. Geol. 56 (2009) 1551-1561.
[22]   S. Sobanska, H. Hwang, M. Choël, H.-J. Jung, H.-J. Eom, H. Kim, J. Barbillat, C.-U. Ro, Anal. Chem. 84 (2012) 3145-3154.
[23]   M.P. Tolocka, T.D. Saul, M.V. Johnston, J. Phys. Chem. A 108 (2004) 2659-2665.
[24]   B.J. Finlayson-Pitts, J.N. Pitts Jr., Chemistry of the upper and lower atmosphere: Theory, experiments, and applications. Academic Press, Florida, 2000.
[25]   D. Migliavacca, E.C. Teixeira, M. Pires, J. Fachel, Atmos. Environ. 38 (2004) 1641-1656.
[26]   H.R. Pruppacher, R. Jaenicke, Atmos. Res. 38 (1995) 283-295.
[27]   P. Vargas Jentzsch, B. Kampe, P. Rösch, J. Popp, J. Phys. Chem. A 115 (2011) 5540-5546.
[28]   P. Vargas Jentzsch, V. Ciobotă, B. Kampe, P. Rösch, J. Popp, J. Raman Spectrosc. 43 (2012) 514-519.
[29]   P. Vargas Jentzsch, R.M. Bolanz, V. Ciobotă, B. Kampe, P. Rösch, J. Majzlan, J. Popp, Vib. Spectrosc. 61 (2012) 206-213.
[30]   K. Omori, P.F. Kerr, Geol. Soc. Am. Bull. 74 (1963) 709-734.
[31]   H.H. Adler, P.F. Kerr, Am. Mineral. 50 (1965) 132-147.

[32]   V. Ciobotă, W. Salama, N. Tarcea, P. Rösch, M.E. Aref, R. Gaupp, J. Popp, J. Raman Spectrosc. 43 (2012) 405-410.
[33]   N. Tarcea, M. Harz, P. Rösch, T. Frosch, M. Schmitt, H. Thiele, R. Hochleitner, J. Popp, Spectrochim. Acta A 68 (2007) 1029-1035.
[34]   S.M. Angel, N.R. Gomer, S.K. Sharma, C. McKay, Appl. Spectrosc. 66 (2012) 137-150.
[35]   G. Schweiger J. Aerosol Sci. 20 (1989) 1621-1624.
[36]   K.H. Fung, D.G. Imre, I.N. Tang, J. Aerosol Sci. 25 (1994) 479-485.
[37]   M. Trunk, J. Popp, I. Hartmann, M. Lankers, E. Urlaub, W. Kiefer, Fresenius J. Anal. Chem. 355 (1996) 354-356.
[38]   M. Trunk, J. Popp, W. Kiefer, Chem. Phys. Lett. 284 (1998) 377-381.
[39]   J. Musick, J. Popp, M. Trunk, W. Kiefer, Appl. Spectrosc. 52 (1998) 692-701.
[40]   J. Musick, J. Popp, W. Kiefer, J. Raman Spectrosc. 31 (2000) 217-219.
[41]   Y. Batonneau, S. Sobanska, J. Laureyns, C. Bremard, Environ. Sci. Technol. 40 (2006) 1300-1306.
[42]   W. Schumacher, M. Kühnert, P. Rösch, J. Popp, J. Raman Spectrosc. 42 (2011) 383–392.
[43]   C.H. Chio, S.K. Sharma, D.W. Muenow, J. Raman Spectrosc. 38 (2007) 87-99.
[44]   A.E. Hill, L.R. Bacon, J. Am. Chem. Soc. 49 (1927) 2487-2495.
[45]   S. Datta, Y. Thibault, W.S. Fyfe, M.A. Powell, B.R. Hart, R.R. Martin, S. Tripthy, Episodes 25 (2002) 236-239.
[46]   R.M. Caven, W. Johnston, J. Chem. Soc. (1928) 2506-2514.
[47]   J.P. Smith, J.R. Lehr, A.W. Frazier, J. Agric. Food Chem. 10 (1962) 77-78.
[48]   J.D.J. Van Doesburg, L. Vergouwen, L. Van der Plas, Am. Mineral. 67 (1982) 1035-1038.
[49]   G. Sekar, V. Ramakrishnan, G. Aruldhas, J. Solid State Chem. 66 (1987) 235-241.
[50]   G. Sekar, V. Ramakrishnan, G. Aruldhas, J. Solid State Chem. 74 (1988) 424-427.
[51]   V.S. Jayakumar, G. Sekar, P. Rajagopal, G. Aruldhas, Phys. Stat. Sol. (a) 109 (1988) 635-640.
[52]   P. Rajagopal, G. Aruldhas, J. Solid State Chem. 80 (1989) 303-307.
[53]   H.-H. Emons, G. Ziegenbalg, R. Naumann, F. Paulik, J. Therm. Anal. Calorim. 36 (1990) 1265-1279.
[54]   V.P. Mahadevan Pillai, V.U. Nayar, V.B. Jordanovska, J. Solid State Chem. 133 (1997) 407-415.
[55]   M.V. Barashkov, A.I. Komyak, S.N. Shashkov, J. Appl. Spectrosc. 67 (2000) 216-225.
[56]   J.T. Kloprogge, M. Broekmans, L.V. Duong, W.N. Martens, L. Hickey, R.L. Frost, J. Mater. Sci. 41 (2006) 3535-3539.
[57]   P. Vargas Jentzsch, R.M. Bolanz, V. Ciobotă, B. Kampe, P. Rösch, J. Majzlan, J. Popp, J. Molec. Struct. 1022 (2012) 147-152.
[58]   R Development Core Team, R: A language and environment for statistical computing, R Foundation for Statistical Computing, Vienna, 2009.
[59]   T. Dörfer, T. Bocklitz, N. Tarcea, M. Schmitt, J. Popp, Z. Phys. Chem. 225 (2011) 753-764.
[60]   E.O. Schlemper, W.C. Hamilton, J. Chem. Phys. 44 (1966) 4498-4509.
[61]   J.A. McGinnety, Acta Cryst. B 28 (1972) 2845-2852.
[62]   B.-K. Choi, D.J. Lockwood, Solid State Commun. 72 (1989) 133-137.
[63]   B. Xu, G. Schweiger, J. Aerosol Sci. 30 (1999) S379-S380.
[64]   J.L. Anderson, R.C. Peterson, I.P. Swainson, Mineral. Mag. 69 (2005) 259-271.
[65]   A. Wang, J.J. Freeman, B.L. Jolliff, I.-M. Chou, Geochim. Cosmochim. Acta 70 (2006) 6118-6135.
[66]   C. Shantakumari, P. Indian. As. – Math. Sci. 37 (1953) 393-400.
[67]   D. Liu, F.G. Ullman, J. Raman Spectrosc. 22 (1991) 525-528.
[68]   W.H. Baur, Acta Cryst. 17 (1964) 1167-1174.
[69]   W.H. Baur, Acta Cryst. 15 (1962) 815-826.
[70]   M. Wildner, G. Giester, Neues Jahrb. Mineral., Mh., (1991) 296-306.
[71]   I.R. Beattie, T.R. Gilson, G.A. Ozin, J. Chem. Soc. A (1968) 2765-2771.
[72]   D. Nicholls, K.R. Seddon, Spectrochim. Acta A 28 (1972) 2399-2402.
[73]   A.A. Jarzęcki, A.D. Anbar, T.G. Spiro, J. Phys. Chem. A 108 (2004) 2726-2732.
[74]   E. Corazza, C. Sabelli, Z. Kristallogr. 124 (1967) 398-408.
[75]   G.B. Bokii, N.A. Pal'chik, M.Y. Antipin, Trudy Instituta Geologii i Geofiziki 487 (1981) 4-8.
[76]   L. Bindi, Acta Crystallogr. E 61 (2005) i135-i136.
[77]   G. Cocco, E. Corazza, C. Sabelli, Z. Kristallogr. 122 (1965) 175-184.
[78]   A.G. Shtukenberg, Y.O. Punin, E. Haegele, H. Klapper, Phys. Chem. Minerals 28 (2001) 665-674.
[79]   H.H. Eysel, J. Eckert, Z. Anorg. Allg. Chem. 424 (1976) 68-80.
[80]   S.P. Best, R.S. Armstrong, J.K. Beattie, Inorg. Chem. 19 (1980) 1958-1961.
[81]   S.P. Best, J.K. Beattie, R.S. Armstrong, J. Chem. Soc. Dalton Trans. (1984) 2611-2624.
[82]   F.C. Hawthorne, R.B. Ferguson, Acta Cryst. B 31 (1975) 1753-1755.
[83]   M. Wildner, D. Stoilova, Z. Kristallogr. 218 (2003) 201-209.

[84]   M. Giglio, Acta Cryst. 11 (1958) 789-794.
[85]   M. Natarajan, E.A. Secco, J. Solid State Chem. 47 (1983) 231-235.
[86]   B.J.M. Rajkumar, V. Ramakrishnan, R.K. Rajaram, Spectrochim. Acta A 54 (1998) 1527-1532.
[87]   A. Leclaire, J.C. Monier, Acta Cryst. B 33 (1977) 1861-1866.
[88]   A. Braibanti, A. Tiripicchio, M.T. Camellini, A.M.M. Lanfredi, F. Bigoli, Acta Cryst. B 25 (1969) 354-361.
[89]   T.-C.G. Chang, D.E. Irish, Can. J. Chem. 51 (1973) 118-125.
[90]   M. Balkanski, M.K. Teng, M. Nusimovici, Phys. Rev. 176 (1968) 1098-1106.
[91]   R. Murugan, P.J. Huang, A. Ghule, H. Chang, Thermochim. Acta 346 (2000) 83-90.
[92]   M.H. Brooker, Can. J. Chem. 55 (1977) 1242-1250.
[93]   H.C. Tang, B.H. Torrie, J. Phys. Chem. Solids 38 (1977) 125-138.
[94]   X. Ding, G. Wu, Spectrochim. Acta A 51 (1995) 709-715.
[95]   H.B. Wu, C.K. Chan, Atmos. Environ. 42 (2008) 313-322.
[96]   M.H. Brooker, J. Phys.Chem. Solids 39 (1978) 657-667.
[97]   D.L. Bernitt, K.O. Hartman, I.C. Hisatsune, J. Chem. Phys. 42 (1965) 3553-3558.
[98]   A.R. Davis, B.G. Oliver, J. Solution Chem. 1 (1972) 329-339.
[99]   R.L. Sass, R.F. Scheuerman, Acta Cryst. 15 (1962) 77-81.
[100]   C.S. Choi, A.D. Mighell, Acta Cryst. B 38 (1982) 2874-2876.
[101]   A. Bertoluzza, P. Monti, M.A. Morelli, M.A. Battaglia, J. Molec. Struct. 73 (1981) 19-29.
[102]   R. Brooks, T.C. Alcock, Nature 166 (1950) 435-436.
[103]   K. Nakamoto, Infrared and Raman spectra of inorganic and coordination compounds: Theory and aplications in inorganic chemistry, sixth ed., Wiley, New Jersey, 2009.
[104]   M.C. Hales, R.L. Frost, W.N. Martens, J. Raman Spectrosc. 39 (2008) 1141-1149.
[105]   G. Behrens, L.T. Kuhn, R. Ubic, A.H. Heuer, Spectrosc. Lett. 28 (1995) 983-995.
[106]   A.J. Skinner, J.P. LaFemina, Am. Mineral. 79 (1994) 205-214.
[107]   S. Martinez-Ramirez, S. Sanchez-Cortes, J.V. Garcia-Ramos, C. Domingo, C. Fortes, M.T. Blanco-Varela, Cement Concrete Res. 33 (2003) 2063-2068.
[108]   J.M. Montejo-Bernardo, S. García-Granda, A. Fernández-González, Acta Cryst. B 66 (2010) 358-365.
[109]   T.Y. Ling, C.K. Chan, Environ. Sci. Technol. 41 (2007) 8077-8083.
[110]   G. Giuseppetti, F. Mazzi, C. Tadini, Neues Jahrb. Mineral., Mh. (1988) 203-221.
[111]   A.V. Korsakov, A.V. Golovin, K. De Gussem, I.S. Sharygin, P. Vandenabeele, Spectrochim. Acta A 73 (2009) 424-427.
[112]   K. Crammer, Y. Singer, Mach. Learn. 47 (2002) 201-233.
[113]   A. Statnikov, C.F. Aliferis, I. Tsamardinos, D. Hardin, S. Levy, Bioinformatics 21 (2005) 631-643.
[114]   B. Caputo, K. Sim, F. Furesjo, A. Smola, Appearance-based object recognition using SVMs: Which kernel should I use? Proc of NIPS workshop on Statistical methods for computational experiments in visual processing and computer vision, Whistler, 2002.
[115]   R. Tibshirani, T. Hastie, J. Mach. Learn. Res. 8 (2007) 637-652.
[116]   F. Murtagh, Multidimensional clustering algorithms. COMPSTAT Lectures 4. Physica-Verlag, Würzburg, 1985.
[117]   R. Tibshirani, MarginTree: Margin trees for high-dimensional classification, 2010. http://CRAN.R-project.org/package=marginTree.
[118]   M.O. Andreae, D. Rosenfeld, Earth-Sci. Rev. 89 (2008) 13-41.
[119]   D.T. Shindell, G. Faluvegi, D.M. Koch, G.A. Schmidt, N. Unger, S.E. Bauer, Science 326 (2009) 716-718.
[120]   R.L. Reynolds, J.C. Yount, M. Reheis, H. Goldstein, P. Chavez Jr., R. Fulton, J. Whitney, C. Fuller, R.M. Forester, Earth Surf. Process. Landforms 32 (2007) 1811-1827.
[121]   P. Vargas Jentzsch, V. Ciobotă, P. Rösch, J. Popp, Angew. Chem. Int. Ed. 52 (2013) 1410-1413.
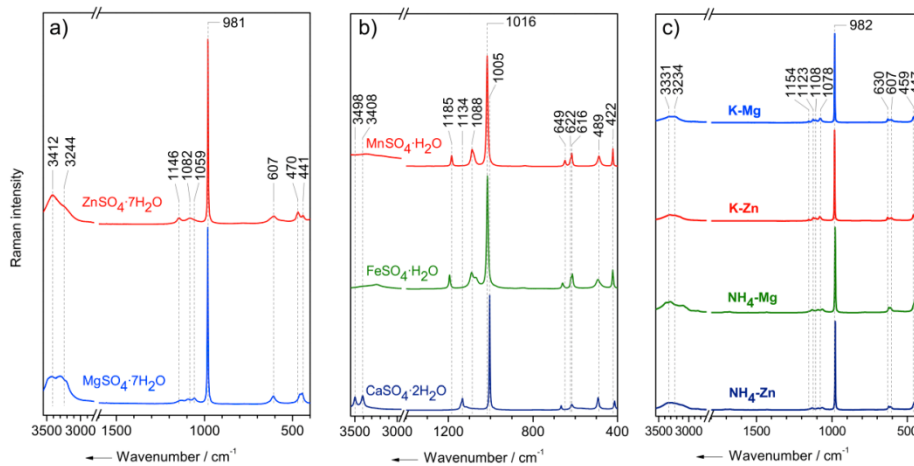
Figure 1. Comparison of the average Raman spectra: a) $ZnSO_4 \cdot 7H_2O$ and $MnSO_4 \cdot 7H_2O$; b) $MnSO_4 \cdot H_2O$, $FeSO_4 \cdot H_2O$ and $CaSO_4 \cdot 2H_2O$; and c) $K_2Mg(SO_4)_2 \cdot 6H_2O$ (K-Mg), $K_2Zn(SO_4)_2 \cdot 6H_2O$ (K-Zn), $(NH_4)_2Mg(SO_4)_2 \cdot 6H_2O$ (NH$_4$-Mg) and $(NH_4)_2Zn(SO_4)_2 \cdot 6H_2O$ (NH$_4$-Zn).
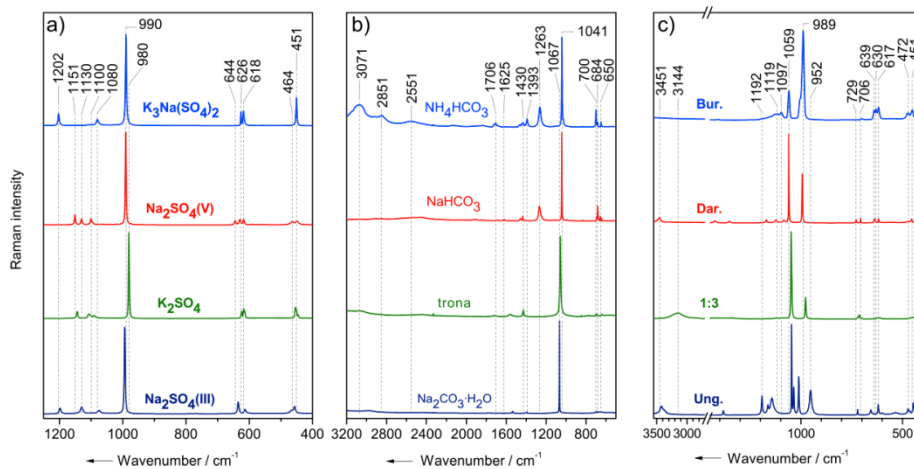
Figure 2. Comparison of the average Raman spectra: a) $K_3Na(SO_4)_2$, Na_2SO_4 (V), K_2SO_4 and Na_2SO_4 (III); b) NH_4HCO_3, $NaHCO_3$, $Na_3(CO_3)(HCO_3) \cdot 2H_2O$ (trona) and $Na_2CO_3 \cdot H_2O$; and c) $Na_6(CO_3)(SO_4)_2$ (Bur.), $Na_3(SO_4)(NO_3) \cdot H_2O$ (Dar.), $(NH_4)_2SO_4 \cdot 3NH_4NO_3$ (1:3) and $K_3Na_8Fe(SO_4)_6(NO_3)_2 \cdot 6H_2O$ (Ung.).
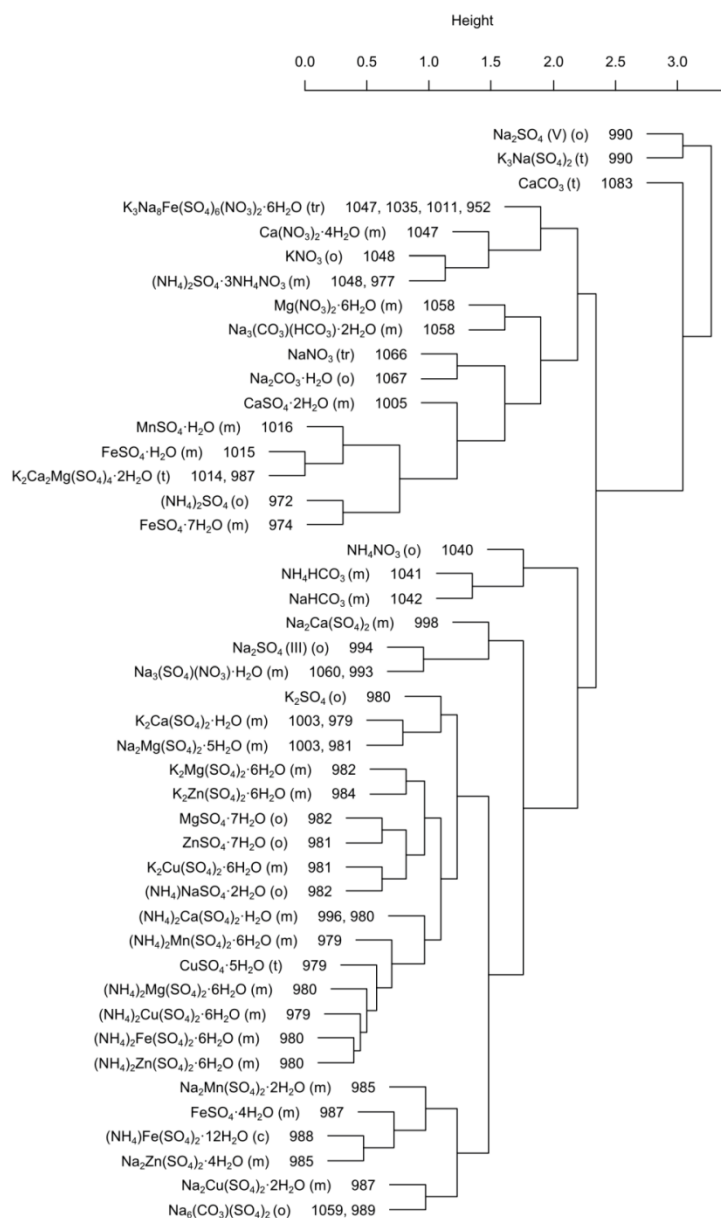
Figure 3. Classification tree for salts without the preselection process. The letters in parenthesis and the numbers beside the salt's formula are the crystal systems in which the salt crystallizes and the wavenumbers (cm^{-1}) of the strongest band(s), respectively. For the crystal system, the following abbreviations are used: t = triclinic, m = monoclinic, o = orthorhombic, tr = trigonal, and c = cubic.
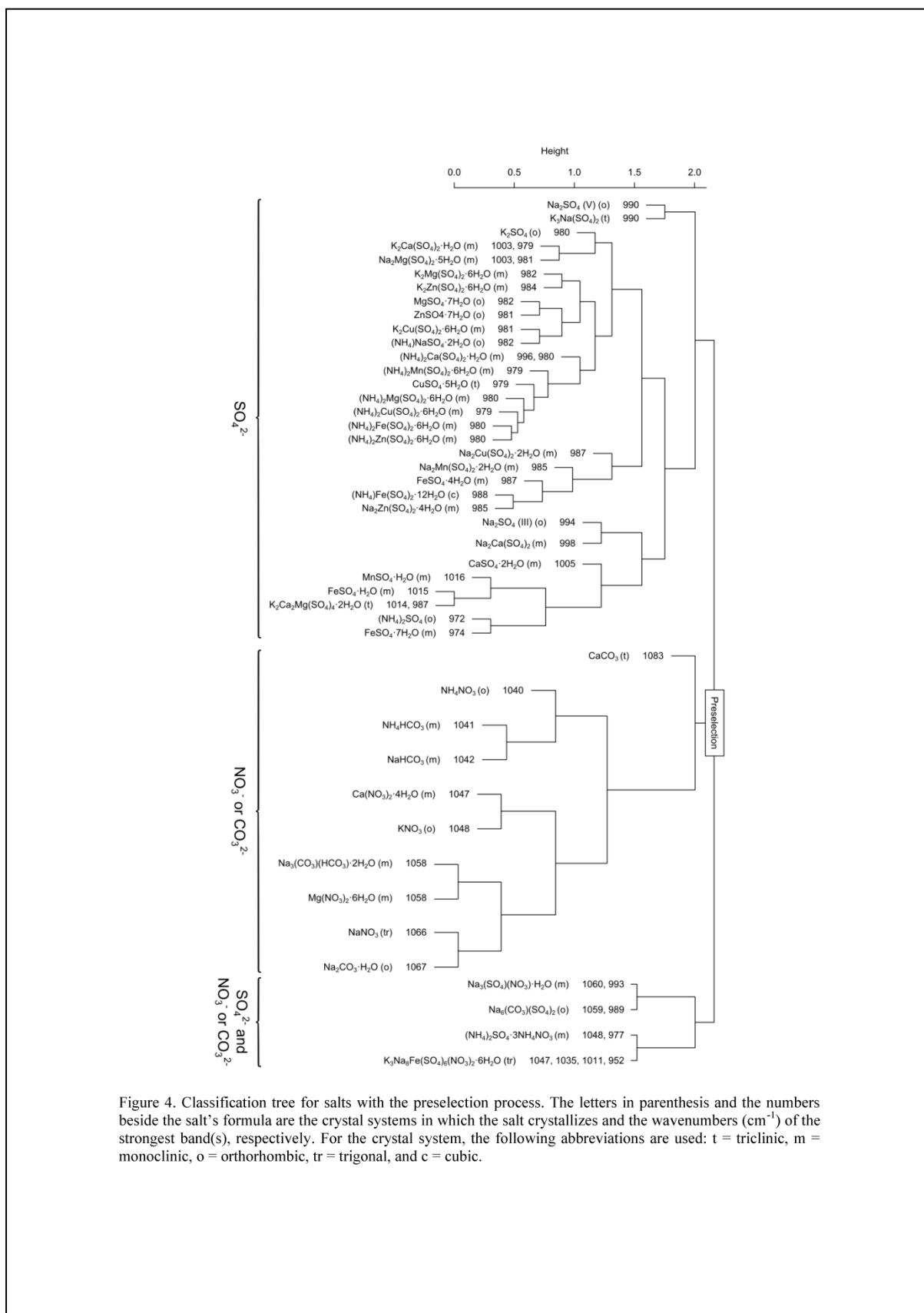
Figure 4. Classification tree for salts with the preselection process. The letters in parenthesis and the numbers beside the salt's formula are the crystal systems in which the salt crystallizes and the wavenumbers (cm^{-1}) of the strongest band(s), respectively. For the crystal system, the following abbreviations are used: t = triclinic, m = monoclinic, o = orthorhombic, tr = trigonal, and c = cubic.

2.6 Reactions of alkaline minerals in the atmosphere [PV6]

Authorship of Publication

Paul Vargas Jentzsch: concept development

salts preparation

Raman measurements

writing of manuscript

Valerian Ciobotă: Raman measurements

discussion of experimental concept and results

Petra Rösch: discussion of experimental concept and results

proofreading of manuscript

Jürgen Popp: project management

discussion of concepts and results

discussion and proofreading of manuscript

Angewandte
Communications

Raman Spectroscopy

Reactions of Alkaline Minerals in the Atmosphere**

Paul Vargas Jentzsch, Valerian Ciobotă, Petra Rösch, and Jürgen Popp

The excessive exploitation of watercourses for human activities affects the water balance of many lakes around the world. A well-known dramatic example is the desiccation of the Aral Sea,[1] which currently has almost disappeared. One of the consequences of the desiccation of saline water bodies as the Aral Sea is the phenomenon known as "salt storms", which transport huge amounts of salt over long distances. Some "soda lakes" (alkaline lakes), for example, the Owens Lake (USA), are also affected by desiccation processes, resulting in the wind transport of the alkaline dust.[2]

In spite of the remarkable scientific efforts to study heterogeneous reactions taking place in the atmosphere, the reactions between solid species under the influence of humid air have not received the necessary attention. To our knowledge, the chemical reaction between $CaCO_3$ and $(NH_4)_2SO_4$ in the presence of humid air[4] is the only report of reactions taking place between solid salts in the presence of humid air. However, there are other salts which should also be considered; $Na_2CO_3 \cdot H_2O$ (thermonatrite) and $Na_3(HCO_3)(CO_3)$ $\cdot 2H_2O$ (trona) were identified in the alkaline dust transported from the Owens (dry) Lake by wind.[2] Trona and $Na_6(CO_3)$-$(SO_4)_2$ (burkeite) were identified in the salt efflorescences of playas of the Mojave Desert (USA), which are periodically removed (and transported) by wind.[3]

Depending on the size of the emitted particles, they can sediment or remain suspended for many days. The suspended material (fine particles) undergoes different atmospheric processes, one of them is coagulation (two particles combining to form one). Coagulation processes can produce internally mixed particles. This means that different solid substances are in contact in single particles (each particle is a mixture). If there is a chemical reaction between two solid compounds present in a single micrometer particle, this reaction takes also place on a macroscale, that is, in a bulk powder mixture. Kinetic differences between experiments on micro- and macroscales can be expected, fundamentally because of the surface area and gas diffusion. Since the reaction rate in a bulk solid mixture may be lower than that in a single particle, it is more likely to detect intermediate products. This is the reason why we use bulk powder mixtures in this work.

We report here, for the first time, solid-state reactions of the alkaline salts thermonatrite, trona, and burkeite with $(NH_4)_2SO_4$ in the presence of humid air (about 70% relative humidity) at ordinary temperatures (21–23 °C). These solid-state reactions can be attributed to the interaction of ions in a liquid film formed on the solids. The observation of changes in the relative amount of reactants over time, as well as the identification of the reaction products were achieved using Raman spectroscopy. We also demonstrate that the reactivity between solid salts is not restricted to alkaline salts.

Considering both the experiments reported by Mori et al.[4] and our own results, the chemical reactivity of the solid powder mixtures seems to be strongly linked to the humidity of the air. When the solid mixtures are exposed to ordinary conditions, that is, temperatures ranging between 21 and 23 °C and a relative humidity (RH) of air below 50%, the chemical reaction rate is very slow; the Raman spectra of mixtures exposed to ambient conditions during 24 h show no or only weak bands of the reaction products (see Figure S1 in the Supporting Information). Remarkable reactivity was observed consistently on exposing the solid powder mixtures to higher RH values. An unequivocal sign that reactions were taking place in the mixtures was the release of NH_3, which is a product of acid–base reactions involving CO_3^{2-} and/or HCO_3^-, and NH_4^+ ions. The formation of CO_2 can be deduced from these reactions.

Figure 1a shows the Raman spectra recorded at different times from an equimolar mixture of $(NH_4)_2SO_4$ and $Na_2CO_3 \cdot H_2O$ (thermonatrite) exposed to humid air (70% RH). After 5 minutes two new bands at 1079 and 996 cm^{-1} are observed, which belong to anhydrous Na_2CO_3 and Na_2SO_4 in phase III, respectively. Na_2SO_4 in phase III (a high-temperature phase) was observed in earlier crystallization experiments of single droplets[5,6] and it is known to transform slowly to phase V (room-temperature phase). After 30 minutes a small band emerges at 1045 cm^{-1} (which can be assigned to $NaHCO_3$ and/or NH_4HCO_3), while the band of anhydrous Na_2CO_3 decreases, obviously as a consequence of the water-vapor absorption to regenerate $Na_2CO_3 \cdot H_2O$. After 3 h the bands belonging to anhydrous Na_2CO_3 and $Na_2CO_3 \cdot H_2O$ (1069 cm^{-1}) disappear, instead a band at 984 cm^{-1} (lecontite, $NH_4NaSO_4 \cdot 2H_2O$) appears. A band emerges and grows gradually at 993 cm^{-1} (Na_2SO_4 in phase V), while the band of Na_2SO_4 in phase III decreases and finally disappears. There is evidence of a phase transition $Na_2SO_4(III) \rightarrow Na_2SO_4(V)$, probably because of the contact with humid air, since the stability of phase III has been associated to dry conditions.[7]

[*] P. Vargas Jentzsch, V. Ciobotă, Dr. P. Rösch, Prof. J. Popp
Institut für Physikalische Chemie and Abbe Center of Photonics
Friedrich-Schiller-Universität Jena
Helmholtzweg 4, 07743 Jena (Germany)
E-mail: juergen.popp@uni-jena.de

Prof. Dr. J. Popp
Institut für Photonische Technologien
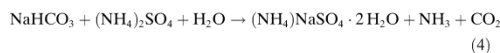Albert-Einstein-Straße 9, 07745 Jena (Germany)
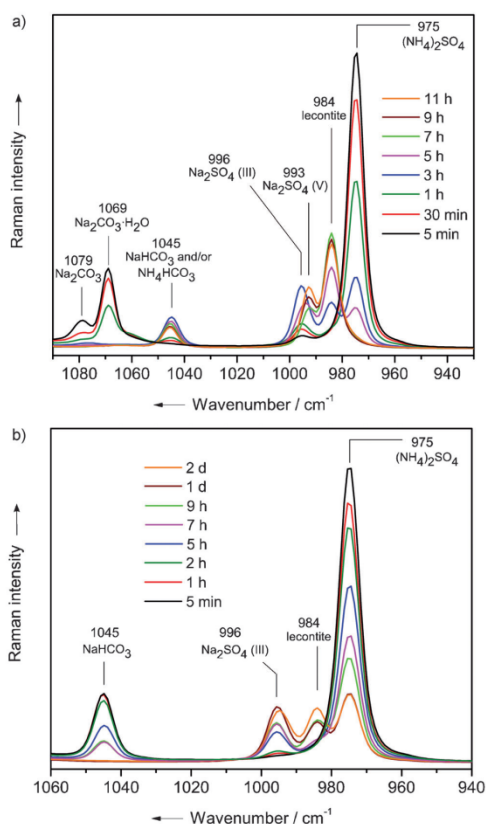
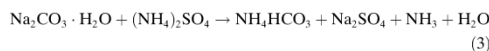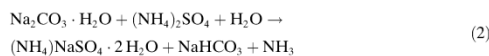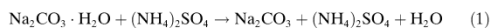**Figure 1.** Raman spectra recorded at different times from equimolar mixtures exposed to humid air (70% RH): a) $(NH_4)_2SO_4$ and $Na_2CO_3 \cdot H_2O$ ($T = 21$–22 °C) and b) $(NH_4)_2SO_4$ and $NaHCO_3$ ($T = 22$–23 °C).

The characteristic band of lecontite increases until 7 h and afterwards a slight decrease is observed, which can be interpreted as a lecontite decomposition reaction.

The Raman spectra acquired at different times from an equimolar mixture of $(NH_4)_2SO_4$ and $NaHCO_3$ exposed to humid air (Figure 1 b) show the formation of both Na_2SO_4 in phase III and lecontite, and again the characteristic band of lecontite decreases towards the end of the experiment. When a new experiment for the $(NH_4)_2SO_4$–$NaHCO_3$ system is performed using a molar ratio of 1:3, only the band of Na_2SO_4 in phase V persists at the end of the experiment (Figure S2), confirming that a lecontite decomposition reaction is taking place. The proposed reactions (1)–(5) for the thermonatrite-$(NH_4)_2SO_4$ system are:

$$Na_2CO_3 \cdot H_2O + (NH_4)_2SO_4 \rightarrow Na_2CO_3 + (NH_4)_2SO_4 + H_2O \quad (1)$$

$$Na_2CO_3 \cdot H_2O + (NH_4)_2SO_4 + H_2O \rightarrow$$
$$(NH_4)NaSO_4 \cdot 2H_2O + NaHCO_3 + NH_3 \quad (2)$$

$$Na_2CO_3 \cdot H_2O + (NH_4)_2SO_4 \rightarrow NH_4HCO_3 + Na_2SO_4 + NH_3 + H_2O \quad (3)$$

$$NaHCO_3 + (NH_4)_2SO_4 + H_2O \rightarrow (NH_4)NaSO_4 \cdot 2H_2O + NH_3 + CO_2 \quad (4)$$

$$(NH_4)NaSO_4 \cdot 2H_2O + NaHCO_3 \rightarrow Na_2SO_4 + NH_3 + 3H_2O + CO_2 \quad (5)$$
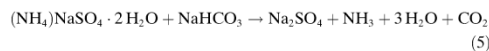
The reaction (1) shows the dehydration of thermonatrite because of the high hygroscopicity of $(NH_4)_2SO_4$. Apparently this strong affinity to H_2O forces the extraction of the H_2O molecule from the thermonatrite structure producing anhydrous Na_2CO_3. The H_2O molecules, initially proceeding from thermonatrite and afterwards from the humid air, deposit on the solid $(NH_4)_2SO_4$. Since $(NH_4)_2SO_4$ and thermonatrite (and anhydrous Na_2CO_3) are intimately mixed, the prolonged exposure to humid air results in the formation of a "liquid H_2O film" on the solids and the partial dissolution of these salts (Figure 2). When CO_3^{2-}, HCO_3^-, and NH_4^+ ions are in
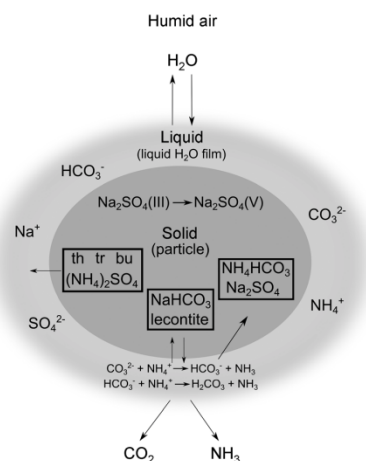
Figure 2. Interaction scheme of a solid particle consisting of a mixture of thermonatrite (th), trona (tr), or burkeite (bu), and $(NH_4)_2SO_4$ suspended in humid air (the actual thickness of the liquid phase compared to the particle size is expected to be much smaller than that shown in the figure).

solution in this "film", acid–base reactions take place eliminating the gaseous products NH_3 and CO_2 and precipitating new salts. This can explain the formation of $NaHCO_3$, $(NH_4)NaSO_4 \cdot 2H_2O$, and Na_2SO_4 in the solid mixture at different times. Na_2SO_4 (phase III) is already observed at 5 minutes and it seems unlikely that the fast formation of Na_2SO_4 is explained only by the two consecutive reactions (2) and (5), therefore reaction (3) is also postulated.
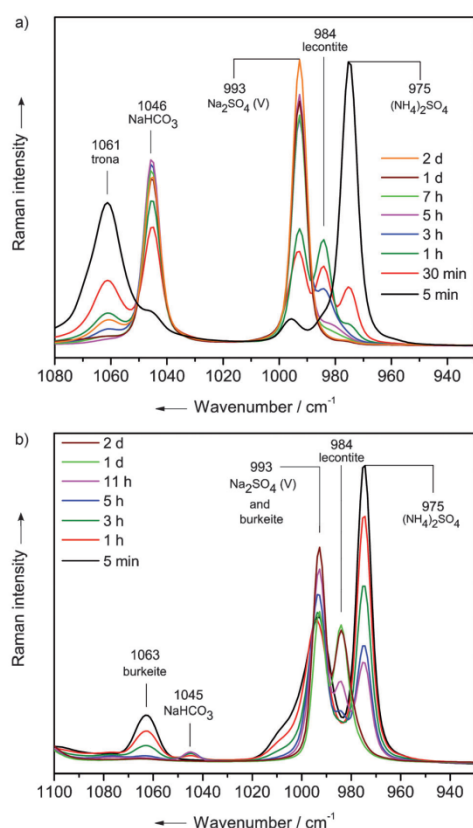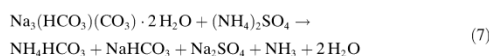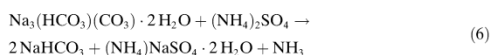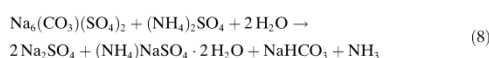
Angewandte
Communications

Figure 3. Raman spectra recorded at different times from equimolar mixtures exposed to humid air (70% RH): a) $(NH_4)_2SO_4$ and $Na_3(HCO_3)(CO_3)\cdot 2H_2O$ ($T = 21–22\,^{\circ}C$) and b) $(NH_4)_2SO_4$ and $Na_6(CO_3)(SO_4)_2$ ($T = 21–22\,^{\circ}C$).

Figure 3a shows the Raman spectra recorded at different times from an equimolar mixture of $(NH_4)_2SO_4$ and $Na_3(HCO_3)(CO_3)\cdot 2H_2O$ (trona) exposed to humid air. After 5 minutes bands at 1046 and 996 cm^{-1} can be observed, indicating that NaHCO$_3$ and Na$_2$SO$_4$ in phase III appear in the solid mixture at this short time. The fast growing of the band at 1046 cm^{-1} suggests that not only NaHCO$_3$, but also NH$_4$HCO$_3$ is formed. After 30 minutes the band at 984 cm^{-1} (lecontite) is clearly distinguishable and starts to decrease as soon as all $(NH_4)_2SO_4$ has reacted. The final products of the reactions are Na$_2$SO$_4$ in phase V, NaHCO$_3$, and NH$_4$HCO$_3$. The proposed reactions (6) and (7) for the trona–$(NH_4)_2SO_4$ system are:

$$Na_3(HCO_3)(CO_3)\cdot 2H_2O + (NH_4)_2SO_4 \rightarrow$$
$$2\,NaHCO_3 + (NH_4)NaSO_4 \cdot 2H_2O + NH_3 \qquad (6)$$

$$Na_3(HCO_3)(CO_3)\cdot 2H_2O + (NH_4)_2SO_4 \rightarrow$$
$$NH_4HCO_3 + NaHCO_3 + Na_2SO_4 + NH_3 + 2H_2O \qquad (7)$$

The formation of NaHCO$_3$ and the evident decomposition of lecontite suggest that the reactions (4) and (5) are also taking place in this system. At the end of the experiment (after two days), a weak band at 1061 cm^{-1} appears; this anomaly can be explained by a local heterogeneity of the mixture resulting in the presence of unreacted trona, or a possible interaction of the mixture with atmospheric CO$_2$ to recrystallize trona. The interaction of alkaline brines with atmospheric CO$_2$ to crystallize trona was proposed by Eugster[8] to explain natural deposits of this mineral.

Figure 3b shows the Raman spectra taken at different times from an equimolar mixture of $(NH_4)_2SO_4$ and Na$_6$(CO$_3$)(SO$_4$)$_2$ (burkeite) exposed to humid air. After 1 h a band at 1045 cm^{-1} (NaHCO$_3$ and/or NH$_4$HCO$_3$) emerges. The SO$_4^{2-}$ symmetric stretching (ν_1) of burkeite is characterized by a strong band at 993 cm^{-1} with a shoulder at 1005 cm^{-1} (see Figure S10), therefore the emergence of the characteristic bands of Na$_2$SO$_4$ in phases III and V (996 and 993 cm^{-1}, respectively) cannot be observed within the first minutes and hours of the experiment. Only at the end of the experiment (after two days) the large increase of the intensity of the band at 993 cm^{-1} and the emergence of the weaker bands of Na$_2$SO$_4$ in phase V indicate the formation of Na$_2$SO$_4$ in this mixture. The band of lecontite (984 cm^{-1}) becomes prominent after 5 h, grows until one day and stabilizes. Taking into account these observations, the main reaction (8) taking place in the burkeite–$(NH_4)_2SO_4$ system is:

$$Na_6(CO_3)(SO_4)_2 + (NH_4)_2SO_4 + 2H_2O \rightarrow$$
$$2\,Na_2SO_4 + (NH_4)NaSO_4 \cdot 2H_2O + NaHCO_3 + NH_3 \qquad (8)$$

The formation of NaHCO$_3$ and lecontite suggests that the reactions (4) and (5) can also take place in this system. The production of NH$_4$HCO$_3$ seems to be unlikely, since the band at 1045 cm^{-1} disappears towards the end of the experiment. This indicates that the signal at 1045 cm^{-1} belongs to NaHCO$_3$ and this salt is completely consumed by the reactions (4) and (5).

The reactions of solid mixtures are not restricted to alkaline materials; in a solid mixture of CaSO$_4\cdot 2H_2O$ (gypsum) and $(NH_4)_2SO_4$ we observed the following reaction (9), see Figure S3:

$$CaSO_4 \cdot 2H_2O + (NH_4)_2SO_4 \rightarrow (NH_4)_2Ca(SO_4)_2\cdot H_2O + H_2O \qquad (9)$$
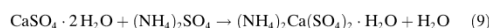
Gypsum, $(NH_4)_2SO_4$ and $(NH_4)_2Ca(SO_4)_2\cdot H_2O$ (koktaite) were reported in atmospheric particulate matter.[9] It is clear that koktaite can be produced not only by precipitation from aerosol solutions,[6] but also by a reaction of solid material in the presence of humid air.

In summary, reactions taking place between alkaline minerals and $(NH_4)_2SO_4$ in the presence of humid air have been studied using Raman spectroscopy. Products such as Na$_2$SO$_4$ (phases III and V), NaHCO$_3$ and/or NH$_4$HCO$_3$, and lecontite have been identified. Moreover, reactions involving solid mixtures are not restricted to alkaline minerals; the

Angewandte
International Edition *Chemie*

formation of koktaite is reported as a product of the reaction between gypsum and $(NH_4)_2SO_4$ in the presence of humid air. This kind of reactions has to be considered in atmospheric studies (aerosol chambers and models), since aerosol coagulation and subsequent chemical reactions may have implications not only on the atmospheric chemistry, but also on the climate.

Experimental Section

Details of the reactants, the synthetic methods of minerals, and the instruments used in this study can be found in the Supporting Information. The reactions of $Na_2CO_3 \cdot H_2O$ (thermonatrite), $Na_3(HCO_3)(CO_3) \cdot 2H_2O$ (trona), $Na_6(CO_3)(SO_4)_2$ (burkeite), and $CaSO_4 \cdot 2H_2O$ (gypsum) with $(NH_4)_2SO_4$ were studied using powder solid mixtures in an equimolar ratio. For normalization purposes, an amount of TiO_2 (anatase) equivalent to about 5% of the mass of $(NH_4)_2SO_4$ was included in the mixtures. To generate the mixtures, appropriate amounts of the salts were placed in a porcelain mortar and finely milled. The temperature and relative humidity (RH) of air during the manipulation of the reactants and the milling process were 21–23 °C and less than 50%, respectively (ambient conditions). The resulting powder was placed in a Petri dish (80 mm diameter), homogeneously distributed, and disposed in a glovebox with an inner RH of 70%. The formation and release of $NH_3(g)$ was verified by its characteristic odor and the color change of a wet piece of pH paper. A powder sample was taken at specific times of exposition to the humid air (starting at 5 minutes) and its Raman spectrum was recorded immediately. The sampling process was performed until no more significant changes were observed in the Raman spectra or the solid mixture deliquesces (the thermonatrite-$(NH_4)_2SO_4$ system). The

samples were collected from the mixture including both the upper (in direct contact with air) and lower (in contact with the Petri dish glass) portion of the bulk mixture. In addition, the reactivity of solid mixtures containing $(NH_4)_2SO_4$ and $NaHCO_3$ in molar ratios 1:1 and 1:3 were evaluated using the same method. To evaluate the reactivity of the mixtures at low relative humidities, the Raman spectra were recorded from small portions of each mixture after 24 h of exposure to ambient conditions. The Raman spectra of all synthetic minerals and reactants used in this study were recorded (see Figures S4–S15).

[1] P. Micklin, *Annu. Rev. Earth Planet. Sci.* **2007**, *35*, 47–72.
[2] M. C. Reheis, *J. Geophys. Res.* **1997**, *102*, 25999–26008.
[3] R. L. Reynolds, J. C. Yount, M. Reheis, H. Goldstein, P. Chavez, Jr., R. Fulton, J. Whitney, C. Fuller, R. M. Forester, *Earth Surf. Processes Landforms* **2007**, *32*, 1811–1827.
[4] I. Mori, M. Nishikawa, Y. Iwasaka, *Sci. Total Environ.* **1998**, *224*, 87–91.
[5] B. Xu, G. Schweiger, *J. Aerosol Sci.* **1999**, *30*, S379–S380.
[6] P. Vargas Jentzsch, R. M. Bolanz, V. Ciobotă, B. Kampe, P. Rösch, J. Majzlan, J. Popp, *Vib. Spectrosc.* **2012**, *61*, 206–213.
[7] B.-K. Choi, H. J. Labbé, D. J. Lockwood, *Solid State Commun.* **1990**, *74*, 109–113.
[8] H. P. Eugster, *Rocky Mountain Geology* **1971**, *10*, 49–55.
[9] R. Voigt, K. H. Lieser, *Naturwissenschaften* **1984**, *71*, 377–378.

3 Conference Contributions

Poster:

1. *Characterization of inorganic mixtures in atmospheric particulate matter using Raman spectroscopy.*
   Scientific Meeting of Photonics4Life **2010**, Paris, France;
   Paul Vargas Jentzsch, Bernd Kampe, Petra Rösch, Jürgen Popp

2. *Analysis of atmospheric particles by micro-Raman spectroscopy: Environmental implications.*
   International Conference on Raman Spectroscopy (ICORS) **2012**, Bangalore, India;
   Paul Vargas Jentzsch, Valerian Ciobotă, Bernd Kampe, Petra Rösch and Jürgen Popp

Oral Presentation:

1. *On the origin of inorganic particles in atmosphere and their characterization using Raman spectroscopy.*
   Doctoral Student's Conference for the Discussion of Optical Concepts,
   March **2011**, Naumburg, Germany.

4 Publication List

Peer-reviewed Publications:

1. Vargas Jentzsch P., Kampe B., Rösch P. and Popp J. (2011) Raman Spectroscopic Study of Crystallization from Solutions Containing $MgSO_4$ and Na_2SO_4: Raman Spectra of Double Salts. *J. Phys. Chem. A* **115**, 5540-5546.

2. Vargas Jentzsch P, Ciobotă V, Kampe B., Rösch P. and Popp J. (2012) Origin of salt mixtures and mixed salts in atmospheric particulate matter. *J. Raman Spectrosc.* **43**, 514-519.

3. Vargas Jentzsch P, Bolanz R. M., Ciobotă V, Kampe B., Rösch P., Majzlan J. and Popp J. (2012) Raman spectroscopic study of calcium mixed salts of atmospheric importance. *Vib. Spectrosc.* **61**, 206-213.

4. Vargas Jentzsch P, Bolanz R. M., Ciobotă V, Kampe B., Rösch P. Majzlan, J. and Popp J. (2012) Raman and infrared spectroscopic study of synthetic ungemachite, $K_3Na_8Fe(SO_4)_6(NO_3)_2.6H_2O$. *J. Mol. Struct.* **1022**, 147-152.

5. Vargas Jentzsch P, Kampe B., Ciobotă V, Rösch P. and Popp J. Origin and significance of inorganic salts in atmospheric particulate matter: Raman spectroscopy as an analytical tool. *Spectrochim. Acta A* (submitted).

6. Vargas Jentzsch P, Ciobotă V, Rösch P. and Popp J. (2013) Reactions of alkaline minerals in the atmosphere. *Angew. Chem. Int. Ed.* **52**, 1410-1413.

Acknowledgments

Curriculum Vitae

2009 – 2012   Doctoral student (DAAD-Scholarship) in the "Institut für Physikalische
               Chemie" (Institute of Physical Chemistry)
               Friedrich-Schiller-Universität Jena, Germany

2008   Researcher (DAAD-Scholarship) in the "Centro de Química Inorgánica"
               (Center of Inorganic Chemistry)
               Universidad Nacional de La Plata, Argentina

2005 – 2007   Researcher in the "Centro de Aguas y Saneamiento Ambiental"
               (Center for Water and Environmental Sanitation)
               Universidad Mayor de San Simón, Cochabamba – Bolivia

2007   Lecturer in Unitary Operations III,
               Universidad del Valle, Cochabamba – Bolivia

2004   Research Assistant in the "Centro de Aguas y Saneamiento Ambiental"
               (Center for Water and Environmental Sanitation)
               Universidad Mayor de San Simón, Cochabamba – Bolivia

2003 – 2007   Lecturer in different subjects (General Chemistry, Analytical Chemistry I,
               Physical Chemistry I, Dissolution Equilibria, Thermodynamics I)
               Universidad Mayor de San Simón, Cochabamba – Bolivia

2002 – 2006   Master in Environmental Engineering
               Universidad Mayor de San Simón, Cochabamba – Bolivia

1999 – 2002   Teaching Assistant in the Organic Chemistry Area
               Universidad Mayor de San Simón, Cochabamba – Bolivia

1997 – 2001   Bachelor's Degree in Chemical Engineering
               Universidad Mayor de San Simón, Cochabamba – Bolivia

Jena, 09.11.12

Selbstständigkeitserklarung

Ich erkläre, dass ich die vorliegende Arbeit selbstständig und unter Verwendung der angegebenen Hilfsmittel, persönlichen Mitteilungen und Quellen angefertigt habe.

Jena, 9. November 2012

Paul Ernesto Vargas Jentzsch